UNIVERSITÀ DEGLI STUDI DI PALERMO
Technological Innovation Engineering
Engineering department
Disciplinary Scientific Sector ING-IND/23

LEAD-ACID BATTERIES WITH NANOSTRUCTURED ELECTRODES

PhD
MARIA GRAZIA INSINGA

COORDINATOR
Prof. SALVATORE GAGLIO

TUTOR
Prof. ALESSANDRO GALIA

CO-TUTOR
Prof. ROSALINDA INGUANTA

CYCLE XXXII
YEAR OF ACHIEVEMENT OF THE TITLE: 2020

Index

Introduction

The lead-acid battery has been widely used for over a century, in fact its production and use continue to grow thanks to new applications in alternative devices and in electric and hybrid vehicles. Currently, the lead-acid batteries are the most widely used device in conventional cars and motorcycles with a combustion engine for starting the engine.
The lead-acid batteries are the oldest and simplest battery systems, with the lowest production/management cost ratio if compared with the modern energy storage systems. They are constructed starting from three essential elements: sulfuric acid as the electrolyte, lead and lead dioxide as negative and positive plate respectively. Each cell is able to supply a voltage of about 2 Volts, while the current is a function of the amount of active material.
Over the years, various studies have been carried out and many solutions have been proposed for improving the performance of lead-acid batteries aimed to increase the life cycles and energy density and also to decrease the sulfurization phenomena. The main studies, to improve the performances of the lead-acid batteries, are focused adding various types of carbon additives in the positive and negative plates or adding substances into the electrolyte to delay the sulfation of both positive and negative electrodes.
Another of the possible methods to obtain these results consists to replace the commercial plates with the nanostructured electrodes of lead and lead oxide.

The research activity of the PhD work was focused on the fabrication of nanostructured electrodes, which have a high surface area and thus high utilization of the active material. This was due to the better diffusion of SO_4^{2-} ions within the active material leading to a more specific energy. Prior to this work, several tests had already been performed for the optimization of the deposition of the nanostructured electrodes of Pb and PbO_2 and subsequently work was carried out on the nanostructured PbO_2 electrode by carrying out various tests on it in various operating conditions. Thanks to the excellent results obtained from the tests performed on the nanostructured PbO_2 electrodes, it was decided to carry out various tests also on the nanostructured Pb electrode and then move on to the tests on entirely nanostructured batteries. The tests were carried out first on the

individual nanostructured electrodes in order to verify the actual performances of these electrodes so as to be able to prevent any malfunctions of an entirely nanostructured battery.
The fabrication method used to obtain nanostructured electrode is based on template electrosynthesis. In particular, nanostructured electrodes were obtained in two steps:

1) Deposition of the current collector;
2) Deposition of nanowires (NWs).

The nanometric dimension of the template pores (polycarbonate membrane) permits to obtain nanostructured electrodes with typical morphology that cannot be obtained with other techniques.
The nanostructured electrodes were assembled in a zero gap configuration (to simulate the commercial battery configuration) using an AGM (Absorbent Glass Mat) type separator. The electrolyte used is an aqueous solution of H_2SO_4 (5M).
The nanostructured electrodes were tested in much more severe conditions than those of conventional batteries. In particular, the tests were carried out at C-rate from 1C (1 hour to complete charge of the battery's capacity) to 10C (6 minutes to complete charge of the battery's capacity), where with "C" we indicate the battery's capacity, and imposing a very deep discharge. In fact, a cut-off voltage of 1.2V was imposed, that is a value well beyond the limits indicated in the literature for lead-acid batteries. This last parameter is very important as significantly differentiates the performance of the nanostructured electrodes compared to the commercial ones. The nanostructured electrodes were tested at room temperature and at temperatures of -20 °C and 40 °C, under galvanostatic charging and discharging conditions and imposing a discharge time equal to 90% of the charge time.
No work, other than those presented by the Laboratory of Applied Chemistry-Physics of the University of Palermo, has ever been carried out on lead-acid batteries with nanostructured electrodes and the results obtained from the tests carried out have shown excellent functioning of this innovative type of lead-acid accumulator, the results obtained are not comparable with the performances presented by current lead-acid batteries.
The research activity also involved the fabrication of hydrogels to use as an electrolyte in nanostructured lead-acid batteries. Furthermore, in the laboratories of the Fraunhofer for Silicate Research of Wűrzburg (Germany) the stability of

carbonaceous materials added to the positive pastes of commercial electrodes were also studied.

Acknowledgments

Many people have contributed, in different ways, to achieving this goal. The first thanks go to my family and my boyfriend who have always supported me in all my decisions, giving me the strength to go on even in the most difficult moments.

A special thanks goes to the two best professors I could meet along my journey, Prof. S. Piazza and Prof. C. Sunseri, two very important figures in my growth path who have been able to give me so much both at didactic level and at human level; Professors who knew how to make a university laboratory a big family.

I would like to thank Professor R. Inguanta as the head of the Laboratory of Applied Physical Chemistry and a reference point for all of us. Thank you for your presence, for helping me in difficult moments and for always being ready to solve my existential doubts.

I thank all the guys, past and present, of the Laboratory of Applied Physical Chemistry for making my days special and unforgettable; I particularly thank the engineer A. Moncada for having instructed me on the world of batteries and for having endured me during my beginnings.

I thank all the students of the XXXII cycle of PhD course, always present during my delusions and with whom I shared the joys and sorrows of the three most beautiful and formative years of my journey.

A final thanks you, but not less important, goes to all the people of the electrochemistry group of the Fraunhofer ISC of Wűrzburge, with particular attention to Jochen Settelein, Begűm Bozkaya and Paul Wulfert-Holzmann, of the group of lead-acid batteries, which they welcomed me as if they had known me always giving me 6 months of fantastic training.

Chapter 1

Lead-acid batteries

Lead-acid batteries are the electrochemical accumulator more diffuse in the world, for their low cost, high efficiency of electrical turnaround (75% - 80%) [1] and recyclability (equal to 95%). These batteries are used for ignition of engine, lights and services of conventional vehicles. In this chapter, it will analyze the main characteristics of lead-acid batteries, the main drawbacks and the current studies that are followed to improve their performance.

1.1 Characteristics of lead-acid batteries

The accumulators can be defined reversible chemical generators. In these devices, chemical energies of reaction between the active substances of electrodes were used to generate electrical energy. Accumulators have two essential parts:

- *the electrodes*, on which the electrochemical reactions take place and the ions are discharged. The electrodes can be positives or negatives and this depends to the potential they have each other during normal work;
- *the electrolyte*, between the electrodes, it is an aqueous solution and in it we have the ions exchange.

An electrochemical cell is constituted to one or more positive electrodes between a couple of negative electrodes all immersed into the electrolyte. Two or more elements, with the same characteristics, connected in series, are named *battery*.
The galvanic cell of lead-acid battery is constituted by a vessel with an aqueous solution of sulfuric acid (1.28 g/cm^3) as the electrolyte in which the electrodes are immersed at a low distance each other. The positive electrode is a layer of lead dioxide (PbO_2) and the negative electrode is a layer of metallic lead (Pb). Figures

1.1 a), b) and c) show the scheme of the discharge, the charge and the assembling respectively of lead-acid battery.

At the positive electrodes, the reaction is:

$$PbO_2 + 4H^+ + SO_4^{2-} + 2e^- \rightarrow PbSO_4 + 2H_2O$$

while at the negative electrode is

$$Pb + SO_4^{2-} \rightarrow PbSO_4 + 2e^-$$

The global reaction is:

$$PbO_2 + Pb + 2H_2SO_4 \rightarrow 2PbSO_4 + 2H_2O$$

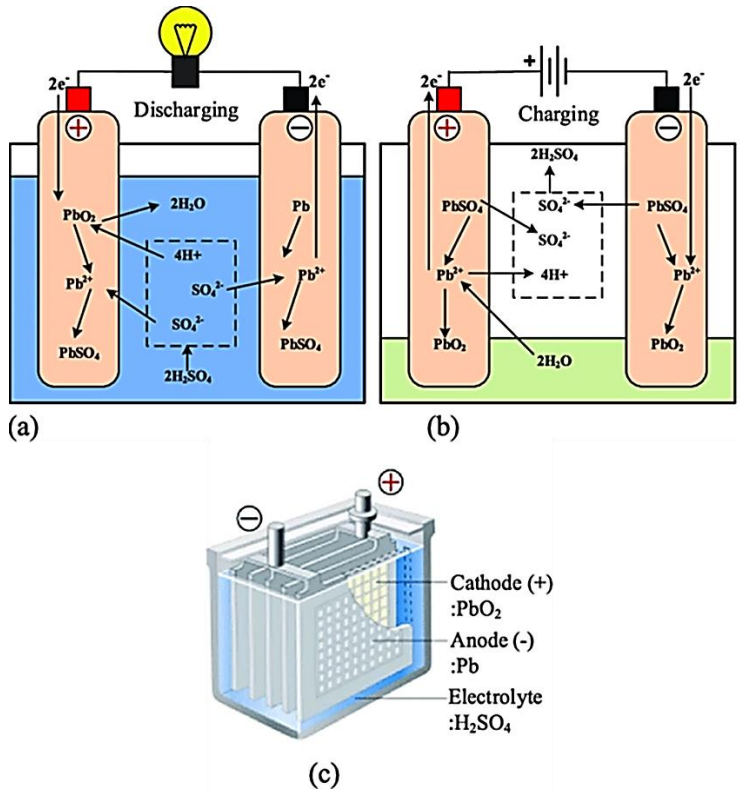

Figure 1.1 Scheme of discharge (a), charge (b) and assembling (c) of lead-acid battery [1].

For a lead-acid battery completely charged the difference of potential between the two electrodes is equal to 2.16V for a concentration of H_2SO_4 equal to 1.32 g/cm^3.

The efforts of the technological research in lead-acid batteries are looking to reach better characteristics such as:

- High specific capacity: the energy content in the reactant system needs to be very high, in order to have, with equal energy demand, minimum size;
- Stability: the reactions need to be only in closed circuit, that means to have low self-discharge;
- Reversibility: the electrochemical reactions must be completely invertible;
- Lifetime: the lifetime of batteries must be as long as possible, according to the performances required.

1.1.1 Components of a lead-acid battery

The lead-acid battery consists of several parts described below.

- ***Plates***

The plates of the lead-acid batteries are generally made by pressing a paste or slurry, containing the lead oxide and the sulfuric acid, into a lead alloy grid designing to prevent material from shedding during the use. The typical grids of the lead-acid battery are shown in figure 1.2.

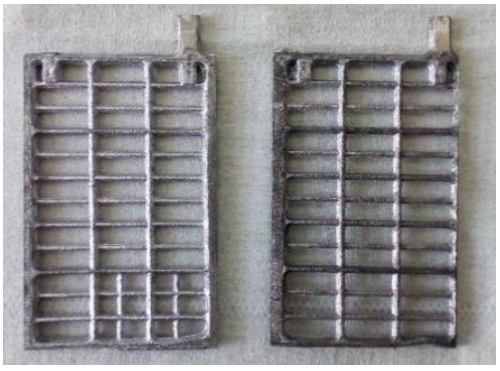

Figure 1.2 Typical grids of lead-acid battery.

The plates are then processed to produce the final positive and negative electrodes, consisting in a sponge of active material. The effective surface area of a typical electrode is about 50÷150 m^2 per Ah capacity. The battery of FIAMM model FG 10121 has plates of lead oxide and lead with the dimensions of about 4 mm length and 11 mm high. The width is different for the two plates, in particular the PbO_2 plate is thicker than the Pb plate. The weight of the PbO_2 plate is around 31.5 g and the weight of the Pb plate is around 23.8 g. The negative electrode with high capacity has a porous mass with the active surface of about 0.4 ÷ 0.8 m^2g^{-1}[22]. The plates are characterised by definite porosity, active surface and hardness of the active mass and of its connection to the grid. The size of the paste particles determines the porosity of the active materials. In order to have a good battery manufacturing the optimum paste particles should be needle-like (prismatic) in shape and have a diameter of 0.4 - 5 mm and a length of 3 - 30 mm. The particles with these size yield positive active mass with appropriate porosity that ensures high specific active surface, adequate hardness of the porous mass and optimum pore distribution allowing easy access of ions of H_2SO_4 and H_2O molecules to every part of the plate volume. Table 1.1 shows the value ranges for the weight coefficients (β) per Ah, and the specific capacity per kg active mass (σ) for PAM and NAM for the basic types of commercial lead-acid batteries: stationary, SLI and traction.

	Specific Energy		β and σ Coefficients			
			PbO_2		Pb	
Battery Type	Wh kg^{-1}	Wh L^{-1}	β_{PbO_2} g Ah^{-1}	σ_{PbO_2} Ah kg^{-1}	β_{Pb} g Ah^{-1}	σ_{Pb} Ah kg^{-1}
SLI (20h rate)	30–40	75–100	10–7.7	100–130	8.7–6.5	115–154
Traction cell (5h rate)	25–32	60–100	16.7–11.1	60–90	12.5–10.0	80–100
Stationary battery: Flooded	20–28	35–60	16.7–10.0	60–100	12.5–10.0	80–100
VRLAB (60Ah)	21–31	45–85	15.2–11.4	66–90	12.5–7.2	80–140

Table 1.1 Specific energy, specific capacity per kg active mass (σ) and weight coefficients per Ah (β) for different battery types [9].

This table also gives the respective specific energies (by volume and weight). The variation in σ and β values for a given battery type is due to differences in the technology of battery design, plate manufacture, and specific or general application requirements [22].

- ***Separators***

The separators are installed between the positive and the negative plates to prevent the short circuits. They should be highly porous, with small pore diameters and high electrical resistance. They are usually made of plastic, rubber or inorganic material (fibres of silica) or a combination of them. Different types of separators are used. Two of the most common types of separator used in lead-acid batteries are shown in figure 1.3.

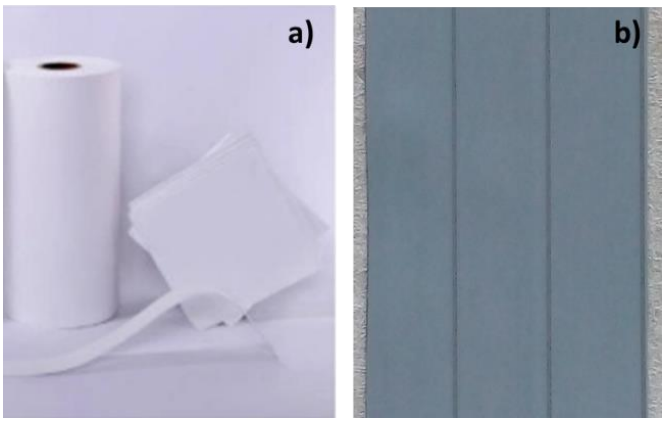

Figure 1.3 Typical separators of lead-acid battery; a) AGM separator, b) Polyethylene separator.

- ***Case***

Different types of case are currently used and they are made with different materials. The urethane cases are best at low temperatures and will not become brittle down to 45°C. They will not crack if the battery freezes, and they are currently available for large batteries. The polypropylene cases, which are becoming increasingly common in automotive batteries, tend to become brittle below -30°C. The rubber cases are somewhat better, but are becoming increasingly rare. At extremely low temperatures, the battery cases are made of hard rubber or plastic may become brittle and fracture on impact, rendering the batteries completely inoperative and possibly allowing sulfuric acid to escape. The figure 1.4 shows an example of a lead-acid battery case.

Figure 1.4 Example of a lead-acid battery case [2].

1.2 Limits of lead-acid batteries

The lead-acid batteries have many drawbacks due to the limited rate of charge (less or equal to C/5, that means 5h to complete charge of the battery's capacity) and the sulfation of the electrodes. The irreversible sulfation of electrodes leads to a partial state of charge of the device causing a low value of the ratio between stored energy/weight, that is the more less than the others types of battery presents on the market.

1.2.1 Charge regime

The charge current is given by:

$$I_c = \frac{V_c - E_c}{R_{ic}}$$

Where I_c is the charge current, V_c is the charge voltage, E_c is the e.m.f. (Electromotive force) of the battery and R_{ic} is the internal resistance of the accumulator.
When the charge is made with a constant value of current with a C-rate equal to C/5 - C/6, the following phenomena occur:

1. Initially, it can be observed a rapid growing of tension until to 2.1V causing an increment of acid concentration in the cell. After, voltage increases slowly until to 2.4V, reached this value, the gas evolution (oxygen on positive plate and hydrogen on negative plate) starts, causing further plate polarization. At 2.75V, being the battery completely charged, all electrical energy is used for water electrolysis with a very high amount of gas evolution. This must be avoided because can cause a mechanical action on the plate surface leading to active material lose, slurry production and capacity decrement.
2. At the end of the process, the electrolyte density increases up to 1.21 ÷ 1.26 and the temperature is equal to 32°C. The increase of electrolyte density is due to the sulfuric acid production and the water consume. To avoid an excessive gas evolution is possible to establish charge regimes gradually slower. This possibility, even if requires longer time of charge, offers many advantages, such as lower gas production, and thus low water consumptions.

In figure 1.5 the characteristic curves of a commercial lead-acid battery charge at 25°C are reported.

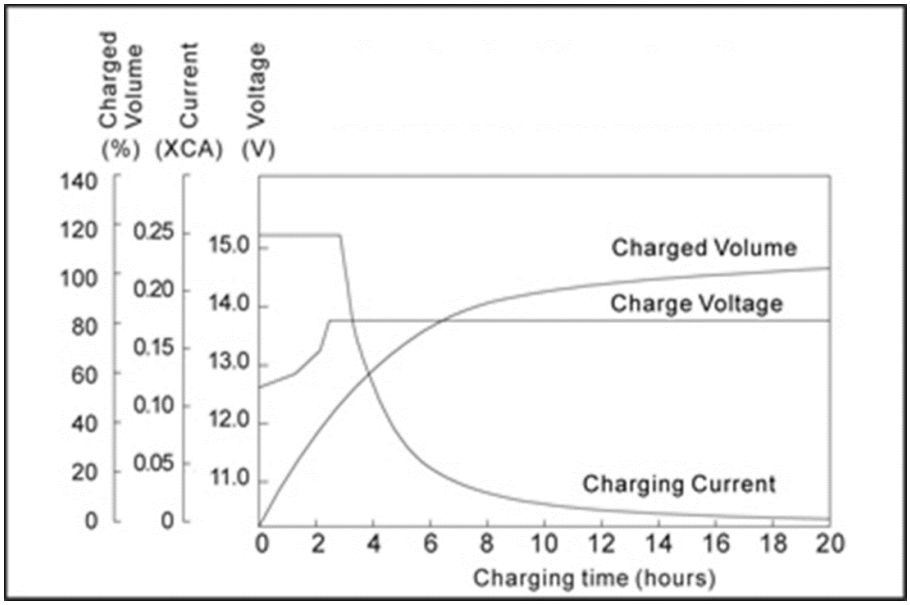

Figure 1.5 Characteristic curves of lead-acid battery charge at constant current at 25°C [3].

In this figure we can see that there are two different steps of the battery charge: the first one is carried out at a constant current until the voltage reaches a value equal to 2.3 ÷ 2.45 V per cell. The second step is carried out at a constant voltage equal to 2.3 ÷ 2.45 V per cell until the complete charge of the battery's capacity. The figure 1.5 also shows an increase in the charged volume of the lead-acid battery.

1.2.2 State of rest

During the state of rest, the battery slowly loses a portion of the charge. This phenomenon can be monitored controlling the density of the electrolyte because its decrease occurs. This self-discharge, due to *local actions*, is proportional to the electrode surface and it is due to the main following causes:

a) The active portions of the plates, in contact with inactive portions, form galvanic couples causing continue internal discharges.
b) The electrolyte density is not constant between the bottom and the top of the plate. In particular, from the bottom to the top the electrolyte density decreases; as a consequence at the bottom of the plates the voltage is little higher than the top. A galvanic macro-couple is then formed between the two parts which tends to charge (self-charge) the lower part and discharge (self-discharge) the upper part.
c) The imperfections of isolation cause dispersion current, that, especially in stacks of batteries connected in series, can assume high values.

To overcome the self-discharge during stop period, a maintaining charge, to compensate the internal losses, is used to keep the Stationaries batteries in full charge state in order to guarantee their good conservation. The maintaining charge is defined as the minimum current needed to one element to maintain the electrolyte density at constant value; if it is too high we have gas production, if it is too low the battery slowly discharge itself.

Another solution consists to maintain the voltage battery between 2.2 ÷ 2.3V for each element with an appropriate charge device.

1.2.3 Discharge regime

At the initial of discharge a voltage drop occurs, attributable to the battery chemical resistance and to the fast decreasing of the acid concentration into the plate pores. This fast voltage drop is frequently followed by a fast voltage increase (coupe de fouet). This effect is not always present, in some cases it is present during the first discharge phase, especially if the battery was stored discharge for many days. After the initial behaviour, the voltage slowly decreases to about 1.8V. In the final part of the discharge, the curve more rapidly drops, this point is known as *curve's knee* and it indicates the proximity of full-discharge. The figure 1.6 shows a typical discharge curve of lead-acid battery.

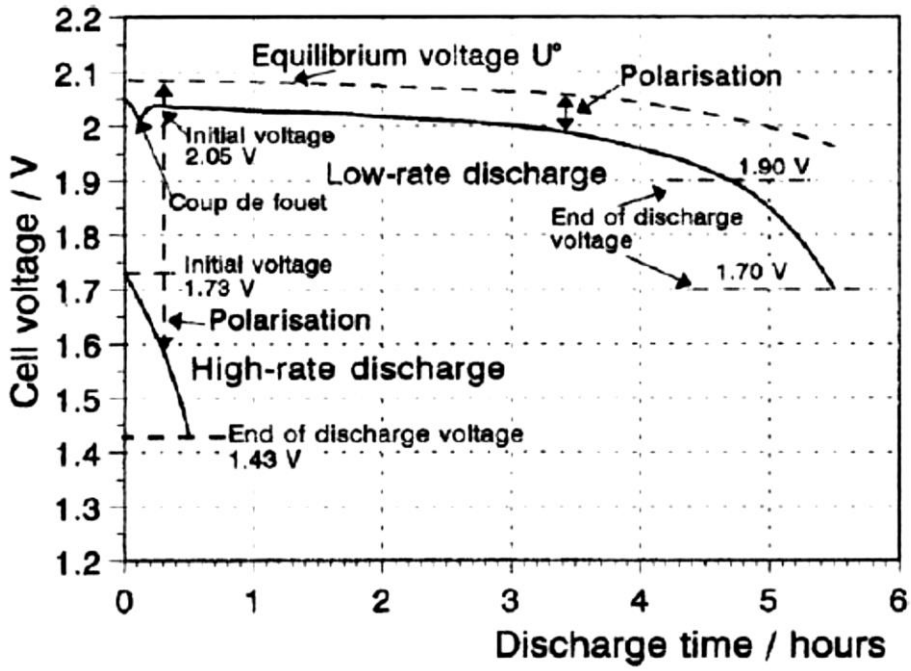

Figure 1.6 Typical discharge curve of lead-acid battery [4].

The average voltage value during discharge is important to determine the energy delivered from the battery. The average value depends on discharge value, type of

battery and also final voltage. The temperature slowly increases during discharge, due to the *reversible heat*, Joule effect, that depends only from the square value of the current density. The specific weight of electrolyte changes quasi linearly during the discharge, thus the measure of this parameter is a good method to know the battery state of charge [2].

The voltage value, during discharge, essentially depends from the electrolyte density into the pores plate. The discharge regime determines the battery behaviour. In fact, if the discharge is slow, all active material can react (superficial and inside the plate pores) obtaining higher discharge capacity. On the contrary, for fast charge, the superficial plate portions react first, leading to the formation of the lead sulphate. The consequent increase of the volume, causes the obstruction of the porosities, hindering the reaction of the actives internal portions, thus the discharge capacity decreases. The figure 1.7 shows the typical curves of discharge and charge of the lead-acid battery.

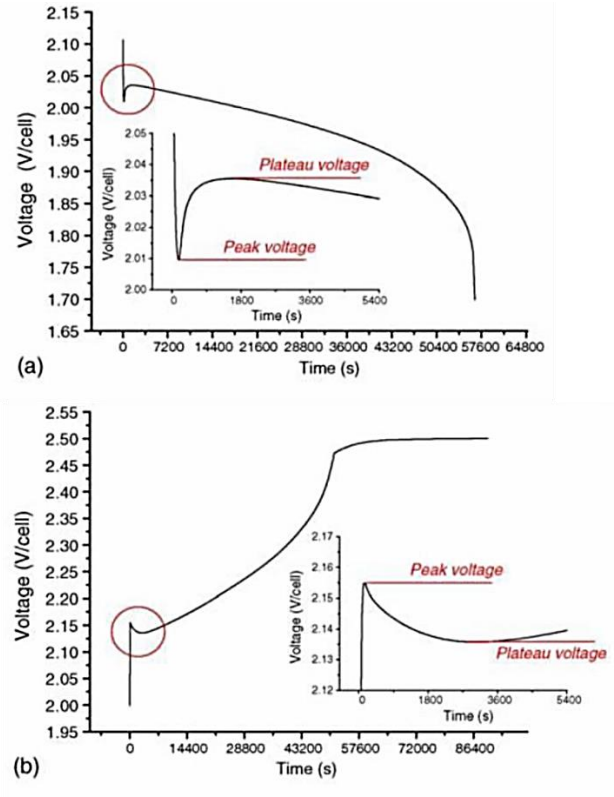

Figure 1.7 Typical curves of discharge (a) and charge (b) of lead-acid battery.

1.2.4 Electrode sulfation

The discharge processes in a lead-acid battery lead to the formation of the lead sulfate ($PbSO_4$) that was re-converted on lead and lead oxide during the charge with restoration of the initial sulfuric acid density (H_2SO_4). After numerous discharge processes, the lead sulphate tends to crystallize, forming a compact, solid structure, making difficult the re-conversion of the active paste of the electrodes. This process is known as *sulfation*, and if a large part of the active electrode paste is involved, the battery is irreversibly damaged. The causes of the electrodes sulfation are multiple, but the main cause is the stay of the battery in a partial state of discharge. Then to guarantee a long life of the lead-acid battery it is necessary to avoid its stay in a partial state of discharge for a long time. The temperature increases the sulfation phenomena. The batteries with liquid electrolyte are more affected by this problem.

1.2.5 Efficiency of lead-acid batteries

The capacity of an electrochemical cell to store energy depends on the quantity of the active paste in the electrodes in real contact with electrolyte. The electrodes with a porous surface have very high electrochemical active area than another one with a compact and dense surface. However, the porous electrodes have less mechanical and structural resistance, and they are not able to bear deep discharge cycles. On the contrary, the thick and compact electrodes, are not able to acquire/release strong currents, but guarantee high life cycle and can reach a depth of discharge around 80% of the nominal capacity. From an electrochemical point of view, assuming a maximum theoretical efficiency, it is possible to calculate the theoretical ratio between storable energy and weight, in the figure 1.8 are reported the value of the ratio Energy/Weight for different type of lead-acid batteries . The theoretical value of this ratio is 160 Wh/kg for each element and in the commercial batteries the value of this ratio is between 25÷50 Wh/kg [3].

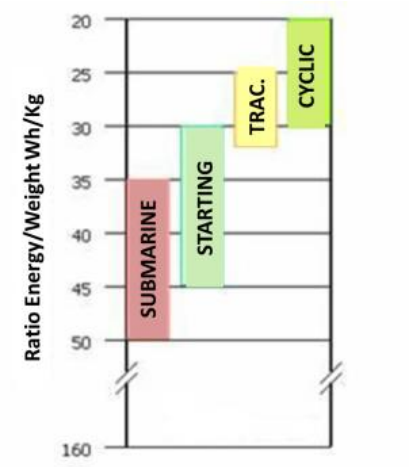

Figure 1.8 Ratio Energy/Weight for different type of lead-acid batteries [5].

1.2.6 Comparison with other types of secondary batteries

To compare the different types of battery (in table1.2 the characteristics of some secondary batteries were reported) at their performances, it is necessary to study the *Ragone Plot* (figure 1.9). This plot shows the specific energy as a function of the specific power (the last one is generally represented on a logarithmic scale) of the different devices.

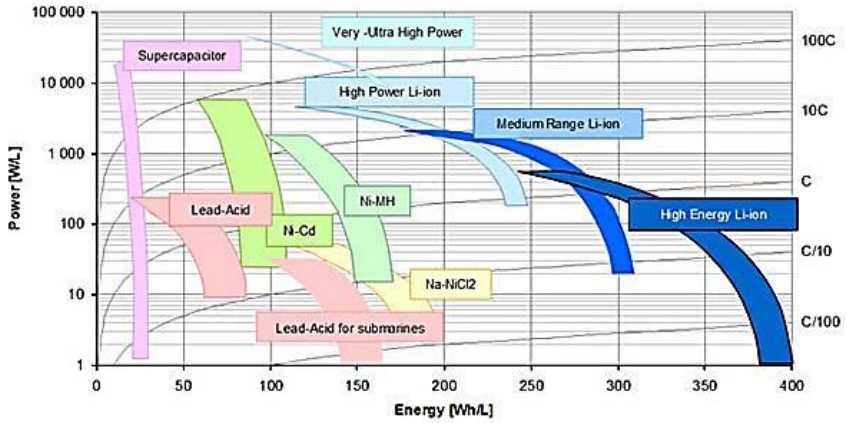

Figure 1.9 Ragone plot [6].

	Lead Acid	Nickel Cadmium	Nickel Metal Hydride	Lithium Cobalt	Lithium Manganese	Lithium Iron Phosphate
Capacity	0.5	1.2	1.8	2.6->2.9AH	2.2-2.45AH	1.3-1.6AH
Voltage	2V	1.2V	1.2V	3.7V	3.7V	3.V
Energy Density(W/Kg)	35	45	70	167	110	100
Cycle Life	400	500	500	>500	>500	>1000
Life (Yrs) @ one charge/day	1	2	2	2	2	3
Charging Time	8 hrs	1.5 hrs	4 hrs	2-4 hrs	2-4 hrs	1-2 hrs
Self Discharge Rate (%/mo)	20%	30%	35%	10%	10%	8%
Safety	Good	Good	Good	Poor	Average	Good
High Temp Performance	Good	Good	Good	Average	Poor	Good
Cold Temp (0°F) Charge	Good	Fair	Fair	Fails	Fails	Fails
Cold Temp (0°F) Discharge	Good	Good	Poor	Poor	Good	Good

Table 1.2 Technical characteristics of some secondary batteries [7].

1.2.7 Performance of lead-acid batteries at different temperature

The lead-acid batteries are still used today in multiple applications and this means that they must work in different operating temperatures. The lead-acid batteries achieved an excellent efficiency under high temperatures for kinetics reason, but in these conditions their life cycle decreases [4]. A battery for stationary applications is used for 10 years if it works at 25 °C, only for 5 years if continuously exposed to 33 °C and only 30 months if it constantly works at 41°C. Instead, at low temperature, the electrolyte becomes viscous retarding the sulfation, but the efficiency of the battery decreases. Moreover, the low temperature leads to freezing of the electrolyte that can cause the crack of the case and damage the plates. For the batteries that have to work at low temperatures an electrolyte with a specific gravity between 1.3 g/cm^3 and 1.36 g/cm^3 must be used. Figure 1.10 shows the effect of the temperature and the specific gravity of the electrolyte on the state of charge of the battery.

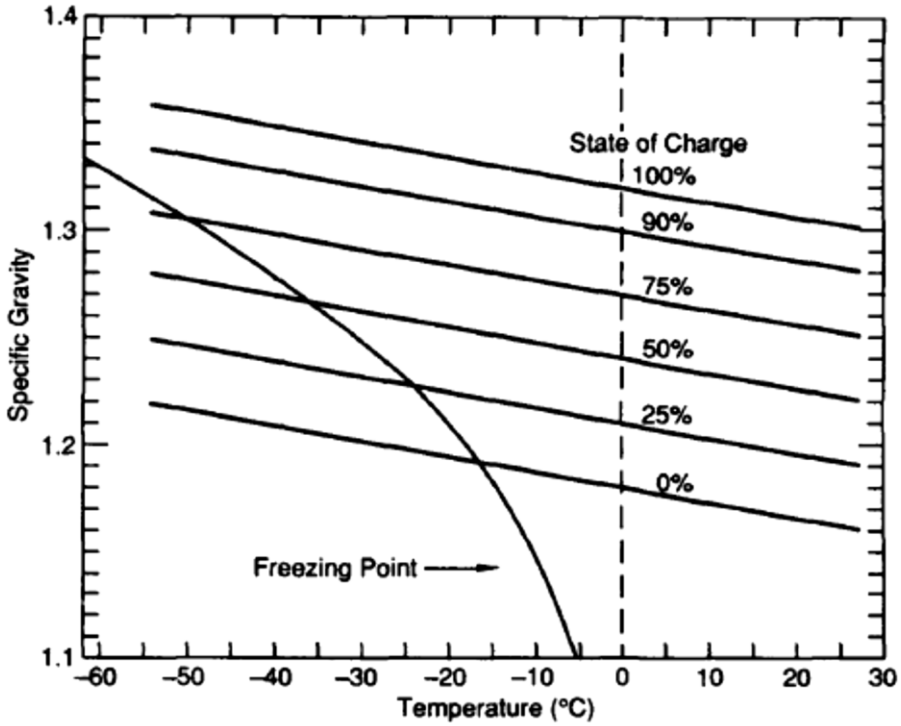

Figure 1.10 Effect of temperature and the specific gravity of electrolyte on the state of charge of battery [8].

1.3 Types of lead-acid batteries

There are different types of lead-acid batteries, as the figure 1.8 shows, each used for specific applications. They are classified on the basis of construction technology and they can be divided into:

- *Cyclical batteries;*
- *Starter batteries;*
- *Traction batteries.*

They are distinguished from the quantity of material with which electrodes are made and the concentration of the electrolyte; the energy density of all these types of batteries varies between 25Wh/kg and 50Wh/kg.

1.3.1 Cyclical batteries

This type of battery is intended for typically cyclic use, such as that required for use as an alternative energy source, where the electrical network is not available or cannot be used. Depending on the use made of it, they can be classified into two different families:

- *Stationary cyclic batteries;*
- *Portable cyclic batteries.*

The *Stationary cyclic batteries* are generally used for static use in large backup systems for telecommunication systems, computing, automation and control centres [3]. For reasons attributable both to logistical problems (spaces) and to problems related to safety standards, for these applications are exclusively using the sealed batteries with electrolyte-gel (SVR and AGM).

The *Portable cyclic batteries* are designed to withstand a high number of discharge cycles, but generally they have much smaller capacities; they find their main use in the supply of the portable devices (equipment, measuring instruments, power tools, etc.). The capacities are in the range between 1 A/h and 20 A/h and they are made with immobilized electrolyte (gel) in hermetic version.

For cyclic batteries, the capacity/weight ratio is generally unfavourable and averages between 20 and 30 Wh/kg. When choosing a cyclic battery, an important factor is the correct evaluation of the "life cycle" parameter (number of discharge and recharge cycles that the battery can withstand), which must always be expressed with reference to the relative percentage and to the depth of discharge. Therefore, in the comparison between two different cyclic batteries, it is important to check that the data relating to the life cycle refer to the same percentage of discharge.

1.3.2 Starter batteries

For the automotive batteries six lead-acid cells are connected in series, to have a total voltage equal to 12.7V. The ability to start the engine is given by the discharge current I, expressed in amperes (A) and established by the manufacturer. This value corresponds to that the battery can supply at a temperature equal to -18 °C for a fixed duration, before reaching a certain minimum voltage. The aptitude for starting is the most important characteristic of the battery, given that it performs its primary function. When sizing, it must be taken into account that it must guarantee start-up even in the most adverse conditions; in fact, when the outside temperature decreases, the battery greatly reduces its ability to start, as shown in the figure 1.11.

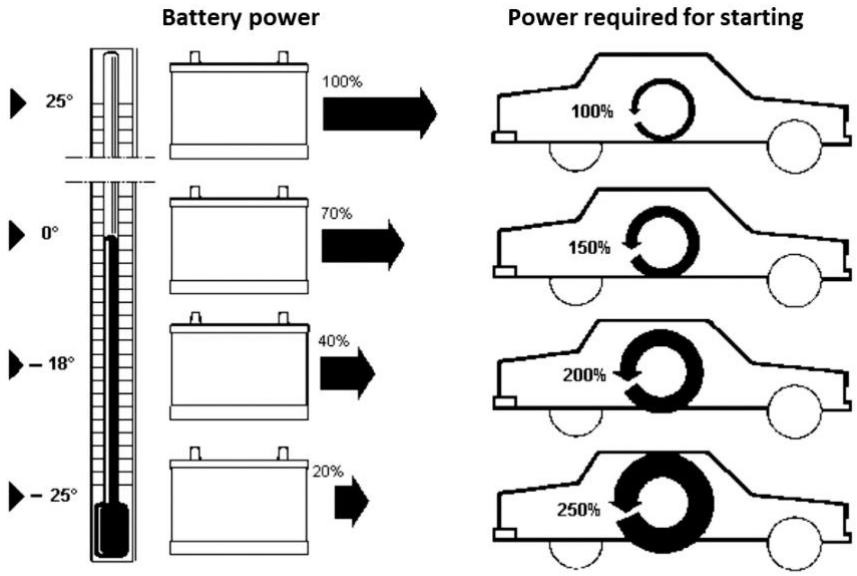

Figure 1.11 Starting ability at different temperatures.

The starter batteries are designed to deliver high current spikes in very short periods of time (in the order of seconds) [7]. They are used in the automotive sector for starting engines and have a variable capacity between 20 Ah and 100 Ah. In order to supply such high currents, these batteries have a very low internal resistance, of the order of 0.002 Ω per cell. To make this resistance so small, numerous lead plates have been added inside the battery, made to be thin and

with pores similar to sponges, so as to maximize the contact surface with the electrolyte. These batteries cannot be used in applications that require numerous discharge cycles, since the discharge cannot exceed 30-40% of the nominal capacity since the lifespan would be significantly reduced, since sulfation phenomena occur in these cases to the electrodes. These accumulators have an energy density between 30-45 Wh/kg.

1.3.3 Traction batteries

This type of accumulator is used for powering electric vehicles. These batteries are designed to deliver a high average of current for long periods of time and suitable for tolerating various discharge cycles. These accumulators have high capacities, between 200-800 Ah, and have lower energy densities than starter batteries, of the order of 25-32 Wh/kg. These batteries are made with thicker internal plates than those of starter batteries in order to allow tolerance to the numerous discharge cycles. One of the aspects that plays a fundamental role in the design of these batteries is the temperature. The figure 1.12 shows the power and energy performance of modern traction batteries.

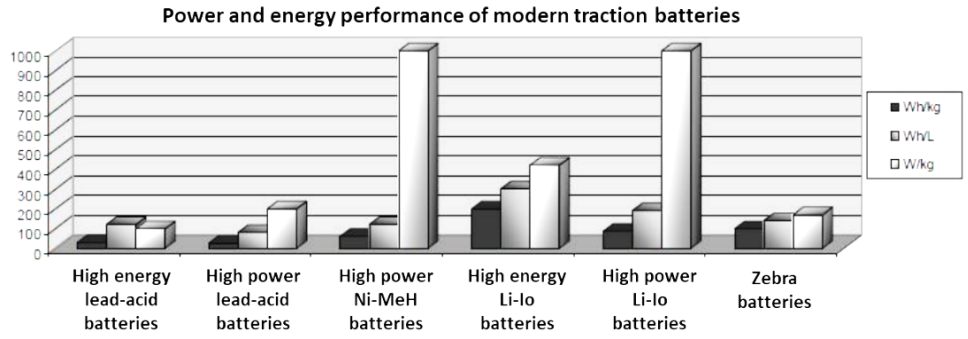

Figure 1.12 Power and energy performance of modern traction batteries.

In the field of the electric traction the lead-acid batteries most used are:

- *Sealed lead batteries*: the electrolyte is immobilized in various ways inside the container, made hermetic (sealed) so as to allow the recombination of the hydrogen and the oxygen during the charging

phase. In this way the refilling operation is not necessary. These accumulators release minimal amounts of hydrogen and corrosive substances and offer greater guarantees of safety.

- *Gel batteries*: essentially the idea is to hold the acid in a special gel. In contrast to the conventional batteries, this arrangement almost completely prevents the emission of hydrogen and oxygen during the charge. The oxygen is widely consumed within the gel by the hydrogen atoms with which it recombines. The gelled electrolyte was obtained by using the silica gel. The main advantage of these batteries is that it is absolutely impossible the release of the acid even if the case is broken. They are sealed and do not require any type of maintenance. However, they have some disadvantages: the main one is that they must be charged with lower currents and voltages than the other batteries, otherwise gas bubbles could form inside the gelled electrolyte causing its damaged.

- *AGM (VRLA)*: in this type of sealed batteries the electrolyte is absorbed in the AGM (Absorbed Glass Mat, or a very fine glass fibre consisting of boron-silicon soaked in acid - aqueous solution of sulfuric acid) that acts also as separator. These accumulators are very safe as they guarantee the non-leakage of the acid even if broken. Almost all AGM batteries are also VRLA (Valve Regulated Lead Acid) type. These batteries have a small valve that keeps a slight positive pressure inside the accumulator compared to the external environment (atmosphere). Therefore, these batteries are slightly under pressure. This type of technology has all the advantages of gel batteries, but without presenting their limits since they can withstand the more sustained high charge currents. This type of lead accumulator is the most suitable for use on the electric propulsion vehicles.

1.4 Improvements in the lead-acid batteries performances

The lead-acid batteries have many advantages:

- Low cost;

- Recyclable to 95%;
- Easy to make in large volume productions;
- Large variety of capacities (from 1Ah to much hundred of Ah), dimensions and forms;
- Usable in a temperature range between -40°C and 60°C;
- Voltage per single cell more than 2V.

However, the lead-acid batteries have also many disadvantages:

- Low life (around 500 cycles with complete discharge);
- Low energy density (30 40 Wh/kg);
- Sulfation phenomena that damage the battery if it is left in discharge conditions;
- The grids contain some additives as antimony or arsenic, that are dangerous for the health;
- Difficult to create in small dimensions;
- The short circuit currents cause irreversible damages.

In the last years, researchers have done many studies to improve the lead-acid battery's performance, these studies are looking to increase the life of batteries and the energy density and decrease the sulfation phenomena.

1.4.1 Effects of additives in the positive plate

The main problem of conventional negative plates is the irreversible sulfation of electrodes caused to deep discharge regimes. The problem is principally due to the not uniform distribution of $PbSO_4$, that hinders the recharge process, promoting the H_2 development. One the method to limit this phenomenon is the addition of some additives to the negative paste of lead-acid batteries.

- ***Carbon***

The addition of carbon to the negative active mass causes a delay in the phenomenon of irreversible sulfation thanks to the steric impediment provided by the carbon to the formation of a compact layer of lead sulfate. Thus, the addition

of carbon leads to an increase of the electrode capacity and to hinder the growth of sulfate crystals [8].

- ***Glass fibres***

The active negative mass of lead-acid batteries has a low specific surface and during the PSoC (partial state of charge) regime has a low charge acceptance; furthermore there is a progressive and irreversible sulfation of negative plates. To overcome this problem, Valenciano et al. [10], used in the negative plates expanded graphite, layers of graphite and glass fibres as additive (1.5% for each one). The utilization of active mass is more uniform and the degradation mechanisms of the negative electrode surface, during PSoC regime, are inhibited. The results show more uniform utilization of the active mass and less degradation mechanism of the surface structure of the negative active mass during PSoC regime and that means an increase of negative electrode cycle life.

- ***Surfactants***

The utilization of surfactants as an electrolyte additive improves the battery capacity. The phosphonate surfactants have to be chemically, thermally and electrochemically stable in high corrosive environments. In a study [11], the phosphonate surfactants used as additives are a mixture of Alkyl Phosphonate and Poly Karboksylsyre Copolymer. The results showed that these polymers improve the electrochemical behaviour of negative electrode. In fact, the addition of surfactants in the H_2SO_4 solution decreases the electrode resistance, confirming the formation of a small amount of $PbSO_4$ on the electrode. The presence of surfactants influences the capacity of the electrode, due to the adsorption of the surfactant on the Pb electrode, causing a change in the morphology of the PbO_2 and $PbSO_4$ crystals on the electrode surface; moreover, as already stated above, the corrosion rate of lead electrodes decrease in the presence of surfactants.

- ***Graphene and Carbon Nanotubes***

Many studies suggest that the addition of graphene to the negative mass may decrease the charge cut-off voltage, increase the discharge cut-off voltage and improve the cyclic life of the VRLA batteries during cycles in a partial state of charge. The best electrochemical performance could be attributed to the inhibiting effect of graphene on the growth of lead sulfate [12]. Also the Carbon Nanotubes

(dCNT) are used as additive in the negative plate of lead-acid batteries. The batteries with CNT show a small variation of the Reserve Capacity, a better Cold Cranking, a greater charge acceptance, and a greater overall efficiency of the system. The tests show an increase in the number of cycles by 60% when the dCNTs are incorporated in the negative electrode (HRPSoC and SBA tests) and reach values up to 500% if they are incorporated in both electrodes (SBA test), with a reduction in the water loss per cycle greater than 20% [13]. A further development of this research was obtained in another work in which multiple-walled carbon nanotubes (MWCNTs) were used as a conductive additive to the negative active mass (NAM) [14]. These MWCNTs added to the negative electrode, allow to obtain a high capacity, excellent cycling at C/10, in a partial state of charge (HRPSoC) and at various discharge speeds. With these additives the irreversible lead sulfate on NAM is significantly reduced, the use of the active material is increased and the performance of the electrode is improved. The capacity improvement and cyclic performance of the cell are attributed to the nanometric size of the MWCNTs used as additives. The MWCNTs allow to improve the electrochemical properties of the NAM. They act first as an ideal conductive support for the transport of electrons and, secondarily, they stabilize the structure of the electrode with a good electrical contact between the particles of lead sulphate and the spongy lead during the process of charge/discharge. The nanostructured additive increases the electrical conductivity of the active mass, therefore the electrochemical performances of lead-acid batteries with MWCNTs are higher than those of batteries that use conventional carbon black (CB) in the same quantity.

1.4.2 Nanostructured PbO_2

The lead oxide nanostructured electrodes can be a good alternative to conventional pasted electrodes, thanks to their high surface area (about 70 times higher than the geometrical one) that implies a high specific energy batteries. The fabrication process of nanostructured PbO_2 electrode consists in two phases:

1. Electrodeposition of current collector
2. Electrodeposition of nanowires

The details of this fabrication process are largely described in the article "*Growth and Electrochemical Performance of Lead and Lead Oxide Nanowire Arrays as Electrodes for Lead-Acid Batteries*" [6]. These new types of electrodes are able to work at very high C-rate without being damaged. In particular, after an initial stabilization (around 100 cycles of charge/discharge), a specific capacity of about 200 mAh g^{-1}, very close to the theoretical one of 224 mAh g^{-1}, was drained for more than 1000 cycles at a C-rate higher than 1C with an efficiency around 90%. This behaviour of PbO_2 nanostructured electrodes is very different from the conventional ones with pasted active material. In addition, the discharge curves maintain a quasi-constant voltage of about 2.1 V, without reaching the cut-off potential also at the high C-rate. This implies a quasi-constant energy drained during fast discharge [19]. The PbO_2 nanowires were obtained by template electrodeposition in polycarbonate membranes and tested as positive electrode for lead-acid battery, using as counter electrode a negative commercial plate. The current collector is electrodeposited on the one side of the polycarbonate membrane and the nanowires in the other side. The last one were grown into the channels of the polycarbonate membrane and supported by current collector. The current collector and the nanowires are constituted of the same material to avoid loss of charge due to galvanic contact.. The nanostructured lead oxide electrodes were assembled in a zero-gap configuration using commercial separator. The electrochemical cell was tested in a 5M H_2SO_4 aqueous electrolyte by galvanostatic charge/discharge cycles [20].

1.4.3 Scope of the thesis

The scope of this PhD thesis was focused in the substitution of commercial plates of a lead - acid battery with the nanostructured electrodes to demonstrate the increase of lead-acid battery performances that use the last type of electrodes. Before this work, there have never been any papers presented in the literature concerning tests on lead-acid batteries having both nanostructured electrodes. In particular my PhD work was divided in two parts, the first one was focused on fabrication, characterization and testing of the Pb nanostructured electrodes and the second one consisted in the testing of lead-acid batteries with both nanostructured electrodes. The test of Pb NWs electrode was fundamental to establish its effective performance, the same work that the laboratory was before

carried out on PbO_2 NWs electrodes. After the Pb NWs electrode tests in different conditions, we carried out the same tests on a lead-acid battery with both nanostructured electrodes and how it is possible to see in the following chapters the performances of nanostructured lead-acid batteries are incomparable with the performances of commercial lead-acid batteries in terms of efficiency and charge and discharge rate.

Chapter 2

Fabrication and characterization of nanostructured lead electrodes

Porosity of the active material is of fundamental importance to guarantee a good diffusion of electrolyte and to obtain a high utilization of the active material, which results in a high Drainable energy from the battery itself. As reported by Fleming [21], although porous electrodes have the enormous advantage of providing a very high surface area, it is also necessary to consider the problems related to the distribution of current, in turn related to the distribution of the pores and their interconnections.

2.1 Negative active material (NAM) preparation

In figure 2.1, a scheme of the preparation of negative plates is shown. For negative plates the precursor of the active material is tribasic lead, fibres and the expanders ($BaSO_4$, lignosulfonates and carbon additives) are mixed with water, then the leady oxide is added and the suspension is mixed again. After this the sulfuric acid (density 1.4 g cm^{-3}) is added slowly, to avoid overheating of the paste, until 3BS crystals are formed, in addition, a cooling system is provided during the process to keep the temperature below 50 °C. This last mixing phase is the most important, because the formation and growth of 3BS occur. The expanders are used to avoid the formation of a continuous layer of $PbSO_4$, that would cause a decrease of electrode capacity until the break. The pastes for positive and negative plates are prepared in separate mixers to avoid contamination of the positive paste with $BaSO_4$ and expanders from the negative paste. The negative electrode with high capacity has a porous mass with active surface of about $0.4 \div 0.8$ m^2g^{-1}.

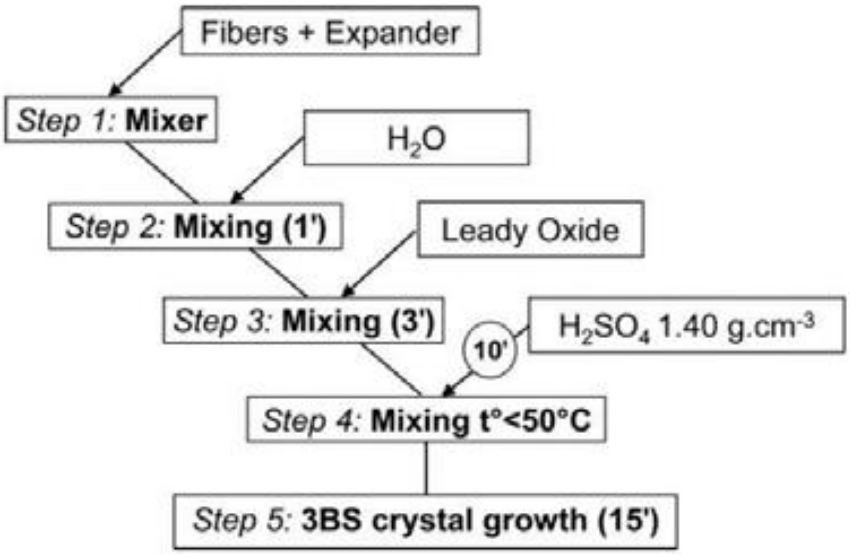

Figure 2.1 Preparation of 3BS pastes for negative plates [9].

The figure 2.2 Scheme of the technological procedures for paste preparation and grid pasting [22].

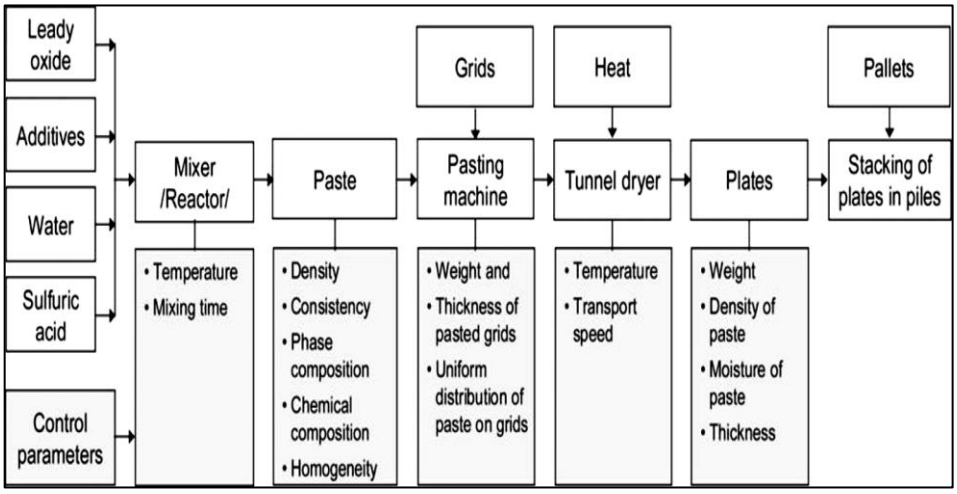

Figure 2.2 Technological scheme for paste preparation and grid pasting [9].

2.2 Lead nanowire electrode

In order to improve the performances of lead-acid batteries it is possible to replace the current commercial plates with nanostructured electrodes. Nanostructured lead electrodes have a high surface area and a better utilization of active material, thanks to the better diffusion of SO_4^{2-} ions into the active material and then they are able to store more specific energy. Furthermore, the fabrication of nanostructured electrodes allows for a simplification of the production process, reducing its costs. The method, used to obtain the Pb nanostructured electrode, is a template electrodeposition and it consists in two phases:

1) Current collector electrodeposition
2) Pb NWs electrodeposition.

The polycarbonate membrane, used as a template for the electrodeposition, is a polymeric film with pores interconnected each other and not parallels. The nanometric dimensions of the membrane pores have made possible the electrodeposition of Pb nanowires and therefore the formation of a nanoelectrode whose morphology depends precisely on the properties of the membrane used as a template. In the figure 2.3 are reported the main steps of electrodeposition process.

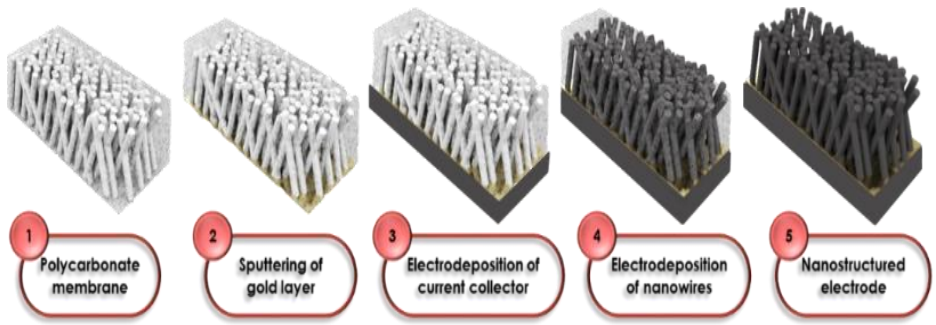

Figure 2.3 Electrodeposition process.

The fabrication process of Pb NWs electrode was studied and optimized during the years in the Applied Chemical-Physical Laboratory and it is largely discussed in the article "*Growth and Electrochemical Performance of Lead and Lead Oxide Nanowire Arrays as Electrodes for Lead-Acid Batteries*" [6].

2.2.1 Polycarbonate membrane

The Whatman polycarbonate membrane, used as a template for the fabrication of nanostructured electrodes, has pores with a nominal diameter equal to 200 nm, an average thickness of about 15μm, pore density of 10^{11} pores per m^2 and porosity of 15-20%. These membranes are produced from polycarbonate films using the track-etch method and usually they are used in micro-nanofiltration processes. The membrane morphology was analysed by electron microscope and the figure 2.4 shows the images of the typical interconnections of this type of membrane.

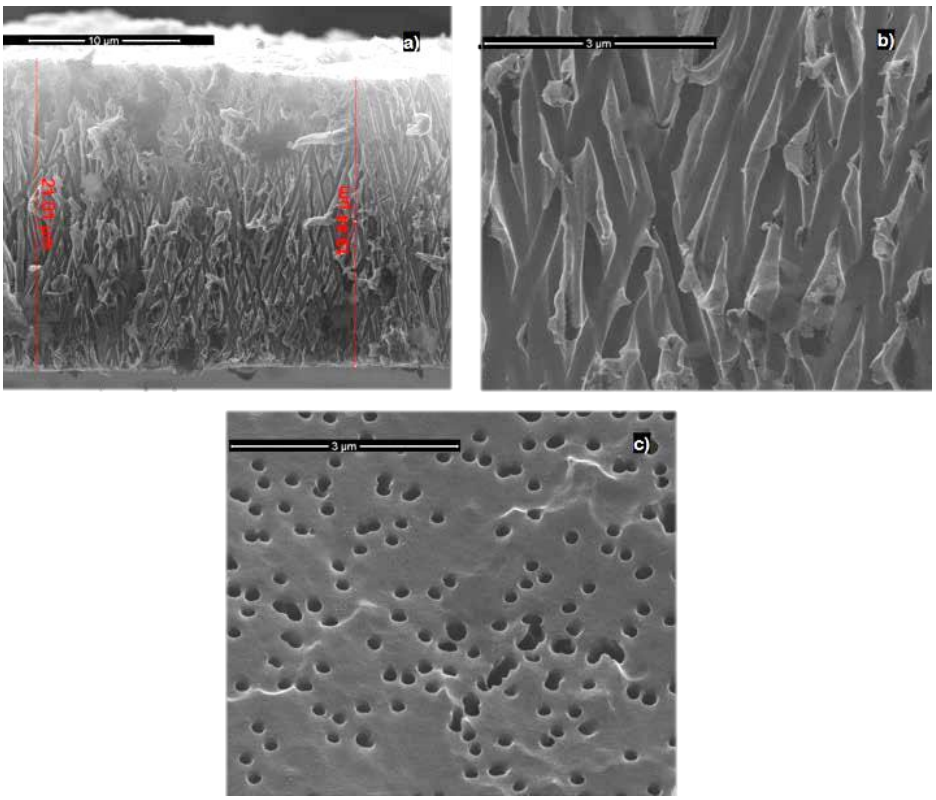

Figure 2.4 Micrographs of a PC membrane, a) and b) cross section at different magnifications and c) viewed from the top [4].

The polycarbonate membrane has a uniform porous capillary structure with a high distribution of pores. The polycarbonate membranes are hydrophilic and they are available in different dimensions. The main characteristics of the

polycarbonate membrane are reported in the table 2.1. The membranes used for this research activity have the following characteristics:

- Average diameter of pores: 200 nm;
- Average thickness: 15 μm;
- Pore density: 10^{11} pores/m^2;
- Porosity: 15%.

The main advantages in using a polycarbonate membrane are:

- This membrane is easy to remove by chemical dissolution in dichloromethane without damaging the nanostructures;
- The polycarbonate is able to be recovered, after membrane dissolution, using a batch distillation [23].

Characteristics of polycarbonate membrane	
Thickness	7 – 20 μm
Weight	from 0.7 to 2.0 mg/cm^2
Maximum temperature	140°C
Porosity (vacuum volume)	4 – 20%
Pore density	10^5 - 6*10^8 pores/cm^2
Opacity	Translucent
Density	1.21 g/cm^2
Flammability	Low flammable
Compliance	Neglectable
Biological compatibility	Inert

Table 2.1 Main characteristics of polycarbonate membrane.

2.2.2 Fabrication process of lead nanowire electrode

The process used to manufacture the nanostructured lead electrodes is the template electrodeposition. Before current collector electrodeposition, a thin layer of gold was sputtered on one side of the membrane, for making it electrically conductive. After sputtering, a compact layer of lead was electrodeposited on the gold film. This layer has two different aims: mechanical support for nanostructures and electrical connection between them and the power supply, furthermore, it is of the same material of nanostructures to avoid self-discharge effects. For lead electrodeposition was used a solution with a proper composition of tetrafluoroboric acid (H_3BO_3) and lignin sulfonate ($C_{20}H_{26}O_{10}S_2$), to avoid the dendritic growth of lead, in fact these compounds are complexing agents of lead ion. In particular the solution contains 4.5 g L^{-1} lignin sulfonate, 15 g L^{-1} H_3BO_3, 35.2 g L^{-1} HBF_4, and 40.5 g L^{-1} $Pb(BF_4)_2$. The electrochemical cell was assembled with a Pt mesh as a counter electrode and powered by a pulsed rectangular current (duty cycle = 0.952) supplied by a PAR Potentiostat/Galvanostat (mod. PARSTAT 2273). The deposition of current collector was carried out applying a cathodic current density equal to -10 mA/cm^2 for 5 s, followed by an anodic current density, equal to 1 mA/cm^2 for 0.25 s, that prevents the dendritic growth of lead and promotes the formation of a compact Pb layer. Deposition was carried out in three identical steps of 960 s each and at the end of every step, the solution was replaced with a fresh one, avoiding any relevant modification of the precursor concentration. The figure 2.5 shows an interval of the rectangular current pulses powering the electrochemical cell together with the voltage response, which was changing with the advancement of the deposition process, as shown by comparing figures 2.5 a) - c). It can be observed that the voltage remains constant at about −2.25 V during the first stage of deposition, while shows an increasing trend to −2.19 V during the successive two steps. During the first stage, lead is deposited on gold, whose coverage is completely likely at the end of this stage. In the successive stages, deposition of lead on lead occurs. This probably is the reason of the slightly higher voltage during the first stage (−2.5 V) because the deposition of lead on gold is kinetically more difficult than deposition of lead on lead where there is not crystal lattice mismatching. The increasing trend of the voltage in figures 2.5 b and c can be attributed to the onset of concentration polarization which is removed during the current inversion.

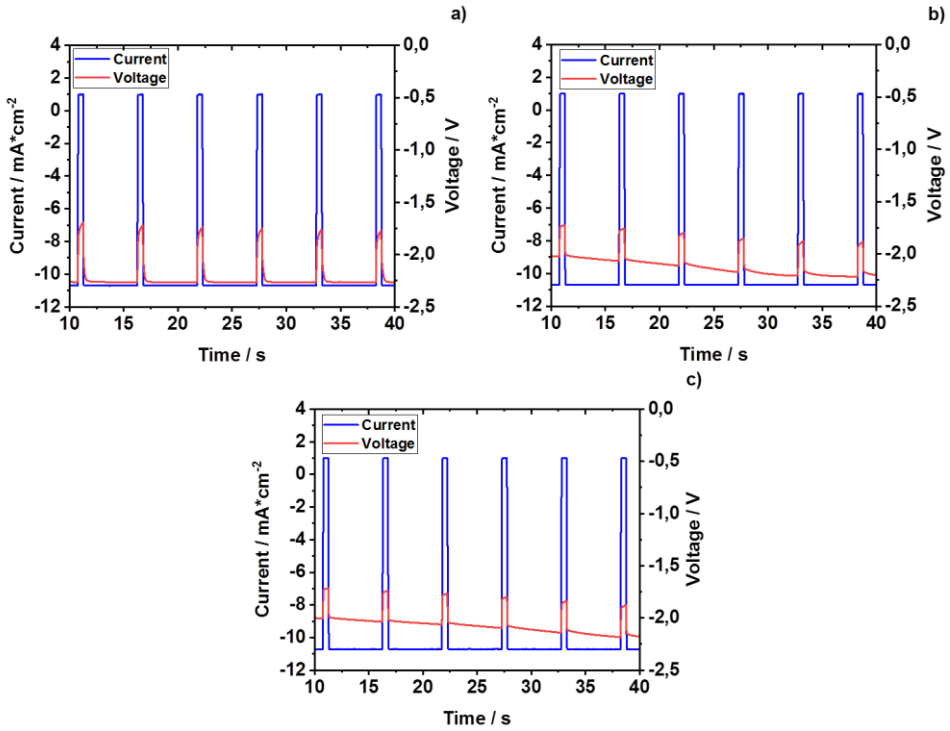

Figure 2.5 Rectangular current pulses, with relative voltage response, powering the electrochemical cell for depositing a lead layer on sputtered gold film covering one side of the template. a) step1, b) step 2, c) step 3.

The substitution of the solution, after each step, was due to eliminate any risk of dendrite or acicular deposit formation that are favoured by decreasing lead concentration. In these conditions we obtained a compact layer of Pb with a thickness of 30 µm. The figure 2.6 shows the SEM image of a transverse section of Pb current collector. From this image we can see that the current collector, obtained by electrochemical deposition, is compact. The deposition of lead nanostructures was carried out in identical conditions of the current collector deposition. In particular, the nature and composition of solution were identical and the current pulse shape was rectangular with a duty cycle equal to 0.91. Also in this case we used a Pt mesh as counter electrode and we applied a pulsed current with the same Potentiostat/Galvanstat used for current collector electrodeposition. The figure 2.7 shows an interval of the NWs deposition.

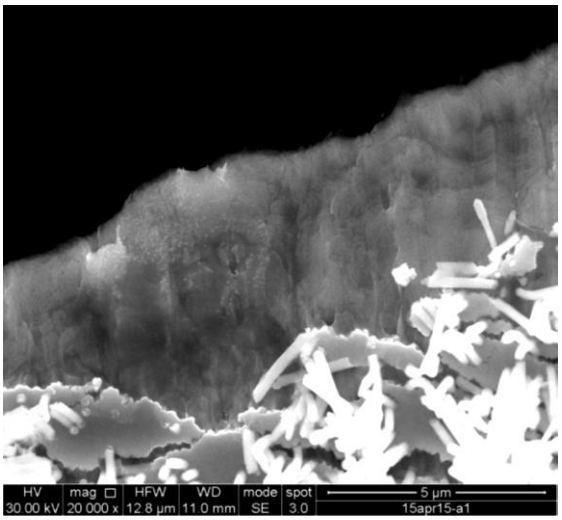

Figure 2.6 SEM image of transverse section of Pb current collector.

The NWs growth was carried out in a single step with a total duration of 450 s and the nanostructures were obtained with a length about of 10 µm.

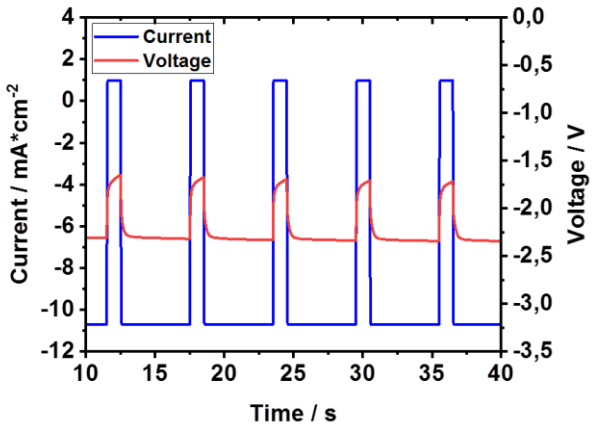

Figure 2.7 Rectangular current pulses with relative voltage response of nanostructures deposition.

In this phase, there is the prevalent polarization in the initial instants of the cathodic pulse, likely due to the combined effects of ohmic drop and concentration overpotential in a confined ambient such as nanosized template

channels. Also here the concentration overpotential was removed on the current inversion. After synthesis and dissolution of the template the nanostructures were characterized. The dissolution of the template is a very critical step and it must be conducted with care for avoiding collapse of the deposited Pb NWs with consequent uselessness of the electrode. This operation of dissolution was carried out in successive steps for complete removal of the polycarbonate. A Field Emission Gun Environmental Scanning Electron Microscope (FEI Quanta 200 FEG-ESEM) was employed for morphological analysis while solid-state characterization was performed through a RIGAKU Xray diffractometer (model: D-MAX 25600 HK). X-ray diffraction patterns were obtained in the 2θ range from 10° to 100° with a sampling width of 0.004° and a scan speed of 3 deg/min, using Ni-filtered Cu Kα radiation (λ=1.54 Å). The diffraction peaks were identified by comparison with ICDD database (International Centre for Diffraction Data 2007). The morphology of the as-prepared lead nanostructures was first investigated by LSM (Laser Scanning Microscope) analysis and then a more detailed analysis was performed using SEM (Scanning Electron Microscope). In figure 2.8 a) - c) we can see the images of LSM analysis.

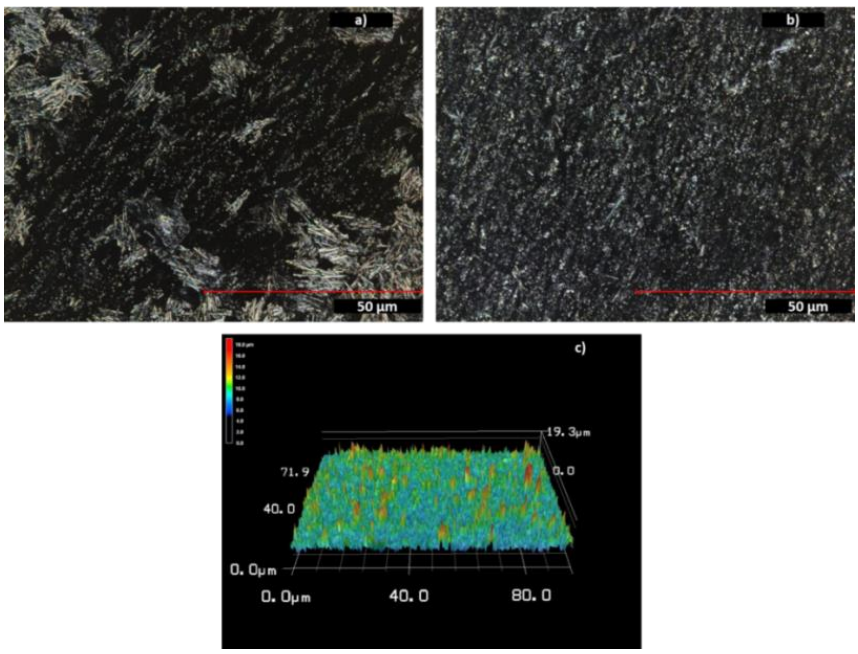

Figure 2.8 LSM images of the Pb electrode after dissolution of the membrane: a) wisps of Pb NWs; b) top view of Pb NWs electrode; c) 3D image of Pb NWs electrode.

The figure 2.9 shows the typical morphology of the as-prepared lead nanostructures. The sectional view of figure 2.9a shows the sturdy connection of NWs to the support, and the void space useful for accommodating the volume increase on discharging and from the figure 2.9b we can see that the surface is uniformly covert from nanowires. Porosity generated by the uniform distribution of NWs is clearly visible in figures 2.9c and d. The NWs interconnection is conformal to the template morphology.

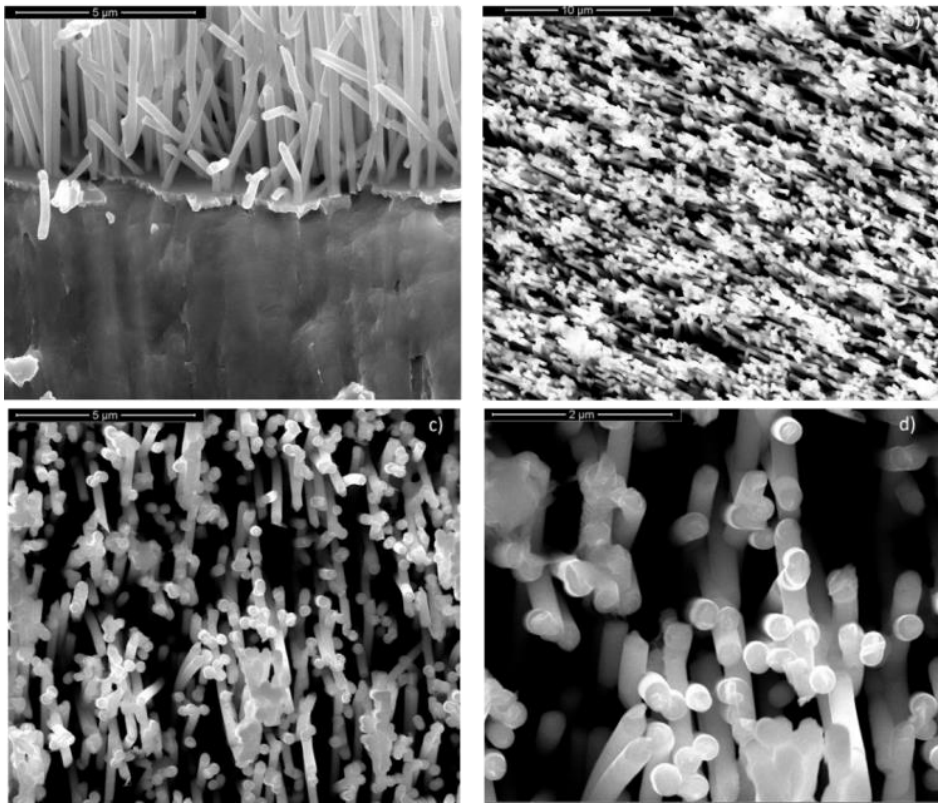

Figure 2.9 Typical morphology of the as-prepared lead nanostructure array at different magnifications: (a) cross-sectional view, (b-c) top-view.

The typical crystal structure of the lead electrode is shown in figure 2.10, where XRD patterns of the as-prepared (figure 2.10a) and cycled electrode up to end of life (figure 2.10b) are shown. In figure 2.10a, very strong lead peaks are evident together with some weak peaks attributed to more or less hydrated β-PbO, likely formed on the air exposition of the as-prepared Pb NWs. In practice, XRD

analysis reveals the extreme purity of the as-prepared deposit. For the purpose of comparison, the typical XRD pattern of an electrode disassembled after cycling in 5M H_2SO_4 up to end of life is shown in figure 2.10b. Strong $PbSO_4$ peaks are largely present together with some weaker peaks of lead, which might be attributed to either residual lead or to the underlying layer supporting the nanostructures. The peaks indicated with * and ° are related to β-PbO and β-PbO xH_2O respectively. The XRD analysis performed in the post-cycled Pb electrode is shown in Figure 2.10b and in this graph are indicated with # and * the peaks related to $PbSO_4$ and Pb respectively. The XRD pattern at the end of life is independent of the cycling C-rate. In the case of pure Pb (figure 2.10a) from literature [24] we know that the characteristic peaks of Pb are found at the angles 2-theta 31.27°, 36.26° and 52.22°, so we have a perfect superposition of the peaks.

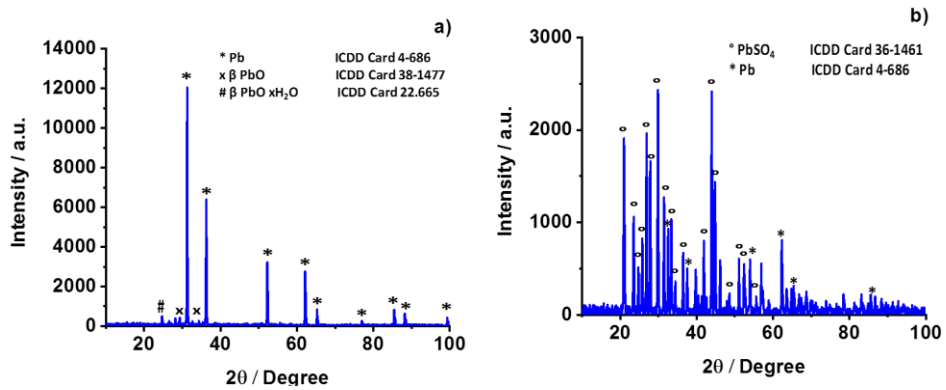

Figure 2.10 Typical X-ray diffraction patterns of a) as-prepared lead nanostructure array, b) porous mass after cycling under constant current up to end of life.

The nanostructured Pb electrodes were tested in various conditions and in the table 2.2 it is possible to see a summary of all electrochemical tests that we carried out on them. On these electrodes all electrochemical tests were carried out at 25°C.

	Battery of 2V	Battery of 6V
1C (1h for full charge)	Investigated	Investigated
2C (30 min. for full charge)	Investigated	Not investigated
5C (12 min. for full charge)	Investigated	Not investigated
10C (6 min. for full charge)	Investigated	Investigated
From 10C to 1C	Investigated	Not investigated

Table 2.1 Summary table of all electrochemical tests on nanostructured lead electrodes.

2.2.3 Electrochemical test

The nanostructured lead was tested as a negative electrode in an electrochemical cell simulating a LAB (lead-acid battery), with a commercial PbO_2 plate as the positive electrode. The two electrodes were vertically assembled, isolated by an AGM separator, and immersed in 5 M H_2SO_4. A zero-gap cell, kept at 25 ± 2 °C, was assembled to exclude any effect on the electrochemical results of both cell configuration and uncontrolled temperature oscillations. The cell was powered at constant current through a Cell Test System (Solartron, Mod. 1470 E, 8 channels) controlled by a desk computer via MultiStat Software (Mod. UBS147010ES). The voltage value reported in the following is the difference in electric potential between positive (PbO_2) and negative (Pb) electrodes. It was not used any reference electrode in order to compare the cell voltage value directly, with a real

LAB, whose performances and the State of Charge are evidenced just through the cell voltage. The nominal charge capacity of the negative electrode was determined by weight according to the following steps.

1) The membrane was weighed after sputtering of the gold in one of its sides;
2) Then, the Pb current collector was deposited on the gold film. The membrane was again weighed;
3) Then, nanowires were electrochemically deposited inside the membrane pores and weight of the membrane was determined;
4) The weight difference prior to and after nanowires deposition gave the nanowires mass deposited;
5) Only the weight of the NWs was considered in evaluating the nominal capacity, because dedicated experiments showed that the Pb layer supporting the NWs does not participate in the battery cycling. The weight determinations were operated by a SARTORIUS microbalance (mod.: ME36S Premium Microbalance). More than 100 times higher electrical capacity of PbO_2 counter-electrode was selected, so that the nanostructured electrode was controlling the cell performance.

The figure 2.11 shows a 3D-scheme of the final cell assembled with Pb NWs electrode, lead oxide commercial plate, sulfuric acid as an electrolyte and AGM separator.
The first electrochemical test was carried out at constant current corresponding to 1C-rate (1h to reach the complete charge). The first charging was carried out by stepwise grown from 0.2C-rate to the C-rate of the final test. This charging procedure was successfully experienced previously in case of the PbO_2 NWs electrode [19] [20]. Discharge stage was carried out at the same C-rate of the charging. Two limits were imposed for electrochemical tests consisting in cut-off cell voltage and discharging time length. The first one was set at 1.2 V in order to check the lifetime of the nanostructured negative electrode under deep discharge that determines rapid sulfurization of the commercial LABs. The duration of discharging was limited to drawing 90% of the nominal capacity; therefore, the time was set at 54 min. Such a 90% limit was selected for avoiding of converting all available lead into insulating sulfate, with consequent voltage spike above 2.85 V on the starting of the successive charging. The double limit on discharging gives a more complete picture of the performance of the electrode under study. In

fact, if the electrode polarizes to the cut-off voltage within the selected time, discharging stops and a new charging starts. On the contrary, if the electrode polarization remains for all the selected duration less than the cut-off voltage, then the process inverts at an established time. In this case, it can be assumed that 90% of the accepted charge is drawn; therefore a cycling efficiency of 100% has to be estimated, as the ratio of the drained charge to the accepted one.

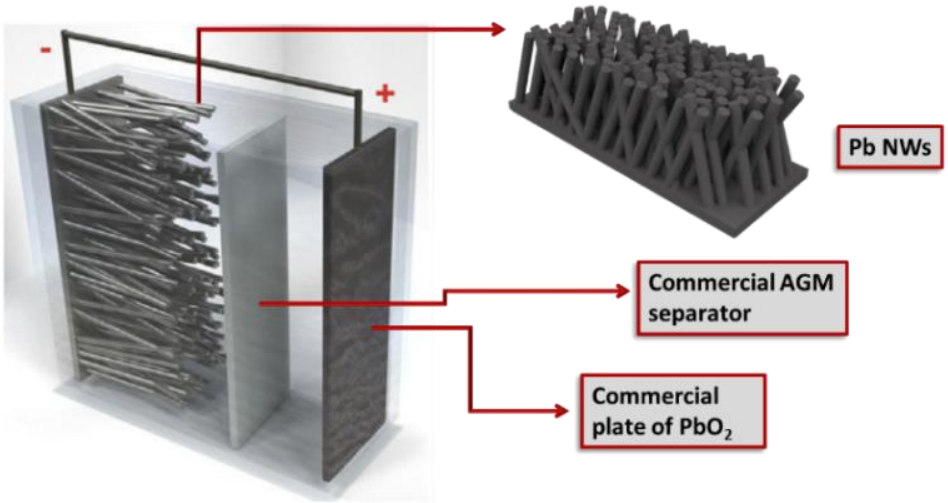

Figure 2.11 3D-scheme of lead-acid battery with negative nanowire electrode.

The performance test of the nanostructured lead as a negative electrode of a simulated LAB was conducted at 1C-rate (figure 2.12). High C-rate and deep depth of discharge were selected for severely stressing the electrode in comparison with LAB pasted one, which cannot sustain such conditions without fast sulfurization [25]. The figures 2.12a shows the initial step-by-step charge up to 1C. The stepwise implements of the C-rate for charging the as-prepared lead NWs was found extremely effective for maintaining the cell voltage below 3.0 V, so preserving the active material from any damage due to turbulent gas evolution. The first discharging curve shows a fast polarization of the electrode, likely due to the high reactivity of the NWs, which convert in sulfate almost instantaneously. In practice, the first discharge does not deliver any useful electrical charge. In cycling after the stepwise initial charging, the delivered charge always increases independently of the C-rate. The figure 2.12a shows that the first discharge is so fast that no electrical charge is drained, because, likely,

the low wettability of the nanostructured electrode so that only the top of the nanowire is converted into lead sulfate with immediate polarization to the cut-off voltage. As cycling is continued, the drained charge progressively increases, as shown in figures 2.12b because both wettability and porosity increase. The enhancement of the reacting area determines a decrease of the electrode polarization with a consequent increase of the drained charge on discharging, as clearly shown in figures 2.12b. The figure 2.12b and c shows the cycling curves at 1C-rate of the lead NWs electrode (2.12b), and the related faradic efficiency (2.12c). The figure 2.1b shows one advantage of the nanostructured negative electrode, in fact, it is possible to see that in this case the performances improve under cycling. The figure 2.12c shows a typical plot of cycling efficiency at 1C-rate vs cycles. The efficiency curve is consistent with the cycling curves of figure 2.12b, because it is evidence that the efficiency not only never reaches the value of 100%, but remains almost constant at around 80% from about 280^{th} cycle to the 450^{th}. Over cycling, conversion reaction of lead sulfate to lead and vice-versa occurs, therefore, the initial morphology is progressively lost.
The morphology change is likely due to the continuous volume variation during the conversion reaction of Pb to $PbSO_4$ and vice-versa. After around 200 cycles the electrode was subject to SEM analysis and we saw that the initial nanowires were changing in micropillars, with very different length, but still well attached to the substrate. Besides, it can be seen that a free space separates neighbouring micropillars. This morphological variation leads to an active material that has both a high surface area, vital for the electrochemical reactions, and a high degree of porosity, which facilitates the transport of the electrolyte throughout active material. The change of electrode morphology was also investigated at the end of the discharge, when the active material was converted in lead sulfate. After cyclization the SEM analysis was carried out to verify how the cycles influenced the electrode morphology. The figures 2.13 a) - d) show the results of this analysis. The lead electrode after cyclization has a porous surface, thus it is possible to use this electrode for more charge and discharge cycles with a deep discharge.

After the tests reported above, we carried out other tests at different C-rate to confirm the good performances of lead nanowires electrodes at high C-rate. In particular, we carried out tests at 2C, 5C 10C. Furthermore, we also conducted some tests at different create on the same battery (from 10C o 1C).

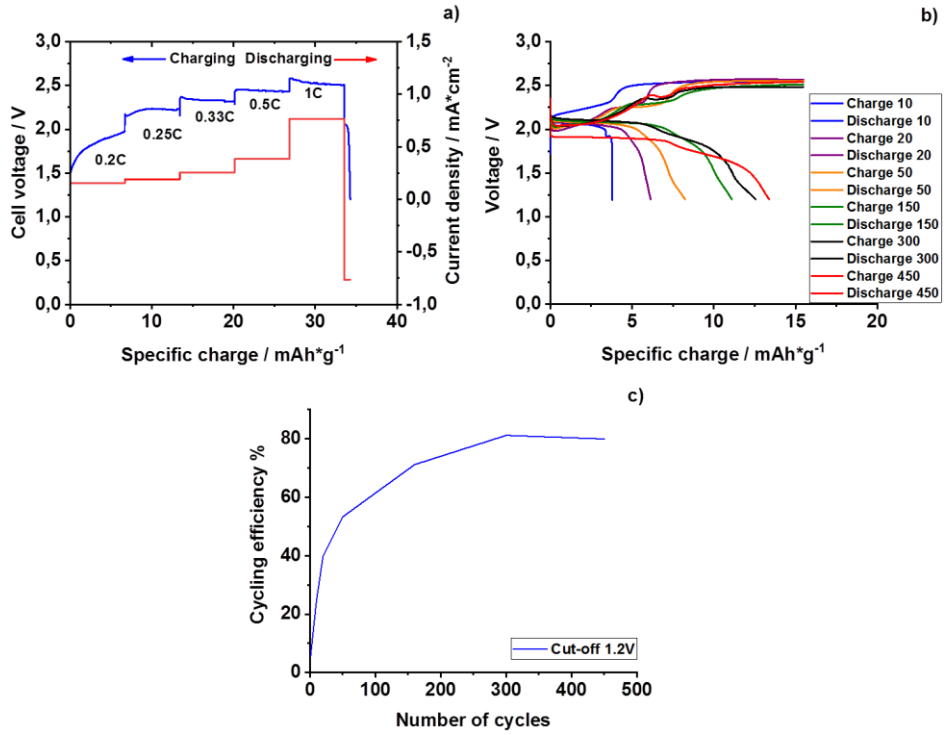

Figure 2.12 Electrochemical performance of nanostructured lead acting as a negative electrode of an electrochemical cell simulating a lead acid battery operating at 25 ± 2 °C and 1C: a) First charging and discharging curves; b) Charging and discharging curves of different cycles; c) Cycling efficiency on discharging of nanostructured.

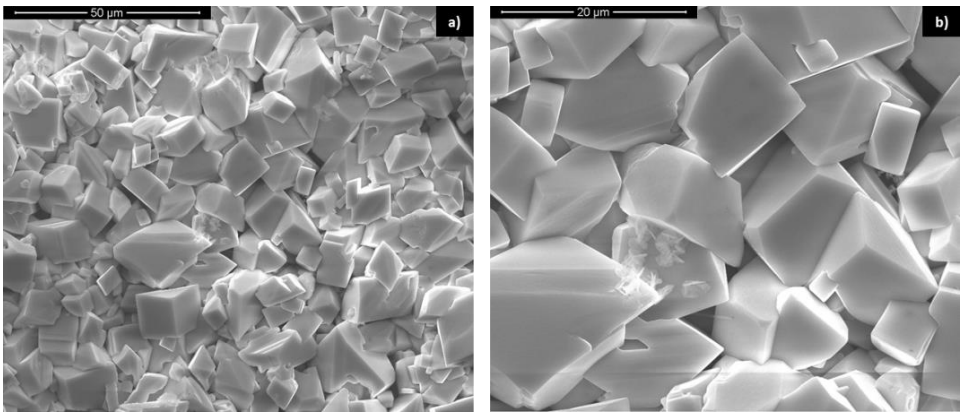

Figure 2.13 SEM images of lead electrode after cyclization at different magnifications.

- ***Performance at 2C***

The electrochemical tests were carried out at constant current corresponding to 2C-rate (limiting charging duration of 30 min), with a cut-off equal to 1.2V and using 5M sulfuric acid as the electrolyte. The separator used to avoid the short-cut was a commercial AGM separator and we choose as counter electrode the PbO_2 commercial plate.

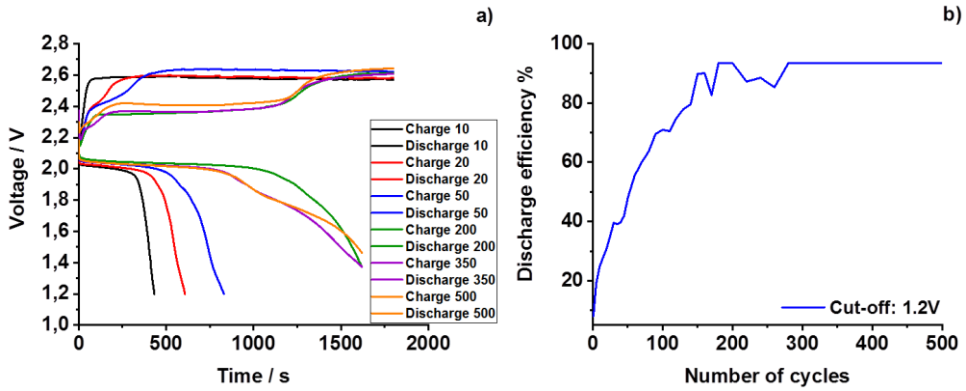

Figure 2.14 Electrochemical performance of nanostructured lead acting as a negative electrode of an electrochemical cell simulating a lead acid battery operating at 25 ± 2 °C and 2C: a) Charging and discharging curves of different cycles; b) Cycling efficiency on discharging of nanostructured.

The figure 2.14 shows the result of this test. In particular, from figure 2.14 a) it is possible to see that the charge curves have a regular pattern and they don't shown the presence of spikes. The discharge curves have an increase of the plateau increasing the number of cycles, that means an increase of the usable energy during battery utilization. In this case the battery reaches an efficiency equal to 90% after 300 cycles. The figure 2.15 shows the SEM images at different magnification of Pb NWs electrode after cyclization. The morphology of nanostructures completely changes after cyclization. Despite the change of nanowires morphology, the electrode has a high porosity so a high surface area for charge/discharge reactions. On the electrode cycled at 2C a quantitative XRD analysis to determine the quantitative of lead and lead sulfate in the electrode after cyclization was carried out. The figure 2.16 shows the result of this analysis. After cyclization the amount of $PbSO_4$ is equal to 98.7% and the amount of Pb is

equal to 1.3%, thus at the end of life the electrode is almost totally sulfated, as aspected.

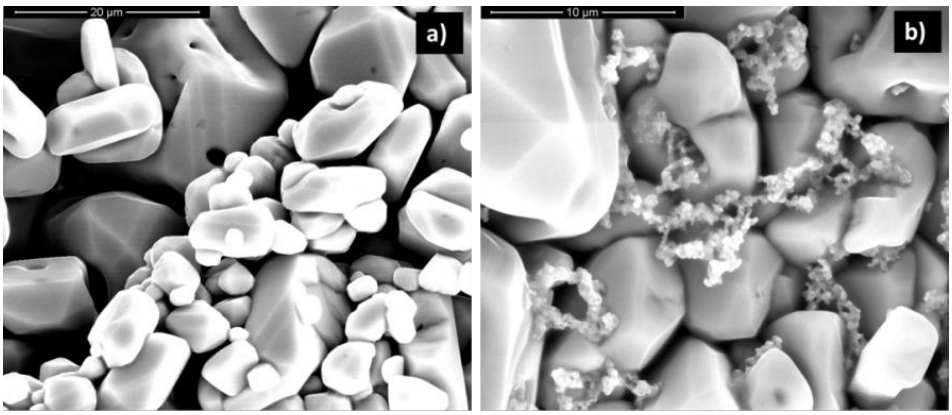

Figure 2.15 Comparison of the morphology of negative nanostructured electrodes after cycling at different magnification: a) 2C after 500 cycles 5000x (end of the life); b) 2C after 500 cycles 10000x (end of the life).

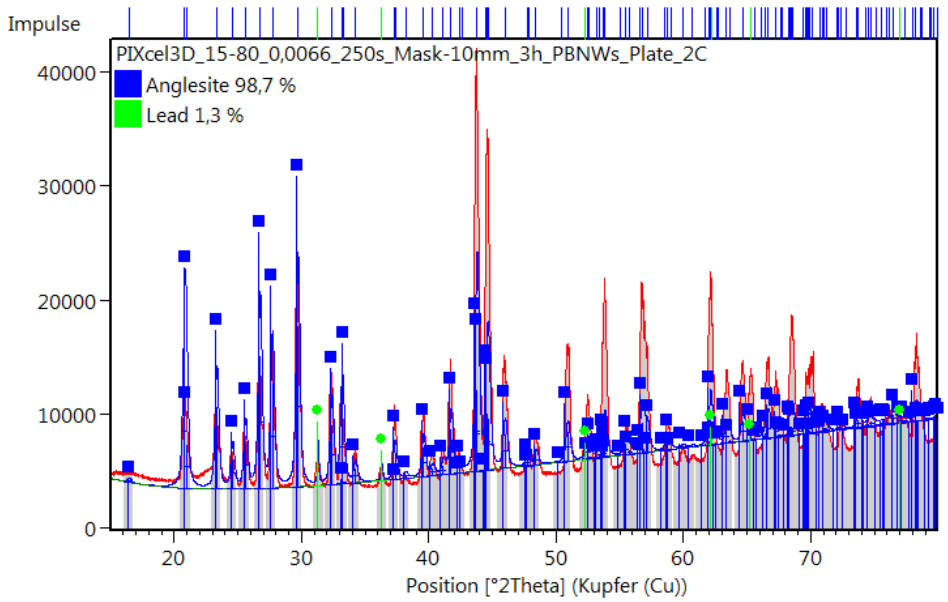

Figure 2.16 Spectrum of quantitative XRD analysis on Pb NWs electrode after cyclization at 2C.

- ***Performance at 5C***

The test carried out at 5C (limiting charging duration of 12 min) was set with the same conditions used for the previous tests, so with a cut-off voltage equal to 1.2 V and using the commercial AGM separator and a commercial PbO_2 plate as counter electrode. The figures 2.17 a) and b) show, respectively the charge/discharge curves of nanostructured Pb electrode at 5C and the efficiency of discharge of this electrode.

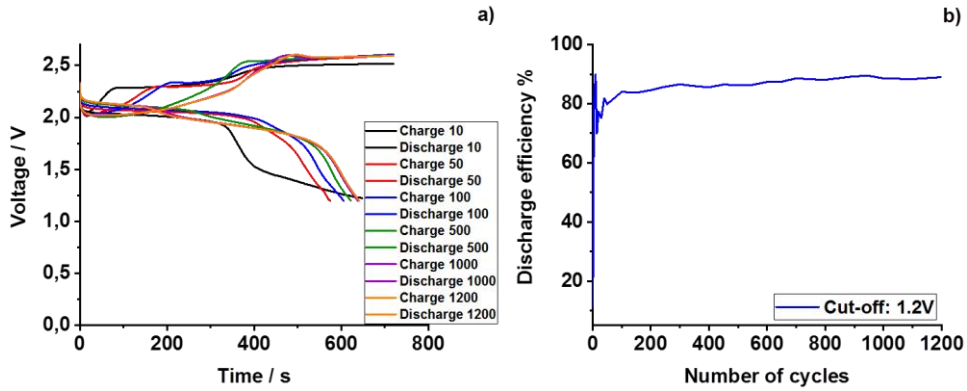

Figure 2.17 Electrochemical performance of nanostructured lead acting as a negative electrode of an electrochemical cell simulating a lead acid battery operating at 25 ± 2 °C and 5C: a) Charging and discharging curves of different cycles; b) Cycling efficiency on discharging of nanostructured.

In this case, battery reaches an efficiency equal to 90% after 100 cycles and this value is constant for all the life of the battery. Furthermore, there is not high gas evolution on the surface of the electrode, in fact the charge curves have a regular trend, and the discharge curves have an increase in the plateau with increasing of number of cycles. On the electrode at the end of life was carried out the quantitative XRD analysis (figure 2.18). In this case, for the quantitative analysis the $PbSO_4$ was about 99,1% and a Pb about 0.9%.

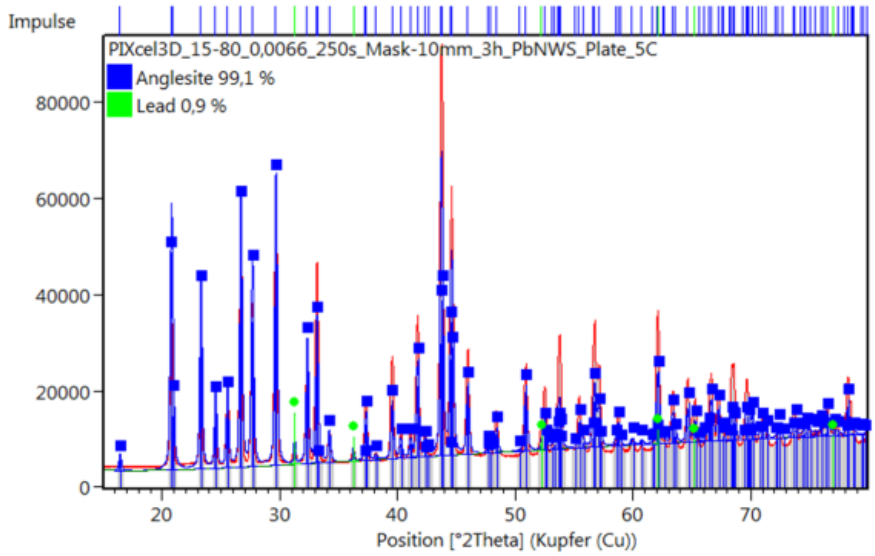

Figure 2.18 Spectrum of quantitative XRD analysis on Pb NWs electrode after cyclization at 5C.

- ***Performance at 10C***

The electrochemical tests were carried out at constant current corresponding to 10C-rate (limiting charging duration of 6 min), with a cut-off equal to 1.2V and using 5 M sulfuric acid as electrolyte. The separator used to avoid the short-cut was a commercial AGM separator and we choose as counter electrode the PbO_2 commercial plate. The figures 2.19a shows the initial step charge carried out on the lead-acid battery with negative nanostructured electrode. The higher voltage drop on reversing the first charging shown in figure 2.19a in comparison with 2.12a has to be attributed to higher current at 10C than 1C-rate. Of course, at 10C-rate the conversion of Pb to $PbSO_4$ is ten times faster and, consequently the ohmic drop is higher. A role can be also attributed to the wettability of the porous mass, because the wettability of solid nanostructure and its permeation by a liquid solution is an important aspect for the behaviour of nanostructured materials.

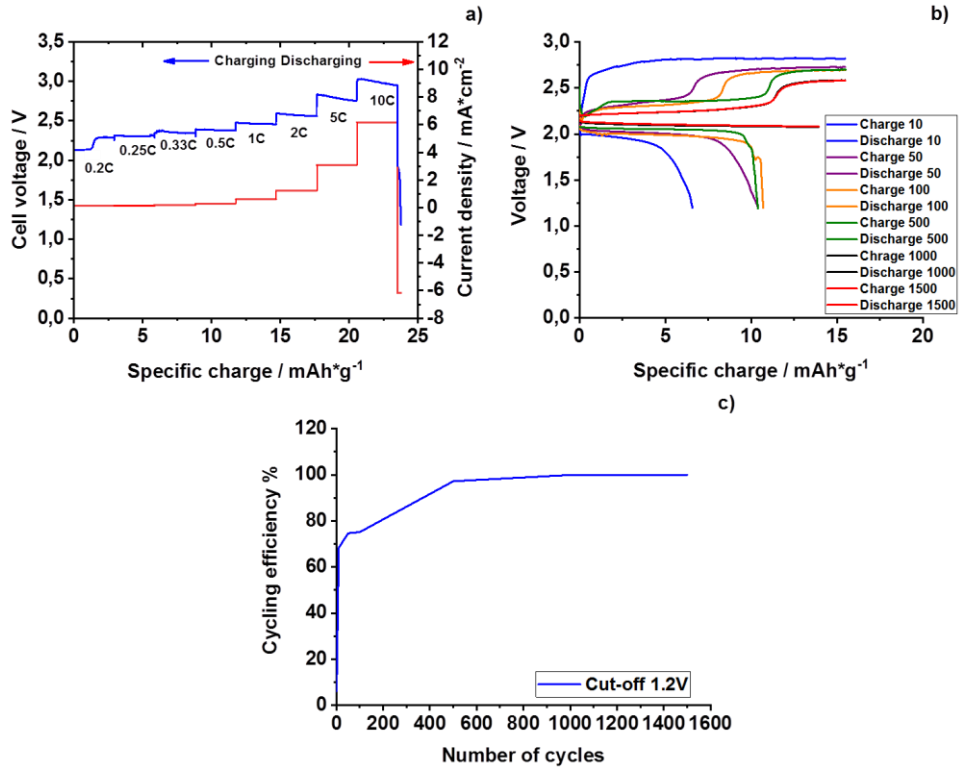

Figure 2.19 Electrochemical performance of nanostructured lead acting as a negative electrode of an electrochemical cell simulating a lead acid battery operating at 25 ± 2 °C and 10C: a) First charging and discharging curves; b) Charging and discharging curves of different cycles; c) Cycling efficiency on discharging of nanostructured.

The figure 2.19b evidences a strong polarization on charging of the electrode at cycle 10, where a voltage of 2.8 V close to the limiting value of 2.85 V is reached. The polarization decreases with the cycling as shown by the curve of the 50^{th} cycle featured by an initial low polarization interval followed by an inflection at about 6 mAh g^{-1} leading to a quasi steady-state voltage of about 2.7 V. It is interesting to observe that the low polarization interval length increases with the cycling number up to a value of 11.5 mAh g^{-1} at the 1500^{th} cycle. Besides, also the quasi steady-state voltage following the inflection is decreased to 2.5V over charging. The two levels of polarization can be explained, taking into account the reactions occurring on charging. Neglecting the reduction of the dissolved oxygen owing to its saturation concentration which is as low as 0.61mM in 5.4M H_2SO_4, the reactions that have to be considered are $PbSO_4$ conversion into Pb, and

hydrogen evolution. Initially, the prevailing process is the reduction of $PbSO_4$ to Pb, because it occurs at lower overvoltage than hydrogen evolution on lead. As the $PbSO_4$ conversion into Pb is almost complete, the prevailing reaction becomes hydrogen evolution, which occurs with higher overvoltage. In practice, the applied current of charging is divided up into $PbSO_4$ and H_3O^+ reduction. In the initial stage, the partial current of $PbSO_4$ conversion is prevailing and a low voltage is found. When the partial current of hydrogen evolution becomes a prevalent higher voltage is recorded even if the conversion of $PbSO_4$ continues but at lower partial current. The curve inflection marks the transition from one regime to the other one. This is a typical voltage response of a lead-acid cell at a constant rate charge. The increasing extension of the charging interval prior to the inflection finds its explanation in the discharging curves. Moving from the curve of the 10^{th} cycle towards those relative at the higher cycle number, not only the drained, charge increases but also the discharging process runs with lower overvoltage. In particular, curves of the 100^{th} cycle and the 500^{th} cycle, show an almost rectangular shape matching the theoretical one. Besides, it must be observed that the discharging process is still controlled by the cut-off voltage at the 500^{th} cycle, while time length is controlled at the 1000^{th} cycle and successive. Therefore, the low voltage interval over charging extends progressively because the drained charge is progressively increasing. As the discharging process passes from the cut-off voltage to the time control, then, it can be assumed that the total nominal capacity is drained, otherwise the electrode should have been polarized owing to the formation of insulating $PbSO_4$. This means that the charge/discharge process runs with 100% faradic efficiency, therefore, its curve has to be normalized at 100% like in figure 2.19c. This plot is coherent with the findings of figure 2.19b, because it shows a progressive increase of the efficiency with the number of cycles. Therefore, the LAB under investigation improves its performance on cycling to the point that it works after 1500 cycles without fading. This result is of great relevance in comparison with the pasted negative electrodes of the commercial batteries, which cannot sustain these severe cycling conditions, without undergoing to fast sulfurization. It is possible to see that the electrode polarization is greater at 1C than 10C-rate. In particular, the curve of the 450^{th} cycle (figure 2.12b) shows that the highest charge is drained with the highest overvoltage essentially due to the initial voltage spike. Such sharp drop can be attributed likely to the presence of sulfate that has not converted during the previous stage of charging. Therefore, when LAB is cycled at 1C-rate its lifetime is shorter because hard sulfate is present already at the 450^{th} cycle in such a

quantity to determining high cell polarization, differently from the nanostructured lead electrode that works up to 1500 cycles at 10C-rate without any difficulty (figure 2.19b). The cycling at 10C-rate was stopped at 1500th cycle only for the sake of characterizing the electrode after so long time of immersion (12.5 days); otherwise the cell could continue to cycling. It was estimated that 1500 cycles at 10C-rate without fading had to be considered a so very satisfying result that did not need to prolong the cycling. The depolarization of the electrode processes is more effective at 10C than 1C in otherwise identical conditions, because, at higher C-rate the particle size decreases and porosity increases more. Therefore, at 10C, the cell voltage does not reach the cut-off value (1.2V) during the 324 s (= 0.9*360) long discharge. For this reason, the curves of the 1000th cycle and the 1500th cycle of figure 2.19b are so slow sloping to seem almost flat, in contrast with the usual shape of discharging curves of a battery. After cyclization Pb nanostructured electrode was subject to the SEM analysis and figures 2.20 a) and b) show the images of this analysis. As it is possible to see from these images the Pb NWs electrode shows a porous surface also after cyclization and that means it is possible to use the same electrode for other cycles with high C-rate and deep depth of discharge. Figures of the electrochemical tests at different crate clearly indicate that when electrodeposited nanostructured lead is employed as a negative electrode in a cell simulating a LAB, not only electrode polarization decreases but also efficiency improves under cycling and with C-rate. These findings are different in comparison with the behaviour of current commercial LABs pasted electrodes which decay rapidly if cycled under the stressing conditions selected for testing nanostructured electrodes. In this context, it is mandatory to scrutinize the possible causes of such behaviour. At this aim, dedicated investigations were conducted. First of all, the wettability of the nanostructured electrode was evaluated by contact angle measurements using a 5M sulfuric acid solution as a wetting liquid (FTA 1000 First Ten Ångstroms). Contact angle was performed on different areas of the nanostructured electrodes to evaluate their uniformity. Figure 2.21a shows the contact angle when a droplet of 5 M H_2SO_4 is in contact with the surface of the as-prepared nanostructured lead.

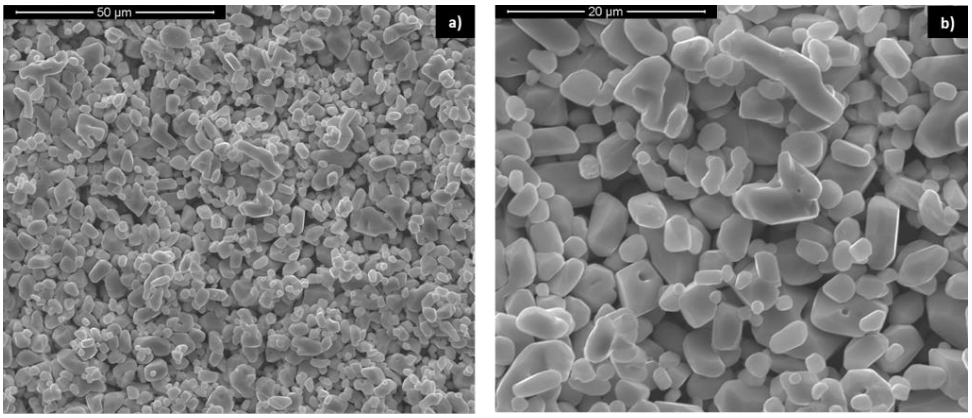

Figure 2.20 SEM image of Pb nanostructured electrode at different magnifications after cyclization.

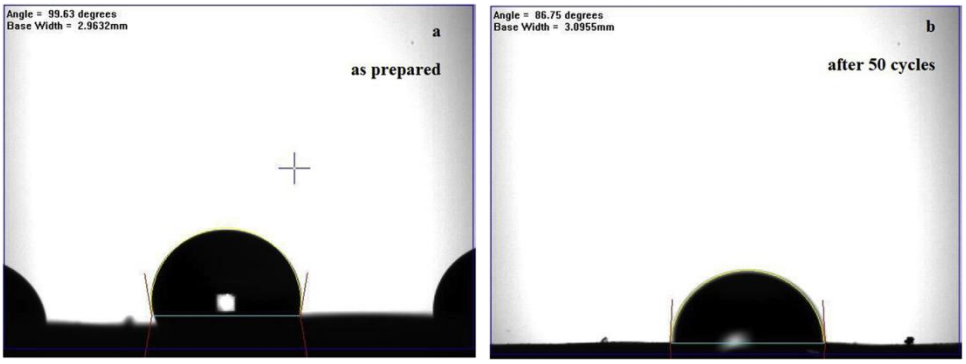

Figure 2.21 Contact angle measured on: (a) as-prepared electrode (b) electrode after 50 charge/discharge cycles [10].

A contact angle of about 100°±2.3 indicates that the surface is scarcely wetted by sulfuric acid solution. Therefore, we can conclude that only the top of the nanowires initially works. After 50 cycles contact angle was about 86°±2.6 (figure 2.21b), while after 200 cycles was not measurable. Likely, initial hydrophobicity of the nanostructures diminishes over cycling owing to the repeated conversion reactions $Pb/PbSO_4$ and vice-versa, which modify the external surface of the nanostructures. Thus, the improvement of the performances is due to the gradual increase of the wetted surface by the electrolyte, therefore polarization decreases. In addition, the modification of the nanowire surface area, due to the conversion reactions $Pb/PbSO_4$ and vice-versa

is coupled with the porosity increase of the active area, as evidenced in figure 2.22 shoving the SEM images of lead electrode cycled at 10C for 200 cycles at the end of the charge. Figure 2.12 shows SEM pictures of nanostructured electrodes cycled at 1C for 450 cycles (a), 10C for 1500 cycles (b) and after 50 cycles at 1C (c) and 10C (d). All images were made at the end of the charge. Obviously, the pillar morphology of the as-prepared electrode is completely lost owing to the conversion in lead sulfate in the form of macroparticles.

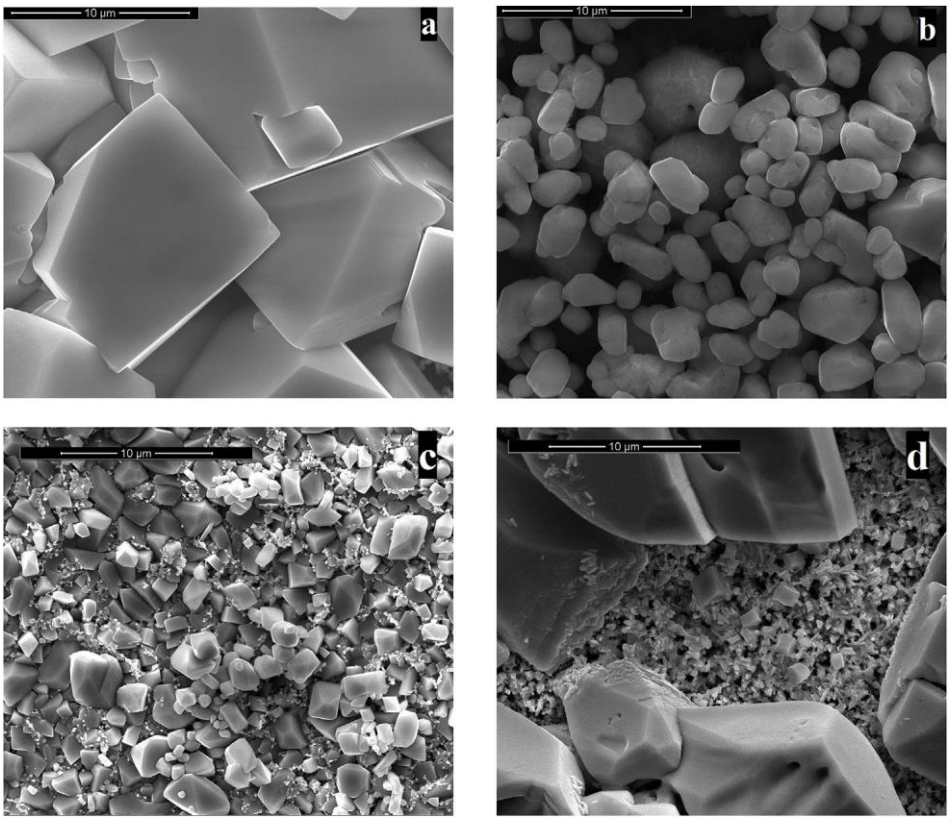

Fig. 2.22 Comparison of the morphology of negative nanostructured electrodes after cycling at different C-rate (at the end of discharge): a) 1C after 450 cycles (end of the life), b) 10C after 1500 cycles; c) 1C after 50 cycles, d) 10C after 50 cycles [10].

In particular, these SEM images show that the particle size after 10C cycling is lower than after 1C, according to the literature showing that as the cycling rate increases, i.e. the current density increases, the mean particle size decreases [26] [27]. Since the magnification of the images is identical, the particle number per

surface unit after cycling at 1C is less than after 10C. Therefore, the surface is more porous in this last case. This conclusion is further confirmed by the images after 50 cycles at 1C (figure 2.22c) and 10C (figure 2.22d) are shown, both at the end of discharge. This figure evidences that after 50 cycles, smaller particles were formed at 10C than 1C. Therefore, according to the previous considerations, a more porous layer is formed at 10C than 1C also at low cycle number. According to these results, we can infer that the change of morphology with the consequent gradual increase of both wettability and porosity over cycling is the most likely cause of the better performances of lead nanostructured electrode in comparison with the pasted one. In detail, fresh formed nanostructured lead shows the pillar morphology of figure 2.9 b) - d).

- ***Performance at C-rate from 10C to 1C***

To establish the response of the electrodes at different C-rate some tests with variable C-rate we performed, in particular from 10C to 1C. In figure 2.23 the efficiency trend at different C-rate was reported. The efficiency of the battery increases by 90% and then decreases when the battery starts the cycles at 1C. In the last case the maximum efficiency reached is around 65%.

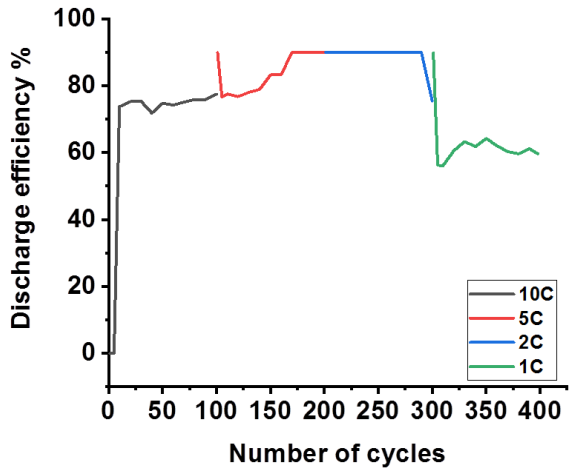

Figure 2.23 Cycling efficiency on discharging of nanostructured at different C-rate.

The figure 2.24 shows the charge/discharge curves at different C-rate. These figures show that gas evolution occurs during the charge phase and the performance of electrode are better at high C-rate, in fact there is increasing in the plateau of discharge curves at 10C and 5C and a little decreasing in the plateau of discharge curves at C-rate equal to 2C and 1C.

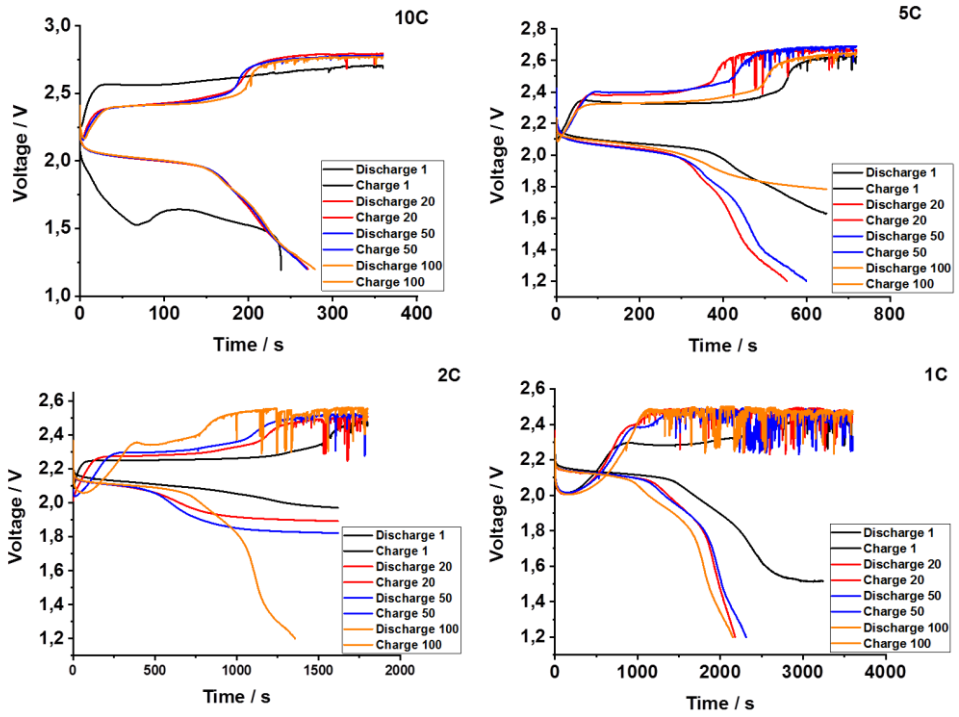

Figure 2.24 Charge/discharge curves at different C-rate: from 10C to 1C.

The quantitative XRD analysis, carried out on this electrode, shows a quantitative of lead sulfate equal to 99% and a quantitative of lead equal to 1%, figure 2.25.

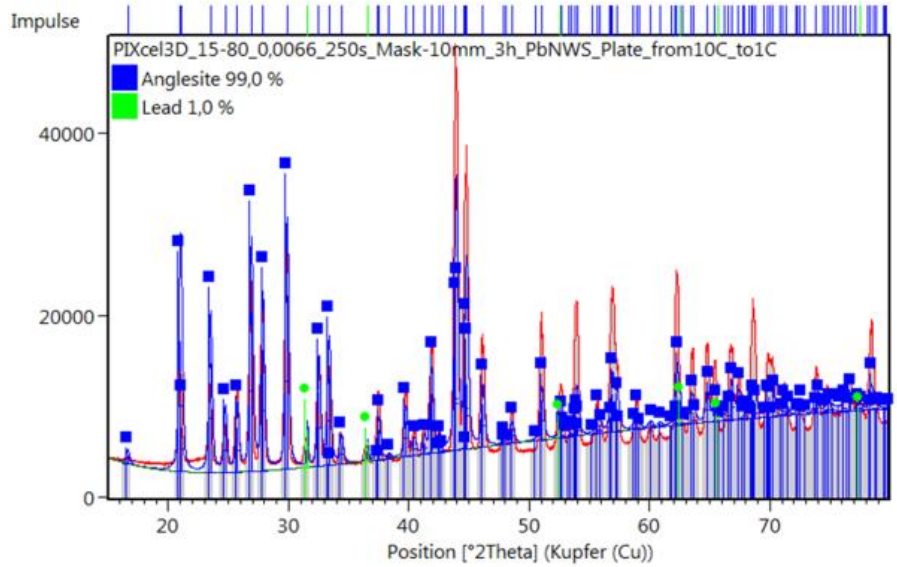

Figure 2.25 Spectrum of quantitative XRD analysis on Pb NWs electrode after cyclization at different C-rate.

- ***Performance of Pb NWs electrode in 6V hybrid prototype***

An hybrid prototype of 6V was designed, made with three Pb NWs electrode as negative electrode, three PbO_2 commercial plates as the positive electrode, commercial AGM separators and 5M sulfuric acid as the electrolyte. The case of this battery was designed using a 3D-modelling program and printed with a 3D printer. This prototype was cycled at 1C and 10C and the figure 2.26 shows the results of these tests in terms of charge/discharge curves and efficiency pattern. How it is possible to see from the plots reported in the figure 2.26 the prototype shows performance, better at 10C than the 1C. In both cases there is not gas evolution and there is an increasing in the plateau of discharge curves, that means an increasing in usable energy.

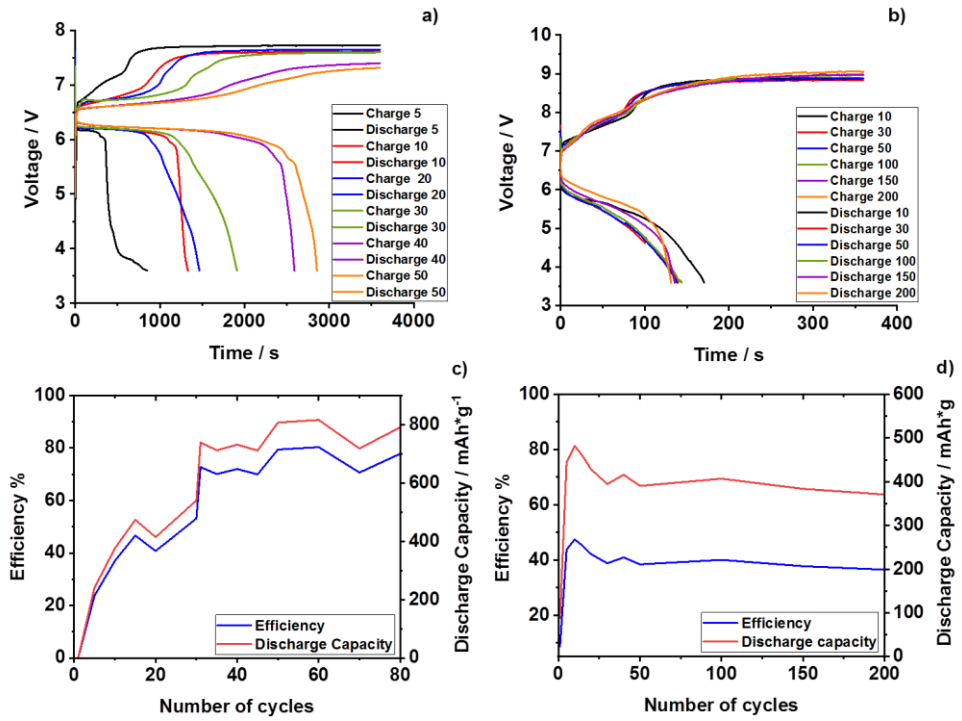

Figure 2.26 Electrochemical performance of nanostructured lead acting as a negative electrode of an electrochemical cell simulating a 6V lead acid battery operating at 25 ± 2 °C: a) Charging and discharging curves at 1C; b) Charging and discharging curves at 10C; c) Cycling efficiency on discharging of nanostructured at 1C; d) Cycling efficiency on discharging of nanostructured at 10C.

The efficiency reached at C-rate equal to 10C is around 80%, while the efficiency reached at 1C is around 40%. A commercial battery cannot reach such high C-rate, in fact by carrying out some tests on a commercial battery it has been seen that the performance of the latter decreases rapidly with increasing the C-rate of the battery, until it breaks after very few cycles carried out at 2C (30 minutes to reach full charge). The performance, in terms of efficiency, of a commercial battery is shown in the figure 2.27.

On the Pb NWs electrode after test quantitative XRD analysis was performed to determine the quantity of lead and lead sulfate in the electrode. The figure 2.28 shows the result of this analysis. $PbSO_4$ was equal to 96.9%, while quantitative of Pb was equal to 3.1%.

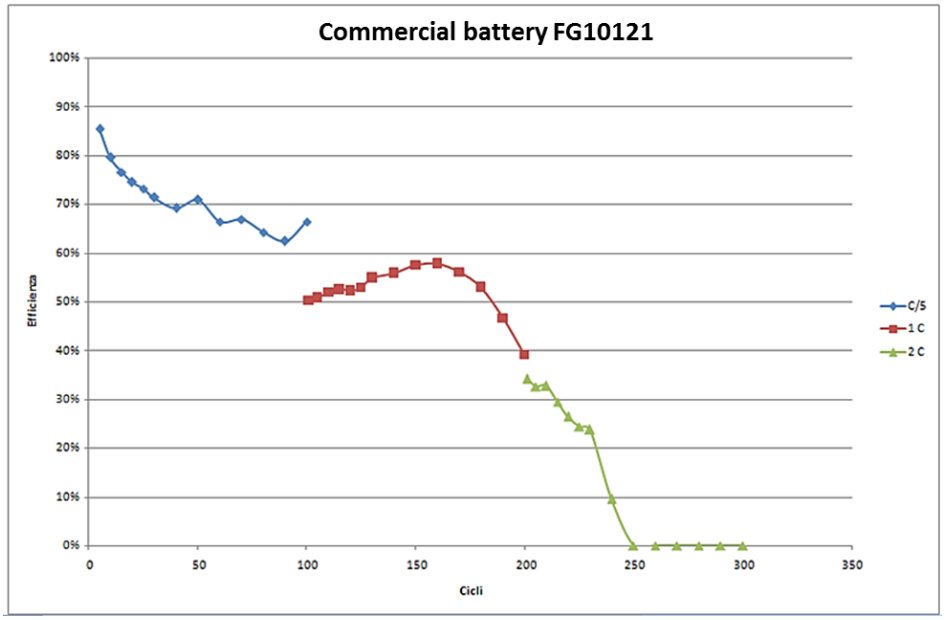

Figure 2.27 Performance of commercial lead-acid battery at different C-rate.

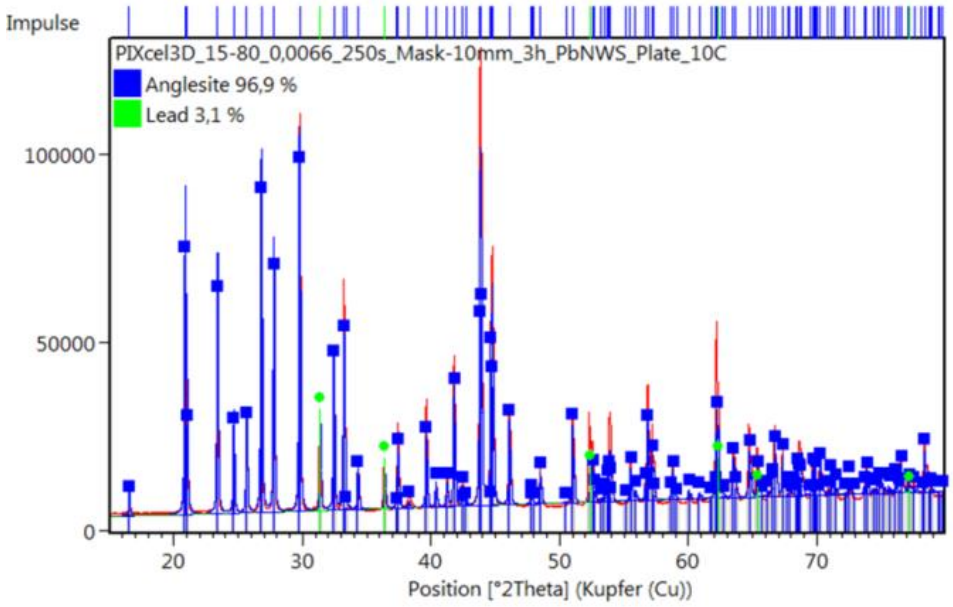

Figure 2.28 Spectrum of quantitative XRD analysis on Pb NWs electrode after cyclization.

How it is possible to see from the results of the various electrochemical tests on nanostructured lead electrodes, in comparison with the performances of commercial lead-acid batteries, it is possible to affirm that the nanostructured electrodes improve the performances of this type of battery in terms of speed of charge and number of cycles.

Chapter 3

Lead-acid battery with both nanostructured electrodes

After the study of the performances of the nanostructured lead and lead oxide electrodes separately, also the lead-acid batteries with both nanostructured electrodes were investigated. The performances of these batteries was also studied at different temperatures, in the range from -20 °C to 40 °C, following the standard BS EN 61427-1: 2013 [28] concerning the operation conditions of commercial lead-acid batteries. Furthermore, in this chapter the performances of nanostructured batteries with gel electrolyte, based on PVA and fabricated in our laboratory, were also discussed.

3.1 Performances of nanostructured lead-acid batteries at different temperature

The electrodes used for the manufacture of the nanostructured battery were fabricated according to the procedures reported in the previous chapters.
The nanostructured battery used for the tests consists of a nanostructured PbO_2 electrode with a geometric area of 1,130 cm^2, a nanostructured Pb electrode with a geometric area of 7,065 cm^2, a commercial separator of the AGM type and an aqueous solution of 5M sulfuric acid as electrolyte. The area of the PbO_2 NWs electrode is smaller than the area of Pb NWs electrode because we choose the first one as the limiting electrode, being it constituted by a fragile material. The figure 3.1 shows a 3D image of the nanostructured battery. The nanostructured batteries was assembled with zero gap, to simulate the same condition of commercial lead-acid batteries,with a C-rate equal to 10C and with a cut-off equal to 1.2V, that mean a depth of discharge equal to 90%, to avoid the not complete formation of lead sulfate insulating on the surface of electrodes. The deep depth of discharge and the high C-rate for each temperature were selected for severely stressing the electrode in comparison with LAB pasted one, which cannot sustain such conditions without fast sulfation [25]. The lead oxide electrode was pre-immersed in 5M sulfuric acid before testing to overcome its

low wettability to avoid higher value of potential which could cause a break of electrodes.

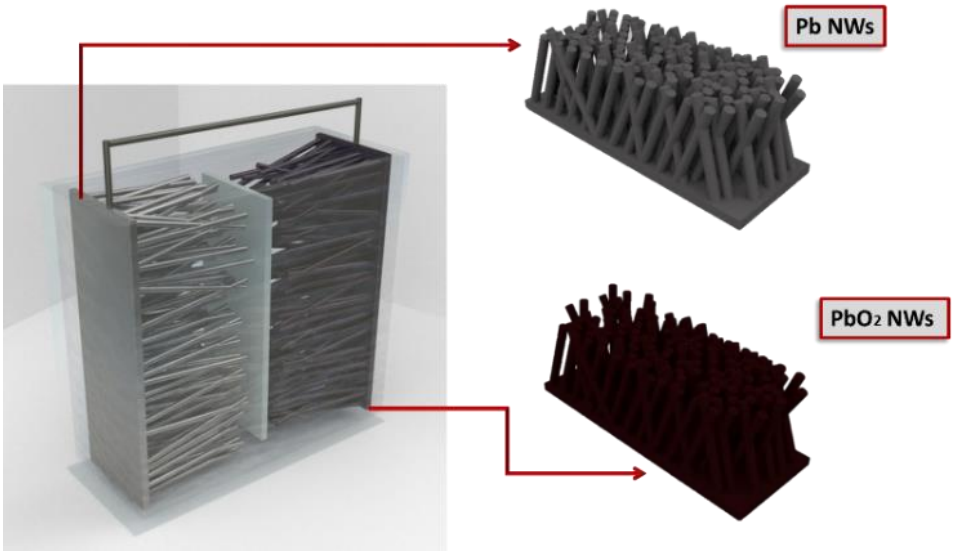

Figure 3.1 3D-scheme of nanostructured lead-acid battery.

The active mass of nanowires was evaluated by gravimetric measurements using a SARTORIUS microbalance (mod. Premium Microbalance ME36S) that it was required to evaluate the nominal capacity of electrodes. In particular, the electrochemical tests were based on the gravimetric capacity of PbO_2 because the positive electrode was limiting respect to electrode of Pb (or negative one) due to lower geometrical surface area. Electrochemical tests were carried out in two-step. First, it was conducted the conditioning of nanostructured cell at 1C, afterwards the same cells were tested at 10C for 1000 cycles and at different temperatures. In particular the temperatures were 25 °C, -20 °C and 40 °C, where the first represents the typical operating conditions of a lead-acid battery under normal conditions, while the last two are extreme temperatures of use of a lead-acid battery according to rules BS EN 61427-1: 2013 [28]. The first charge was carried out with a step charge until reaching the same C-rate of the first discharge. This procedure was adopted to maintain the cell voltage below 3V to avoid the gas evolution, which would cause mechanical stress to the electrode and the migration of acid particles to metal parts causing their corrosion. At the end of this charge the nanostructured batteries were cycled at C-rate equal to 1C for 100

cycles and with a temperature equal to 25 °C. This is the conditioning phase of nanostructured lead-acid batteries and is necessary for stabilization of electrodes. The figure 3.2a shows the initial step-by-step charge up to 1C, C-rate adopted for the conditioning phase of nanostructured lead-acid battery.

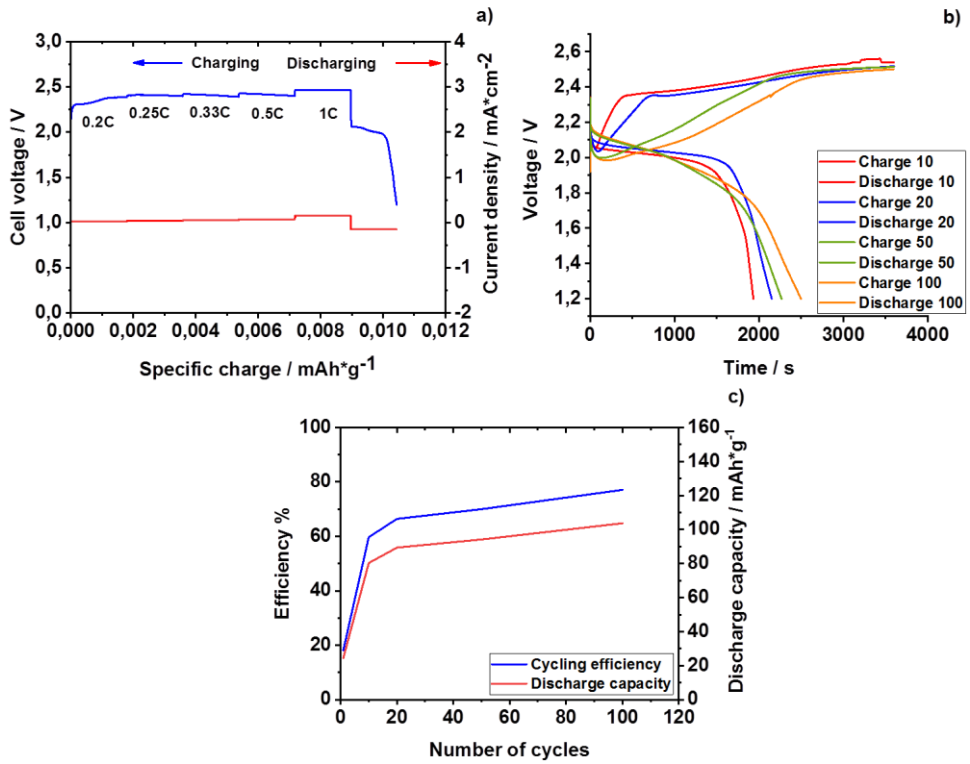

Figure 3.2 Electrochemical performance of nanostructured lead-acid battery operating at 25 ± 2 °C and 1C: a) First charging and discharging curves; b) Charging and discharging curves of different cycles; c) Cycling efficiency on discharging and discharge capacity of nanostructured.

The test starts with a first step-charge. The method of the initial charge with a gradual increase of the current is the same used previously for batteries with only one nanostructured electrode. Using this method, the voltage is less than 2.5V, this value permits to avoid the gas evolution, which would cause mechanical stress to nanostructured electrodes. In figure 3.2b the trend of the charge and discharge curves at 25 °C of the nanostructured battery in the conditioning phase can be observed. The battery has a not constant behaviour, in fact, it is possible to

see that the discharge curves have an irregular pattern. This is the reason of the essential conditioning phase before cycling the nanostructured batteries at C-rate different from 1C. The figure 3.2c shows instead the characteristic curves of efficiency and capacity for a nanostructured lead-acid battery. The battery reaches a maximum value of efficiency around 77% and a maximum value of discharge capacity around 103.7 mAh g^{-1}. The conditioning phase was followed by electron microscopic analysis whit a Scanning Electron Microscope (model FEI Quanta 200) to evaluate the change in electrode morphology. This analysis was performed because the improvement of the battery performance with nanostructured electrodes is associated with the improvement of the wettability of the porous mass of the nanostructured electrodes. In figure 3.3, the morphology presented by a PbO_2 electrode before and after the conditioning phase was shown. In particular, the figure 3.3a shows the initial morphology of the lead oxide electrode, made up of many interconnected wires covering the entire surface of the electrode, with numerous spaces among nanowires that allow the electrolyte (H_2SO_4 5M) to penetrate within them and then encounter a larger active surface for the charge/discharge reactions of the battery. In figure 3.3b instead, the reported micrograph is relative to the morphology of the electrode after the conditioning phase lasting 100 cycles. This figure shows morphology almost similar to the initial one, where the nanowires are still visible even if they have a more marked roughness. Furthermore, lead sulfate macrocrystals are visible on the electrode surface.

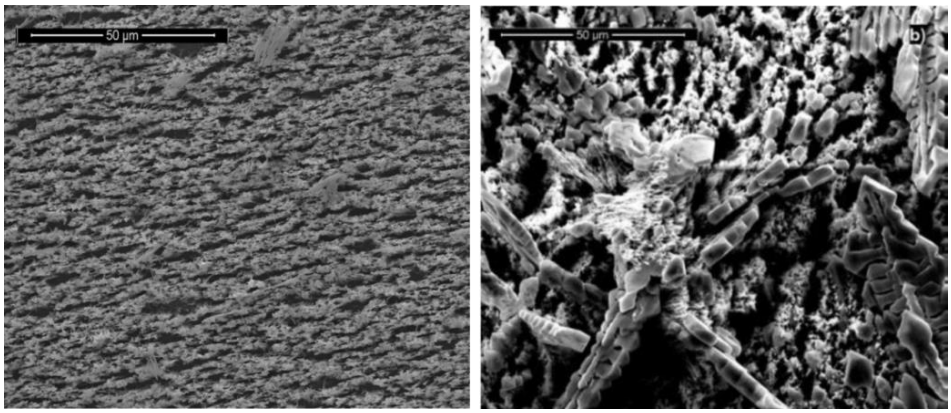

Figure 3.3 SEM images of PbO_2 NWs electrode: a) Micrograph of the morphology of the electrode before the conditioning phase; b) Micrograph of the morphology of the electrode after the conditioning phase [11].

On the basis of these results it can be concluded that the nanostructures formed by template electrodeposition, modify their morphology under cyclization, generating in-situ a porosity that cannot be obtained by other methods. Moreover, and this is certainly the most relevant aspect, the increase in volume during the discharge does not interrupt the electrolytic continuity between the active material of the electrode and the current collector, ensuring a high degree of utilization of the active material. This is perhaps the biggest difference with commercial plates, where the increase in volume associated with the conversion reaction interrupts the electrolytic continuity between the grid and the most distant regions, lowering up to 50% the degree of utilization of the active material, with the related consequences on performance. Also to limit these problems, the commercial plates are cycled at low speeds. After this conditioning phase, the nanostructured batteries were tested at different temperatures. The temperature is a characteristic element of lead-acid batteries and strongly affects their performance. For example, it is found that at high temperatures the internal resistances decrease and the reaction kinetics that take place at the electrodes are facilitated, with a consequent increase in capacity and therefore in energy supplied, in contrast to the high temperatures they also facilitate the self-discharge processes in the process of therefore the capacity loss is stalled. If kinetics is favored at high temperatures, it is unfavourable to the low; the cell reactions slow down, despite this, in the charging phase, a final morphology of macro-porous electrode (very large surface area) is determined which allows to have good performances. On the Pb NWs electrode, post conditioning phase, was carried out a quantitative XRD analysis to determine the quantity of lead and lead sulfate in the electrode. The figure 3.4 shows the result of this analysis. $PbSO_4$ is almost the 98,9%, while Pb is equal to 1.1%.

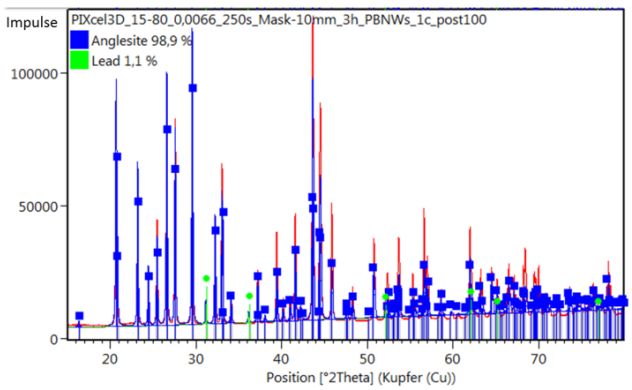

Figure 3.4 Spectrum of quantitative XRD analysis on Pb NWs electrode after conditioning phase.

After conditioning phase the nanostructured lead-acid battery was tested in various conditions. All electrochemical tests carried out on these batteries are reported in the table 3.1

	Battery of 2V	**Battery of 6V**
10C and 25°C	Investigated	Not investigated
10C and -20°C	Investigated	Not investigated
10C and 40°C	Investigated	Not investigated
From 10C to 30C	Investigated	Not investigated
C/5, 1C and 2C	Not investigated	Investigated
Gelled electrolyte and 1C	Investigated	Not investigated

Table 3.1 Summary table of all electrochemical tests on nanostructured lead-acid batteries.

3.1.1 Performance of nanostructured lead-acid batteries at 25 °C

After the conditioning phase, the first test carried out on the nanostructured battery was at a temperature equal to 25 ± 2 °C.
The figures 3.4a and b show the charge and discharge curves of this battery and the relative efficiency. The figure 3.5a evidences a strong polarization of electrodes in the first 50 cycles which decreases with the cyclization, furthermore, the charge curves reported do not have spikes and this means that there is a very limited gas evolution on the surface of the electrodes despite the high speed of cycling. The discharge curves have an increase in the plateau with the cyclization, this means an increase of usable energy of the battery. The charge curves start initially from a voltage slightly lower than 3V and fall to lower voltage values with the increase in the number of cycles. The high voltage value of the charge curves in the first cycles is essentially due to the increase in the speed of cycling that occurs when passing from the conditioning phase to the actual testing phase.

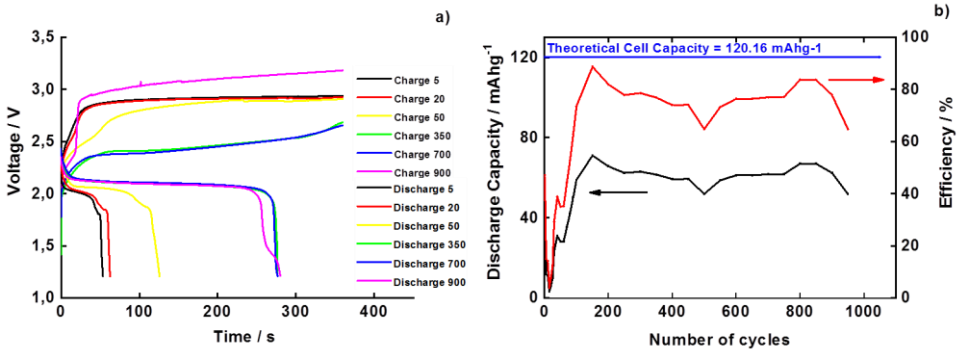

Figure 3.5 Electrochemical performance of nanostructured lead-acid battery operating at 25 ± 2 °C and 10C: a) Charging and discharging curves of different cycles; b) Cycling efficiency on discharging and discharge capacity of nanostructured.

The figure 3.5b shows the efficiency and trends of discharge capacity of the nanostructured battery. The battery reaches a maximum value of efficiency equal to 88.7% (150^{th} cycle) and then it maintains a constant value of efficiency around 76.5% for all its life (figure 3.5b). After cycling, both nanostructured electrodes were analysed by LSM and then SEM to evaluate their morphology change. The figures 3.6 a) - d) show the LSM images of nanostructured electrodes.

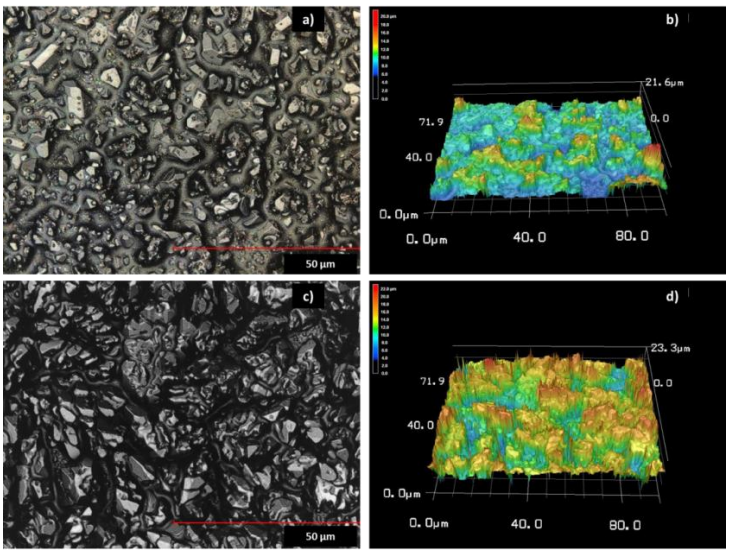

Figure 3.6 LSM images of Pb and PbO_2 NWs electrode: a), b) Images of Pb electrode after 1000 cycles at 10C; c), d) Morphology of the PbO_2 electrode after 1000 cycles at 10C.

The figures 3.7 a) - d) show the images related to the SEM analysis. In particular the figures 3.6a and b show the micrographs related to the morphology of the nanostructured Pb electrode after 1000 cycles; the figures 3.6c and d show the micrographs relating to the naostructured PbO_2 electrode after 1000 cycles. The initial nanowire structure is lost as a result of cyclization in favour of the formation of lead sulfate crystals. The lead sulfate crystals do not form a compact non-conductive layer on the surface of the electrode, but form a highly porous structure which allows the electrodes to be subjected to further charging and discharging cycles at high speeds.

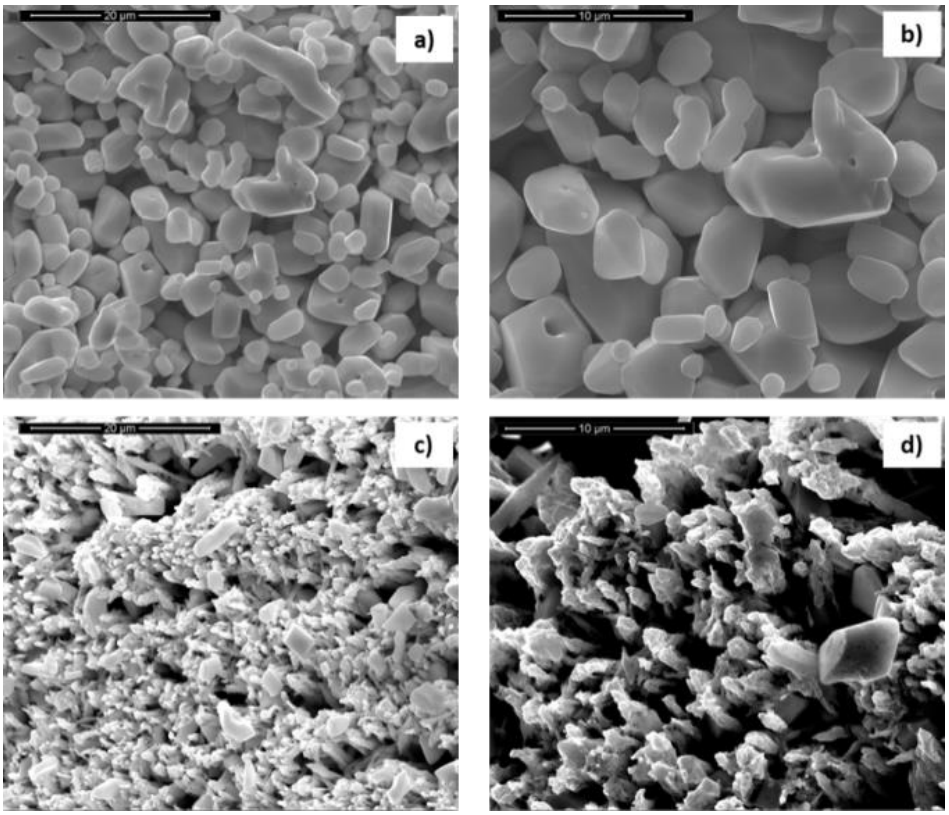

Figure 3.7 SEM images of Pb and PbO_2 NWs electrode: a), b) Micrograph of the morphology of the Pb electrode, at different magnifications, after 1000 cycles at 10C; c), d) Micrograph of the morphology of the PbO_2 electrode, at different magnifications, after 1000 cycles at 10C.

On the Pb NWs electrode cycled at 10C in nanostructured lead-acid battery was carried out a quantitative XRD analysis at different number of cycles. The figures

3.8 a) and b) show the results of this analysis. In particular the image in figure 3.8a shows the spectrum of quantitative analysis after 500 cycles of charge/discharge and in this case there are 97.4% of lead sulfate and 2.6% of lead. In figure 3.8b are reported the spectrum of the quantitative analysis on Pb NWs electrode after 1000 cycles of charge/discharge and in this case, there are 100% $PbSO_4$, so all lead was converted in lead sulfate.

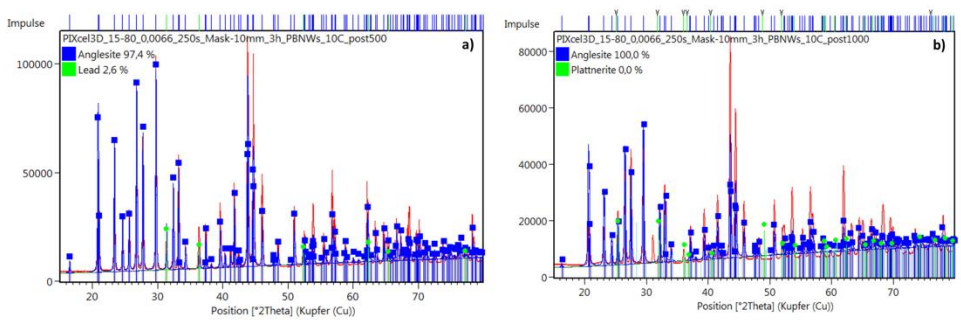

Figure 3.8 Spectra of quantitative XRD analysis on Pb NWs electrode after conditioning phase.

3.1.2 Performance of nanostructured lead-acid batteries at -20°C

A VWR cryostat was used to carry out tests at different temperature. The testing conditions used were the same as those set for 25 °C batteries: 1.2V cut-off, a C-rate equal to 10C and a total of 1000 charge/discharge cycles. The figure 3.9 shows the results obtained from the cyclization of nanostructured batteries at a temperature of -20 ± 2 °C. The figure 3.9a shows the charge/discharge curves of nanostructured batteries. With the increases of the number of cycles the increase in the discharge curve plateau occurs; greater is the horizontal line, greater will be the area under the curve and therefore the usable energy. From the charge and discharge curves it is possible to see that, despite the severe conditions to which the battery has been subjected, from 500^{th} up to 1000^{th} cycle, the behaviour remains almost unchanged and proves that with by increasing the number of cycles it is possible to obtain a constant plateau and therefore a constant capacity value of the device. The charge curves show a behaviour similar to that shown by the batteries cycled at 25 ± 2 °C. In fact an initial voltage value of around 3.2V was measured, probably also in this case due to the sudden change in the C-rate

of the battery, which decreases increasing the number of cycles. Unlike the battery cycled at 25 ± 2 °C in this case the charge curves show the typical trend of the PbO_2 electrodes. At temperature equal to -20 ± 2 °C a percentage efficiency of about 50% was detected, as shown in figure 3.9b, as opposed to a max value of 30% found with conventional batteries according to literature [29].

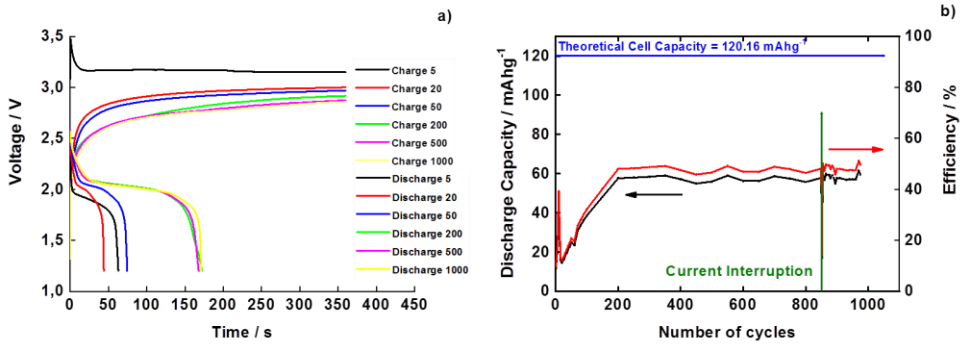

Figure 3.9 Electrochemical performance of nanostructured lead-acid battery operating at -20 ± 2 °C and 10C: a) Charging and discharging curves of different cycles; b) Cycling efficiency on discharging and discharge capacity of nanostructured.

Furthermore, at low temperature a layer of porous $PbSO_4$ is formed which, during charging, is converted into a porous mass of PAM consisting of small particles (<1.5μm) which agglomerate between them forming macro-pores. This type of structure creates a very large contact surface between the PAM and the electrolyte, guaranteeing good performance. After the tests in charge and discharge both the nanostructured electrodes were analysed by SEM to evaluate their morphology variations. In the figures 3.10 a) - d) it can see the results of this analysis for both nanostructured electrodes. The images 3.10a and b show the top view of the Pb nanostructured electrode. It is evident high porosity of the surphace generated by the cyclization of the nanowires. The SEM analysis on the PbO_2 nanostructured electrode was reported in the figures 3.10c and d. These images show a top view of the nanostructured PbO_2 electrode, it can note the presence of sulfate agglomerates (having a similar shape) with a size of about 10÷12 μm distributed on the whole surface, but in particular a highly porous surface is distinguished below the agglomerates.

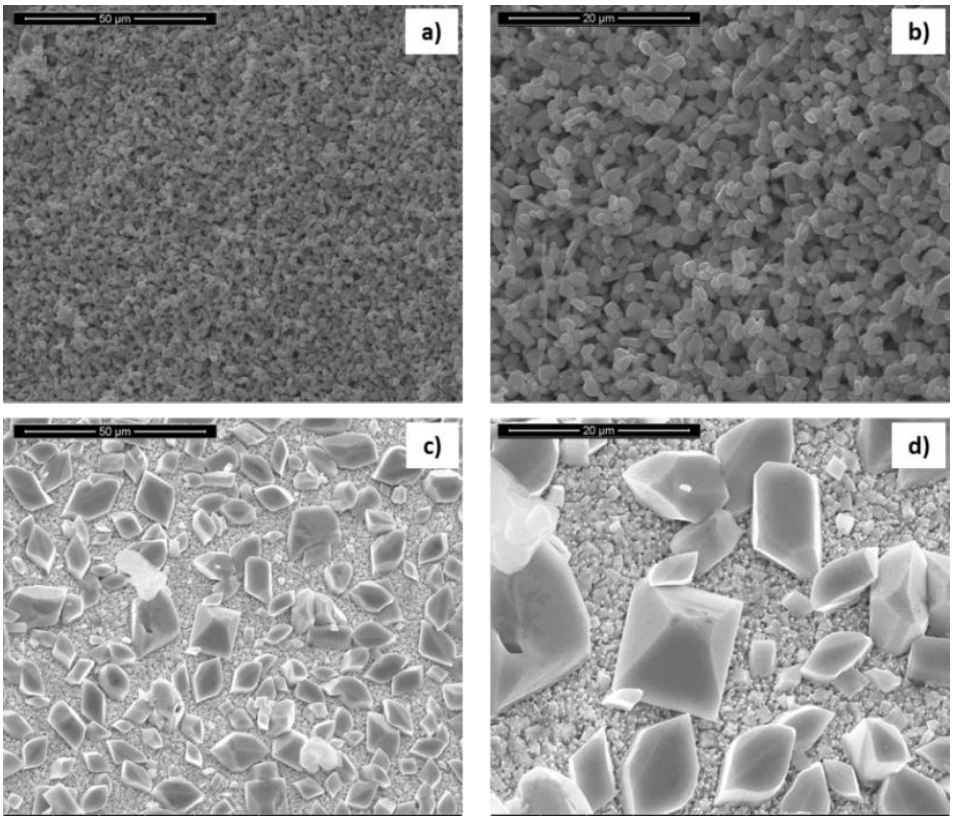

Figure 3.10 SEM images of Pb and PbO_2 NWs electrode: a), b) Micrograph of the morphology of the Pb electrode, at different magnifications, after 1000 cycles at 10C; c), d) Micrograph of the morphology of the PbO_2 electrode, at different magnifications, after 1000 cycles at 10C.

The result of this morphology confirms the trend of the charge and discharge curves shown above and confirms the possibility of diffusion of the electrolyte within the active mass, thus achieving better performance and longer lifetimes despite the critical conditions to which the batteries have been subjected.

3.1.3 Performance of nanostructured lead-acid batteries at 40°C

The tests at temperatures equal to 40 ± 2 °C on nanostructured batteries were performed with the same cryostat used for the tests at -20 ± 2 °C, moreover the

batteries were cycled under the same conditions used for the tests described above. The figure 3.11 shows the results obtained from this test.

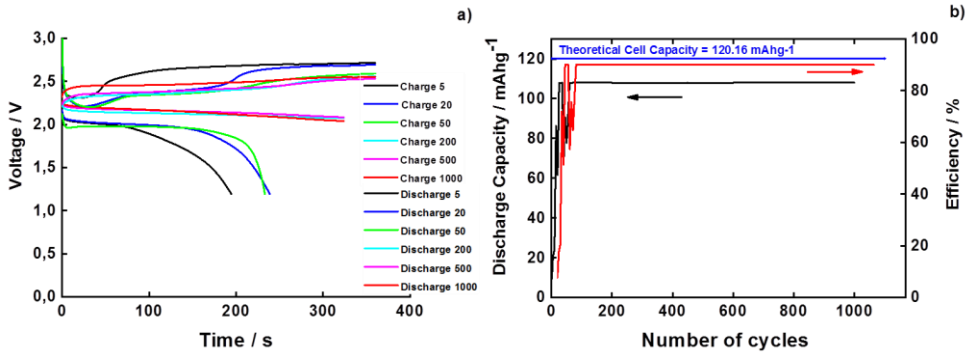

Figure 3.11 Electrochemical performance of nanostructured lead-acid battery operating at 40 ± 2 °C and 10C: a) Charging and discharging curves of different cycles; b) Cycling efficiency on discharging and discharge capacity of nanostructured.

When the number of cycles increases, the plateau of the discharge curves increases. At the 200th cycle, discharge capacity assumes a constant value, while discharge curves reaching a final voltage of about 2.1 V. This behaviour is totally different of that commercial battery, in fact, for the second one the performance decrease with the number of cycles increasing. Also in this case the charge curves have a high initial voltage value, around 2.7V, which decreases with the increase in the number of cycles. Moreover, it is possible to notice that the trend of these curves is the typical trend of the nanostructured lead electrodes, in fact same result were obtained in the case of tests conducted at a temperature of 25 ± 2 °C. Despite the process kinetics are accelerated by the high temperature, the charge curves do not have spikes in their course, which means that even at 40 ± 2 °C there is no excessive production of gas at the electrode-electrolyte interface, a phenomenon that could cause the breakage of the electrodes and then of the entire battery. The results obtained from the tests at a temperature equal to 40 ± 2 °C showed an efficiency of the batteries of 90%, as shown in the figure 3.11b. Thanks to the high temperature, which promote the reaction kinetics, the nanostructured batteries have reached a very high capacity value which allows to accumulate a much greater amount of energy compared to conventional systems under the same operating conditions. With the temperature the morphology of the electrode as the end of charge/discharge processes changes. At high temperatures,

the $PbSO_4$ layer becomes more compact, as reported in the literature [25, 30]. After electrochemical tests, both nanostructured electrodes were analysed by SEM to evaluate their morphology (figures 3.12 a) - d)). The morphology of Pb nanowires was considerably changed compared to the original one. The absence of the nanowires and the presence of large porous agglomerates of the size of about 15 μm are found. The morphology of the PbO_2 electrode is shown in the figures 3.12c and d. The initial morphology typical of NWs has been completely lost in favour of the formation of $PbSO_4$ crystals. The lead oxide electrode still has a porous morphology that allows the electrolyte to penetrate the active part and therefore allow the battery to function for further charging and discharging cycles at high C-rate.

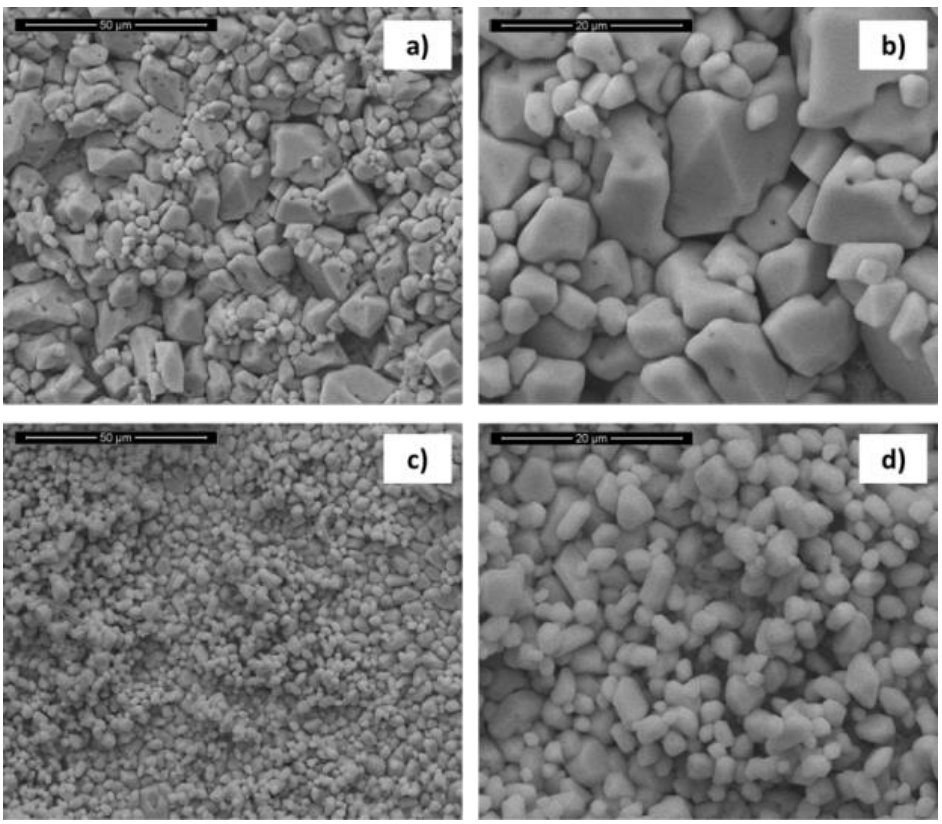

Figure 3.12 SEM images of Pb and PbO_2 NWs electrode: a), b) Micrograph of the morphology of the Pb electrode, at different magnifications, after 1000 cycles at 10C; c), d) Micrograph of the morphology of the PbO_2 electrode, at different magnifications, after 1000 cycles at 10C.

3.1.4 Comparison of the results obtained from nanostructured batteries cycled at different temperatures

The figure 3.13a shows the comparison between the charge curves of the batteries at different temperatures. In all cases the battery maintains a voltage lower than 3V and do not have spikes that would indicate the production of gas at the electrodes surface.

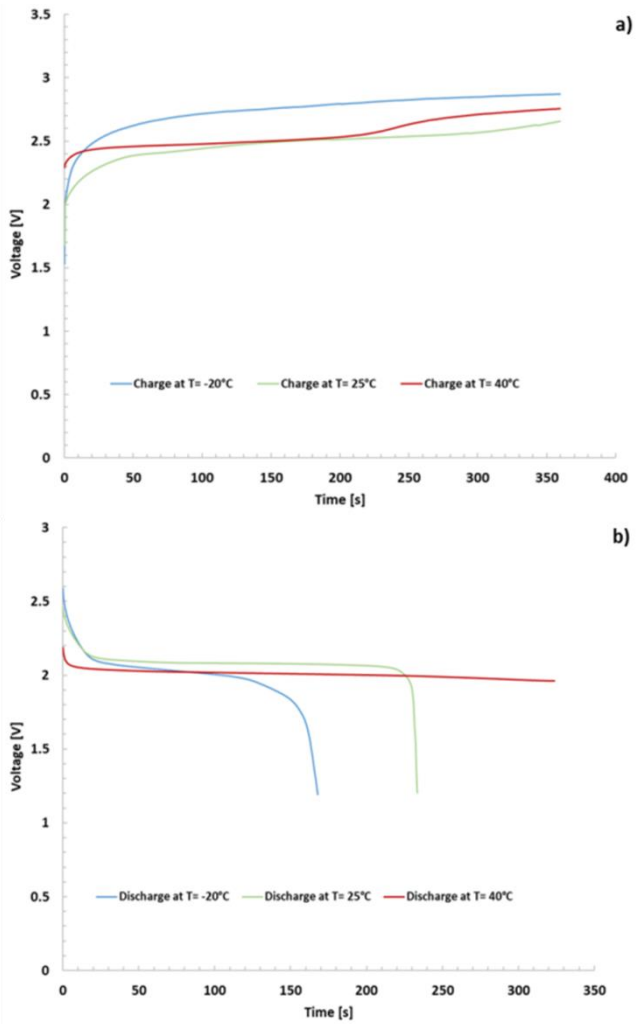

Figure 3.13 Comparison between charge and discharge curves at different temperatures: a) Charge curves at -20 ± 2 °C, 25 ± 2 °C and 40 ± 2 °C; b) Discharge curves at -20 ± 2 °C, 25 ± 2 °C and 40 ± 2 °C [11].

In the figure 3.13b the relative discharge curves are reported and a progressive increase of the plateau of the discharge curves is noticed by the increase of the temperature. This increase indicates a greater usable energy of the battery, and therefore a greater efficiency of the latter [31]. In particular, for the discharge curve relative to the temperature of 40 ± 2 °C, the cut-off is no longer reached. This means that the efficiency of this battery has reached 90% and therefore all the capacity of the battery can be translated into usable energy. The discharge curves remain constant for the whole duration of the cyclization at all three set temperatures, but different levels of efficiency were reached. In particular efficiency battery increases with the temperature. A maximum efficiency reached at -20 ± 2 °C is about 50%. This is a very satisfactory result if compared to the maximum efficiency value of conventional lead-acid batteries that in optimal operating conditions is 30 %. The resume of the results of the cyclization at the various temperatures is shown in table 3.2. The maximum efficiency increases with the temperature, in fact a value of efficiency equal to 90% at a temperature equal to 40 ± 2 °C was reached. The figures 3.14 a) - c) and the figures 3.15 a) - c) show Pb nanostructured electrodes and PbO_2 nanostructured electrodes after testing at different temperature.

Performance	**Working Temperature**		
	T = 25 ± 2 °C	***T = -20 ± 2 °C***	***T = 40 ± 2 °C***
C-rate	1C (Conditioning phase; complete discharge in 1 h) 10C (Complete discharge in 6 minutes)	10C (Complete discharge in 6 minutes)	10C (Complete discharge in 6 minutes)
Efficiency of discharge	77% at 1C 88.7% at 10C	50%	90%

Curves of discharge	Increase of the plateau with number of cycles	Increase of the plateau with number of cycles	Increase of the plateau with number of cycles
Cycle life	>1000	>1000	>1000

Table 3.2 Performance of nanostructured cells at different temperature.

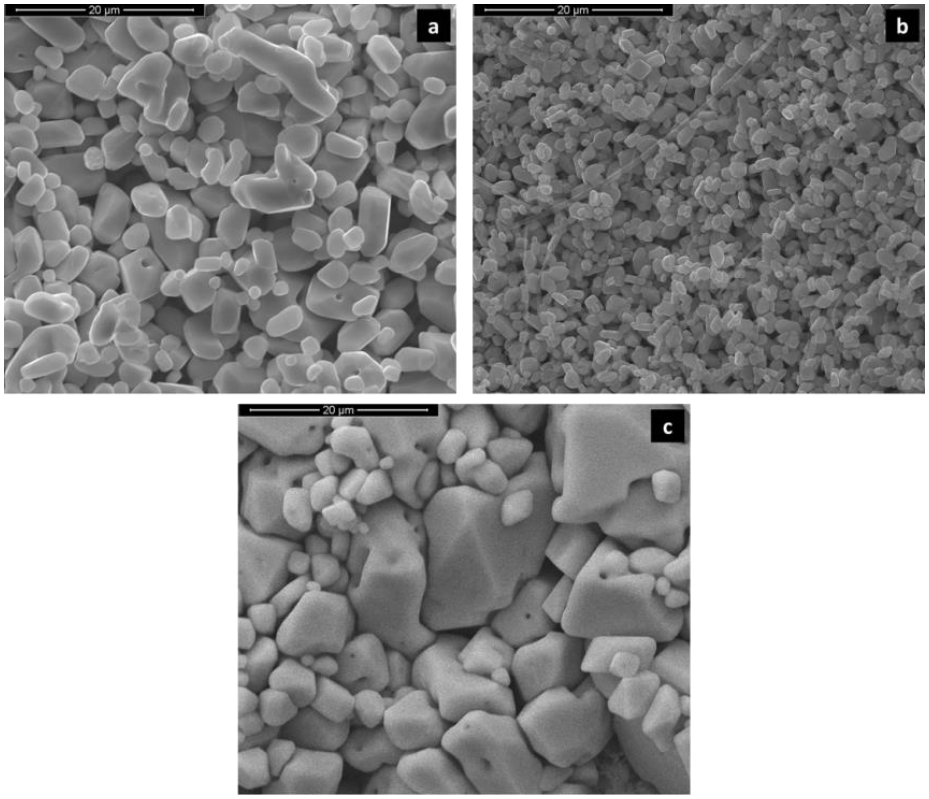

Figure 3.14 SEM images of Pb NWs electrode post-cycling: a) Micrograph of the morphology of the Pb electrode, at T= 25 ± 2 °C after 1000 cycles at 10C; b) Micrograph of the morphology of the Pb electrode, at T= -20 ± 2 °C after 1000 cycles at 10C; c) Micrograph of the morphology of the Pb electrode, at T= 40 ± 2 °C after 1000 cycles at 10C.

In the figures 3.14 a, b, c, Pb electrode, the formation of lead sulfate crystals of different sizes is clear visible on the surface of the electrode, in particular there is

a decrease in the average grain size with the decrease of temperature. However, the surface of the post-cycling electrode at different temperatures remains highly porous and allows the electrolyte to penetrate into the active mass and therefore the use of electrodes for further charge/discharge cycles at high C-rates.

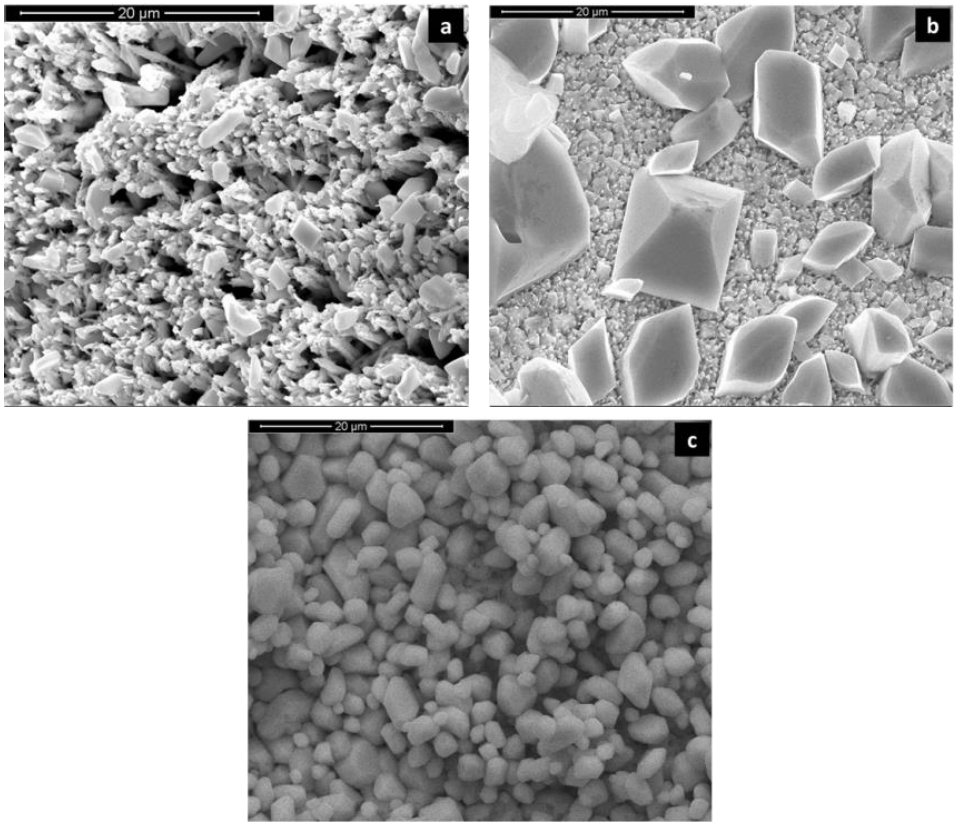

Figure 3.15 SEM images of PbO_2 NWs electrode post-cycling: a) Micrograph of the morphology of the PbO_2 electrode, at T= 25 ± 2 °C after 1000 cycles at 10C; b) Micrograph of the morphology of the PbO_2 electrode, at T= -20 ± 2 °C after 1000 cycles at 10C; c) Micrograph of the morphology of the PbO_2 electrode, at T= 40 ± 2 °C after 1000 cycles at 10C.

The PbO_2 post-cycling electrodes (figures 3.15 a) - c)) have a very variable morphology as the operating conditions vary. In all cases the presence of small sulphate crystals distributed over the entire surface of the electrode can be observed. From the micrographs of the nanostructured lead and lead oxide electrodes we note that the formation of lead sulfate on the surface of the

electrodes never appears as a compact layer, but rather as a set of granules that give the electrode a good porosity, which allows battery operation even after 1000 charge/discharge cycles.

3.1.5 Nanostructured lead-acid batteries at different C-rate

The nanostructured lead-acid battery, after the tests reported above, was cycled at the highest C-rate, in fact, we tested this battery at C-rate from 10C to 30C. Furthermore, we designed a 6V nanostructured lead-acid and we compared its performance with the performance of a commercial lead-acid battery.

- ***Performance at C-rate from 10C to 30C***

On the nanostructured lead-acid batteries were carried out a test at very high C-rate (from 10C to 30C). The figures 3.16 a) – d) show the charge/discharge curves of nanostructured lead-acid battery at different C-rate. In all cases there is not excessive gas evolution, even if at high C-rate (from 6 min. to 2 min. to have a complete charge), in fact in all plots the charge curves have a regular trend without spikes. Also the discharge curves have a regular trend and show an increase of their plateau with increasing in number of cycles, that means an increase in the usable energy with the utilization of the battery. In particular, it is possible to see that in the figure 3.16 d, the discharge curves, from 600^{th} cycle until the end of life of the battery (after 7500 cycles of charge/discharge) have a flat trend, never obtained with current commercial lead-acid batteries. In the figure 3.17 a) and b) the discharge efficiency of the battery cycled at different C-rate is reported. In the figure 3.17a it can be seen that there is an increase of the efficiency with the increase of the C-rate. The battery reaches an efficiency equal to 90% after 300 cycles at 30C and maintains this value constant for all its life.

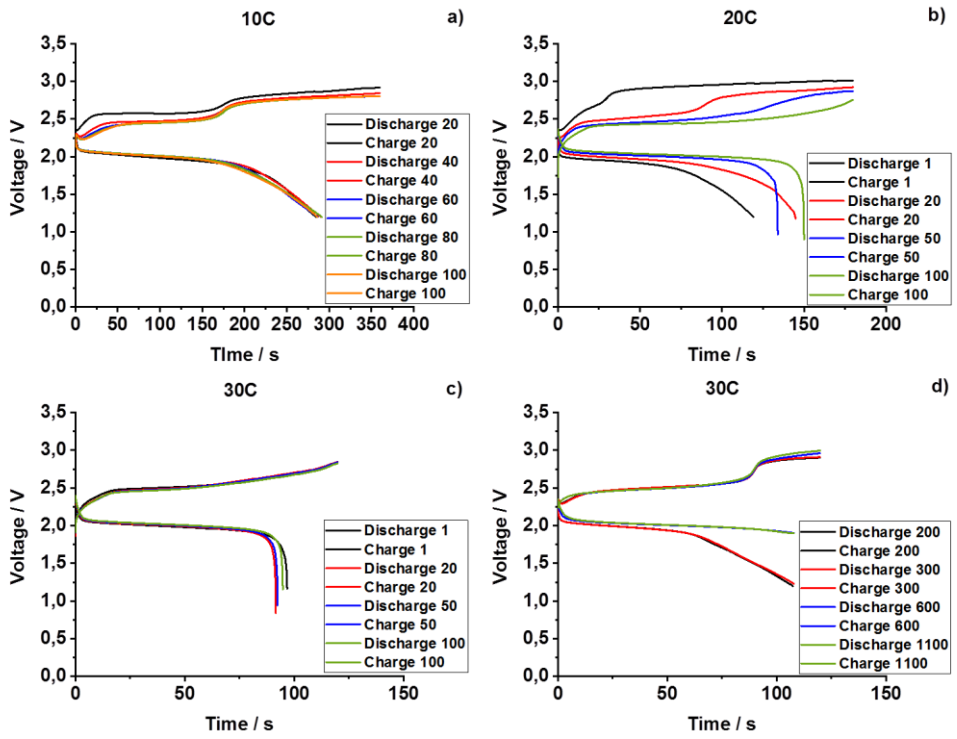

Figure 3.16 Charge/discharge curves at different C-rate: from 10C to 30C.

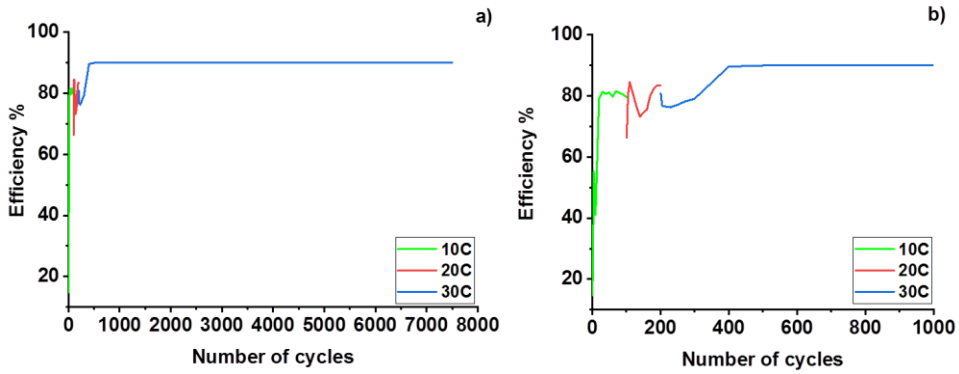

Figure 3.17 Efficiency of nanostructured lead-acid battery from 10C to 30C.

The figure 3.17b shows a magnification of efficiency plot and in this it is possible to see the maximum values of efficiency obtained at 10C and 20C. In particular at

10C the battery reaches a maximum value of efficiency equal to 81.6%, and at 20C the battery reaches a maximum value of efficiency equal to 84.4%.

Other tests carried out on the nanostructured lead-acid batteries are based on asymmetric conditions of charge and discharge. In particular after conditioning phase, the charge was carried out at 10C, 20C and 30C, while the discharge was carried out at 1C. The figures 3.18 a) and b) show the discharge efficiency of this battery.

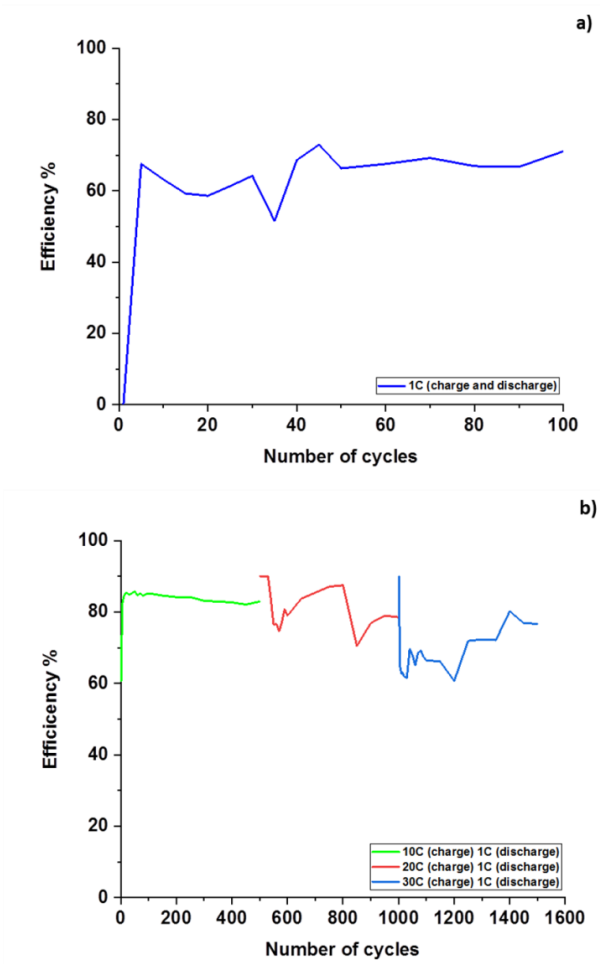

Figure 3.18 Discharge efficiency of nanostructured lead-acid battery: a) Discharge efficiency in conditioning phase (charge and discharge at 1C); b) Discharge efficiency in asymmetric conditions of charge and discharge.

The maximum efficiency reached in the conditioning phase is about 70%. During the charge/discharge cycles a maximum efficiency value about of 86% was obtained with a charging regime at 10C and a discharge regime at 1C; with a charging regime at 20C and a discharge regime at 1C the maximum value of efficiency is about 87.5% and for a charge at 30C and discharge at 1C, the value of efficiency is about 80%.

- ***Performance of 6V prototype***

The 6V nanostructured prototype was also designed and tested. This prototype was made with three nanostructured PbO_2 electrode, three nanostructured Pb electrode, commercial AGM separators and aqueous sulfuric acid 5M as electrolyte. The prototype was cycled at C-rate equal to C/5 (5 h of charge), 1C (1 h of charge) and 2C (30 min of charge). The performance obtained from our prototype were compared with performance of a commercial lead-acid battery (FIAMM FG10121). The figures 3.19 a) and b) show the nanostructured lead-acid battery and commercial lead-acid battery used for this test.

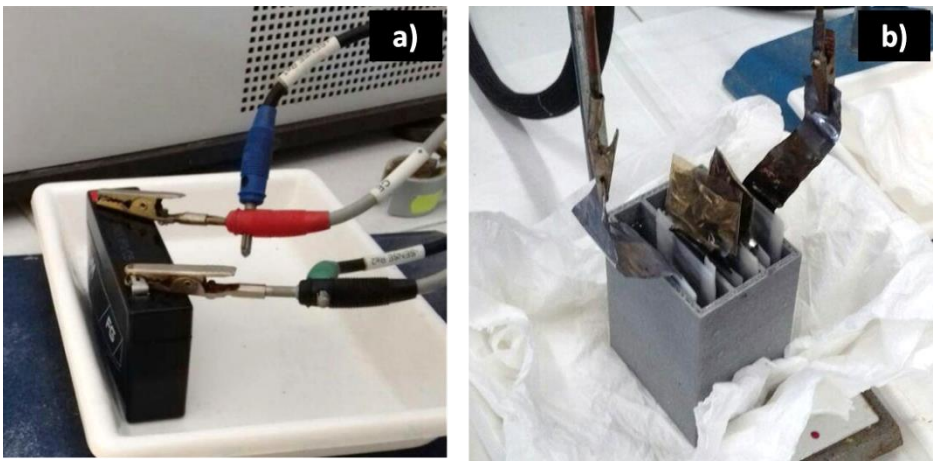

Figure 3.19 6V batteries: a) Commercial lead-acid battery FIAMM FG10121; b) Nanostructured lead-acid battery.

The figures 3.20 and 3.21 show the charge/ discharge curves of commercial (figure 3.20 a) - c)) and nanostructured lead-acid battery (figure 3.21 a) - c)). The charge curves of commercial battery, shown in the figures 3.20, have an almost regular trend without spikes. The discharge curves have a decreasing of their

plateau with increasing of cycle number, so there is a lower usable energy as we use the battery. Probably this trend is due to the formation of a non-conductive layer on the battery commercial plates during discharge reactions, that reduces the active material available for charge and discharge reaction. Furthermore, at C-rate equal to 2C, so 30 minutes of charge, the battery is quasi unusable after 20 cycles of charge and discharge.

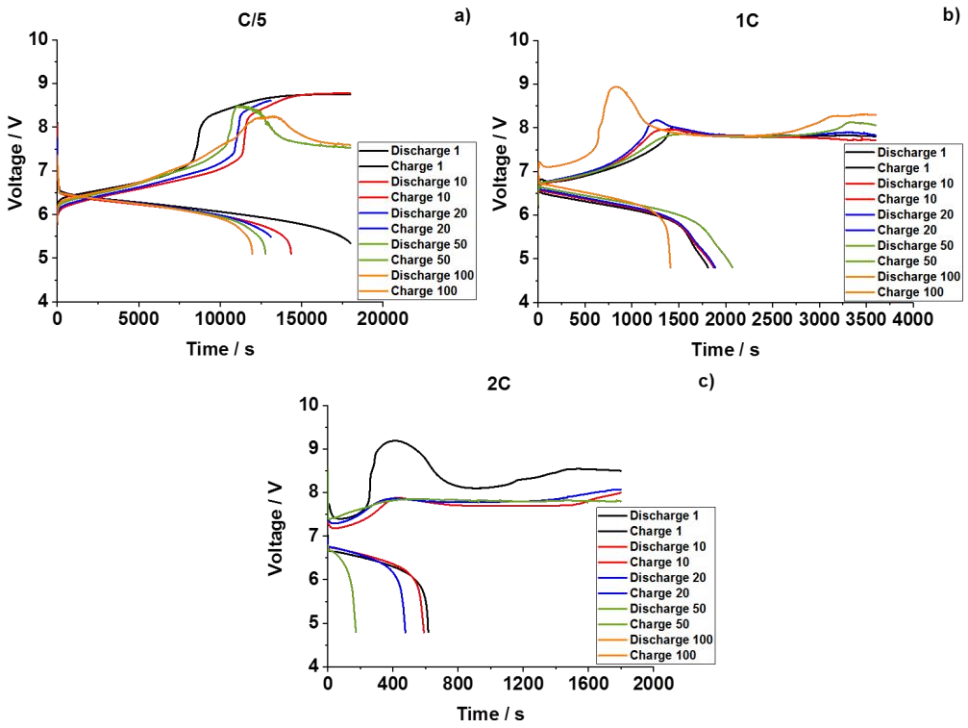

Figure 3.20 Electrochemical performance of lead acid battery operating at 25 ± 2 °C and different C-rate: a) Charging and discharging curves at C/5; b) Charging and discharging curves at 1C; c) Charging and discharging curves at 2C.

The performance of nanostructured lead-acid battery was shown in the figures 3.21 a) - c). In these plots it can be observed that the charge curves are almost regular and in some cases, there is gas evolution but this is not damaging the nanostructures electrodes. Also the discharge curves are regular and there is an increase in their plateau, differently of commercial battery, that means an increase in usable energy. This behaviour is due to the high porosity of nanostructured electrodes that avoid the formation of a non-conductive compact layer of $PbSO_4$

and maintaining a high surface area and then a high value of active material available for charge/discharge reaction. Furthermore, at high C-rate (1C and 2C) the discharge curves have a plateau horizontal, quasi-ideal behaviour, with a drop of voltage value only at the end of discharge.

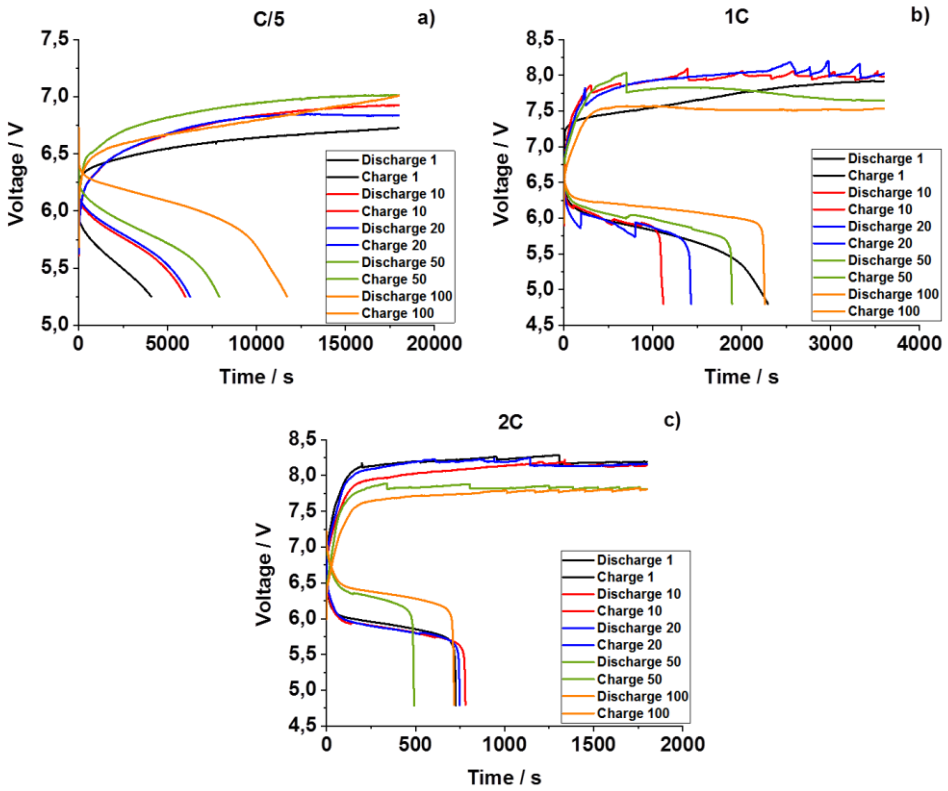

Figure 3.21 Electrochemical performance of nanostructured lead acid battery operating at 25 ± 2 °C and different C-rate: a) Charging and discharging curves at C/5; b) Charging and discharging curves at 1C; c) Charging and discharging curves at 2C.

The figures 3.22 a) and b) show the plots efficiency of commercial and nanostructured lead-acid batteries. From the figure 3.22a it can be see the decreasing in the discharge efficiency of commercial lead-acid battery with increasing of the C-rate, in fact at C-rate equal to 2C the battery reach an efficiency equal to 0% after around 20 ÷ 30 cycles of charge and discharge. The values of the efficiency of nanostructured prototype (figure 3.22b) are, in this particular case, comparable with the values of the efficiency of commercial lead-

acid batteries because the number of cycles were done by battery are not enough to stabilize the performance of nanostructured battery, it needs more than 100 cycles to stabilizes its performance. The performances of 6V nanostructured prototype are lower than the 2V prototype and this depends by the low C-rate of the 6V battery, in fact, this type of batteries have better performance at high C-rate (as 10C, 20C...).

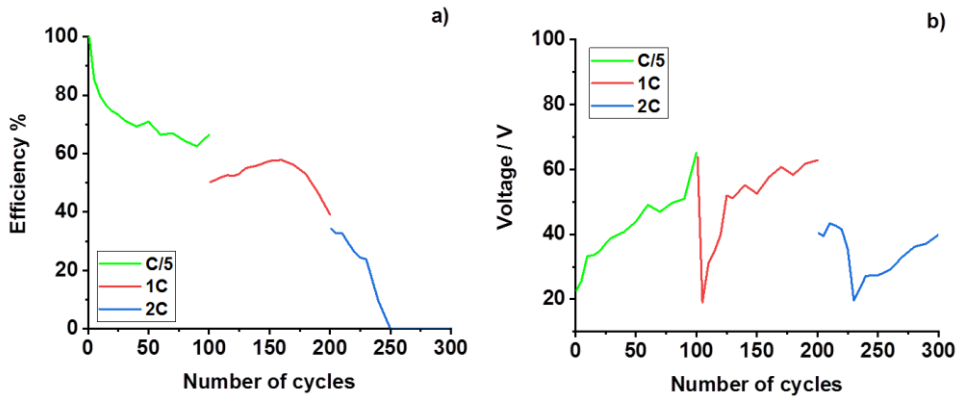

Figure 3.22 Efficiency of lead-acid battery from C/5 to 2C: a) commercial lead-acid battery; b) Nanostructured lead-acid battery.

After cyclization in both of electrode was carried out the quantitative XRD analysis to evaluate the quantitative of lead sulfate in both cases. The figures 3.23 a) and b) show the spectra of this analysis.

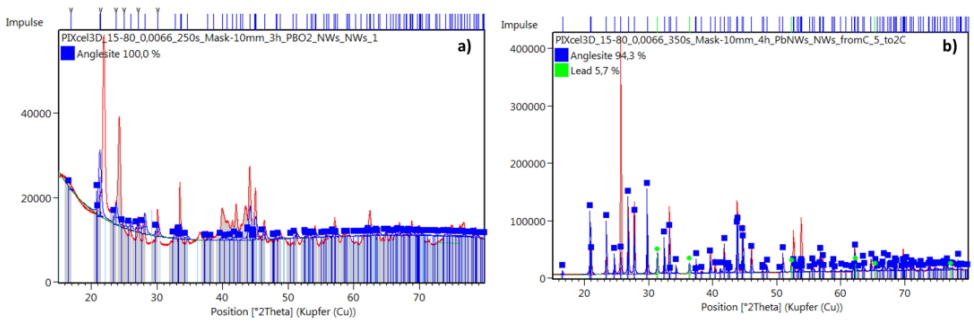

Figure 3.23 Spectra of quantitative XRD analysis on PbO_2 NWs (a) and Pb NWs (b) electrode after cyclization at different C-rate.

The PbO_2 NWs electrode is completely converted in $PbSO_4$ after cyclization, in fact the quantitative analysis show a percentage of lead sulfate equal to 100%, while the Pb NWs is not completely converted and in this case there are an amount of $PbSO_4$ equal to 94.3% and an amount of Pb equal to 5.7%.

3.2 Gelled electrolyte

Polymeric gel electrolytes are often swollen polymer networks, so they possess both the cohesive properties of solids and the properties of the liquids from the point of view of diffusive transport. Thanks to this dual behaviour, gel electrolytes can be used in a wide variety of electrochemical devices. However, their mechanical strength is quite low; for this reason various additives are often used to improve their mechanical stability. In 1975, Feuillade and Perche (1975) produced a gel with a high ionic conductivity (similar to that of the liquid electrolytes) by adding an aprotic solution containing alkali metal salts to the polymeric matrices [32]. In this paragraph, PVA-based hydrogels were made to be used as gel electrolytes in lead-acid battery assembled with nanostructured electrodes. PVA hydrogel preparation, using the freeze-thaw technique, was first reported by Peppas (1975) [33]. In his work, aqueous solutions of PVA (between 2.5 and 15% weight/volume) were frozen at -20 ± 2 °C and then thawed at room temperature. The crystallites formed after this procedure have been characterized by measurements of the turbidity of PVA samples. It has been observed that crystallinity increases with the duration of freezing, instead, during thawing, the crystalline size initially increases and then decreases. This may be due to the breaking of the crystalline structure. After this work, numerous researches have been conducted the production of hydrogels through this technique [34], [35]. The crystallization of the PVA hydrogels was discussed in detail by Bunn (1948) [36]. PVA chains form small sized ordered regions (crystallites) randomly distributed into an amorphous polymeric matrix. The degree of crystallinity, as well as the size of the crystallites, depends on the conditions under which drying takes place [37].

3.2.1 Gelled electrolyte for nanostructured lead-acid batteries

- ***Preparation of hydrogels***

The hydrogels are based on PVA and were prepared by two different techniques. The first one consists in the fabrication of a gel through a "physical gelling", while the second one consists in the preparation of the gel through a "chemical gelling" process. The first step of the preparation of both hydrogels consists in the preparation of a 10% (w/v) PVA aqueous solution. In order to produce the hydrogel by "physical" cross-linking method, the solution was cooled to room temperature, then it was kept at -20 ± 2 °C for 24 h during which the hydrogel was formed, which was stabilized at room temperature for further 24 h [38]. The hydrogel obtained with this method is shown in figure 3.24.

Figure 3.24 Hydrogel obtained with one cycle of freezing – thawin [12].

The second type of hydrogel was produced by using borax (sodium tetraborate decahydrate, $Na_2B_4O_7$ * 10 H_2O) as a cross-linking agent. An aqueous PVA solution and 4% (w/v) borax aqueous solution were prepared. The borate ions $B(OH)_4^-$ reacted with the hydroxyl groups of the PVA generating weak transversal bonds between the polymer chains with the formation of a viscous and elastic hydrogel. The figure 3.25 shows the hydrogel obtained with this method.

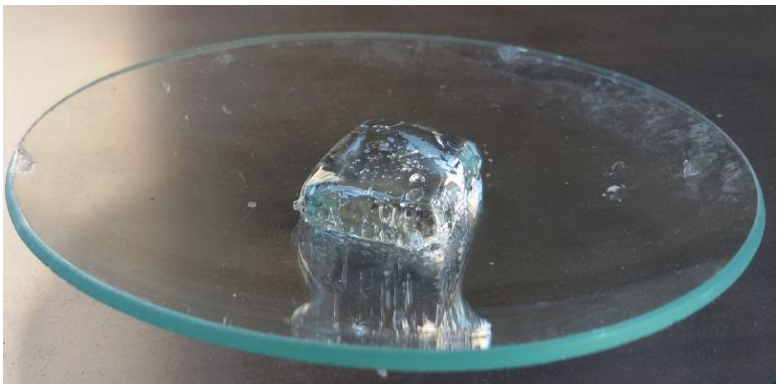

Figure 3.25 Hydrogel PVA – borax [12].

For the sake of simplicity, in the following, the two types of hydrogel will be identified as physical hydrogel and borax hydrogel. Both the types of hydrogels were dried in an oven for 24 h, at a temperature of 40 °C, and then were ground to dust, showed in the figure 3.26.

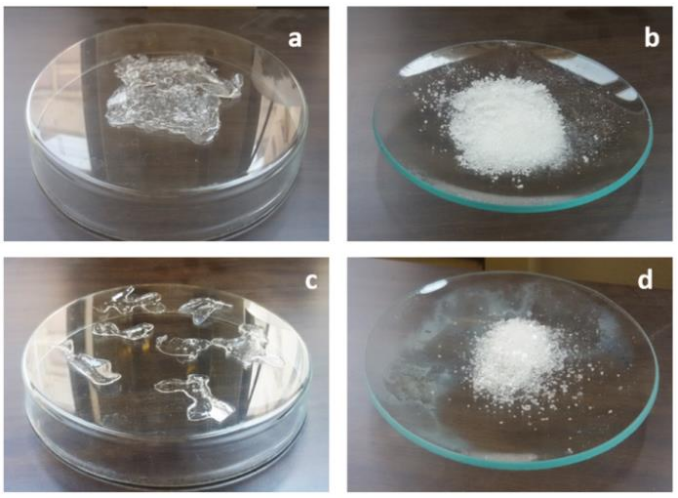

Figure 3.26 Different types of hydrogels: a) and b) Hydrogel obtained through a freezing cycle - dry and ground thawing, c) and d) PVA hydrogel - dry and ground borax [12].

Tests of swelling of the hydrogel powders were conducted in 5 M sulfuric acid (the electrolyte used in the lead acid battery) to evaluate their absorption capacity. It has been found that 1 g of physical hydrogel absorbs 2.95 g of acid, while 1 g

of borax hydrogel can absorb 1.7 g. Of course, this difference results in different performance of the battery. The gels obtained were used as electrolyte in nanostructured lead-acid batteries.

- ***Performance tests***

The electrochemical cell simulating a lead acid battery was assembled with nanostructured PbO_2 and Pb electrodes separated by a layer of hydrogel acting as an electrolyte and a separator for avoiding short circuit. Before testing, the nanostructured electrodes were dipped in 5 M sulfuric acid in order to soak the porous mass. To find the influence of the immersion time on the battery performance, the electrodes were immersed for different times from 24 hours to five days. After extraction from the sulfuric acid, additional acid was poured on the electrodes. Finally, one surface of both PbO_2 and Pb electrodes was spread by the hydrogel powder, which immediately swelled up owing to absorption of sulfuric acid. In this way, the electrolyte, in the form of swollen hydrogel, adhered perfectly to the two electrodes, which were coupled in a zero gap configuration. Nanostructured electrode capacity was determined through gravimetric measurements. All tests were conducted at a constant current of 1C and room temperature, with a cut-off potential of 1.2 V. Since the Pb and PbO_2 electrodes have different capacity, the 1C-rate was referred to the PbO_2 mass. Besides, the discharge time was set at 90% of 3600 s, so that a part of Pb and PbO_2 remained unconverted. This is beneficial for the negative electrode, because its real C-rate is a little less than 1C, which is evaluated according to the mass of PbO_2. In such a way, the total sulfation of the electrodes on cycling is avoided. The figure 3.27 shows the cycling efficiency and specific drained charge as a function of the number of cycles when the two types of hydrogel are employed as electrolytes. For comparison, the same curves are shown when the liquid electrolyte was used (figure 3.27c). The curves of figure 3.27 show, first of all, a significant difference when liquid electrolyte is replaced by the gelled one. In addition, it is evident that physical hydrogel guarantees better performance than the borax one. In particular, the battery equipped with the physical hydrogel achieved an efficiency of about 70% from 40th to 80^{th} cycle followed by fast decay, while the battery with borax hydrogel achieved the maximum efficiency of about 45% in the initial cycles, followed by a very fast decay. The different behaviour under cycling of the two hydrogels can be attributed to the higher amount of acid absorbed by the physical hydrogel.

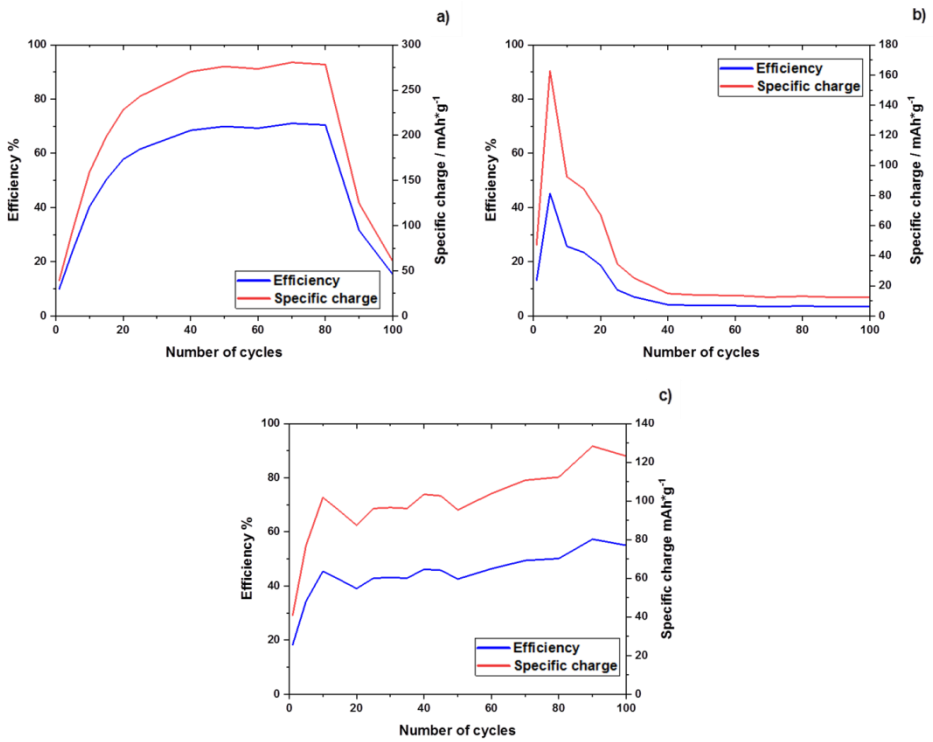

Figure 3.27 Cycling efficiency and electrical charge drained vs. cycle number at 1C and room temperature for a cell with: a) physical hydrogel; b) borax hydrogel; c) liquid electrolyte. Before cycling, electrode was held for 5 days in 5 M H_2SO_4.

The rapid falling-off of the battery performance at low cycle number is due to different causes. The most probable decay of the battery may be due to an unfinished design of the cell, where a progressive flow down of the hydrogels occurs because the electrodes are not permanently blocked in the initial zero-gap configuration. Under cycling, electrodes can move each other with consequent loss of the zero-gap configuration. The electrodes are vertically assembled, therefore, when the distance between them increases, the hydrogel layer can freely flow down, leaving the superior part of the electrode uncovered, which, consequently, stops to work. In practice, tiny, little motions of the electrodes from the zero-gap assembly favour the slow dropping down of the hydrogel with consequent shortening of the lifetime of the battery. The more research activity is in progress aimed to improve the time life of battery equipped with PVA physically gelled, because the challenge appears of great value in comparison

with a battery using a liquid electrolyte. Figure 3.27 also evidences that the physically gelled electrolyte shows a more favourable behaviour than a battery with liquid electrolyte. The weak point is the short lifetime, which can be extended by improving the cell design. Figure 3.28 shows the charge/discharge curves of cells equipped with physical and borax hydrogels. The comparison between figure 3.28 a) and b) confirm the poor performance of the cell with borax hydrogel evidenced by the decreasing of the drained charge from the 40th cycle onwards. Therefore, the stored energy that can be used is irrelevant. On the contrary, far better performance is shown in the cell equipped with physical hydrogel. From the charge/discharge curves, it is clear that the performance of the batteries with the first type of hydrogel turned out to be better: the discharge curve plateau, which represents the range of use of the device, is quite pronounced up to the 50th cycle. The fact that in the last few cycles the performance of the battery collapsed because of the mechanical stability of the hydrogel: the electrolyte in contact with the electrodes gradually fell by gravity until some areas of the electrodes remained without electrolyte, causing the sudden deterioration in performance.

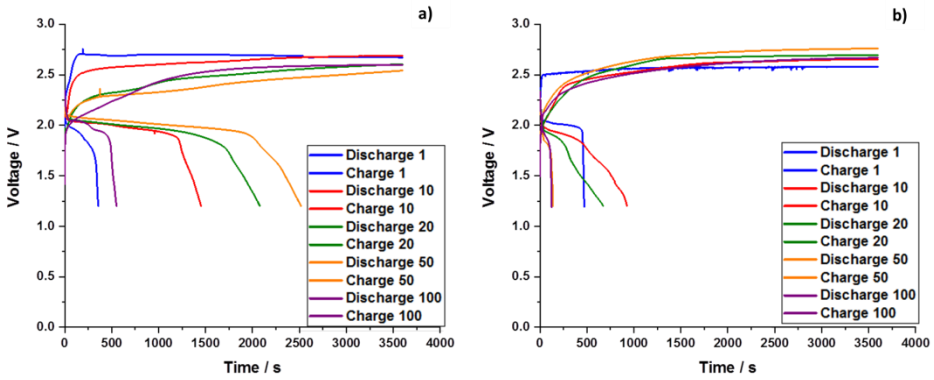

Figure 3.28 Charge/discharge curves at 1C and room temperature of a battery with: a) physical hydrogel; b) borax hydrogel.

At the end of the cycling, the Pb and PbO_2 electrodes that had worked with either physical or borax hydrogel were analysed by SEM (figure 3.29 a) - d)) to evaluate how their morphology had changed as a result of cyclization.

Figure 3.29 shows that under cycling the original nanowires has been lost, replaced by particles that guarantee high porosity. The morphology change is not

due to the presence of the hydrogel, because identical modification has been observed in Pb and PbO_2 cycled in no gelled electrolyte how we saw in the previous chapters. The capability of the battery with gelled electrolyte to restore the water split in oxygen and hydrogen during charging was also investigated. A gas meter coupled with the cell was used to check gas production under charging. It was found the practical absence of gas production, so that battery with gelled electrolyte avoids water consume under cycling that is one of the principal disadvantages of the commercial lead-acid battery with liquid electrolyte.

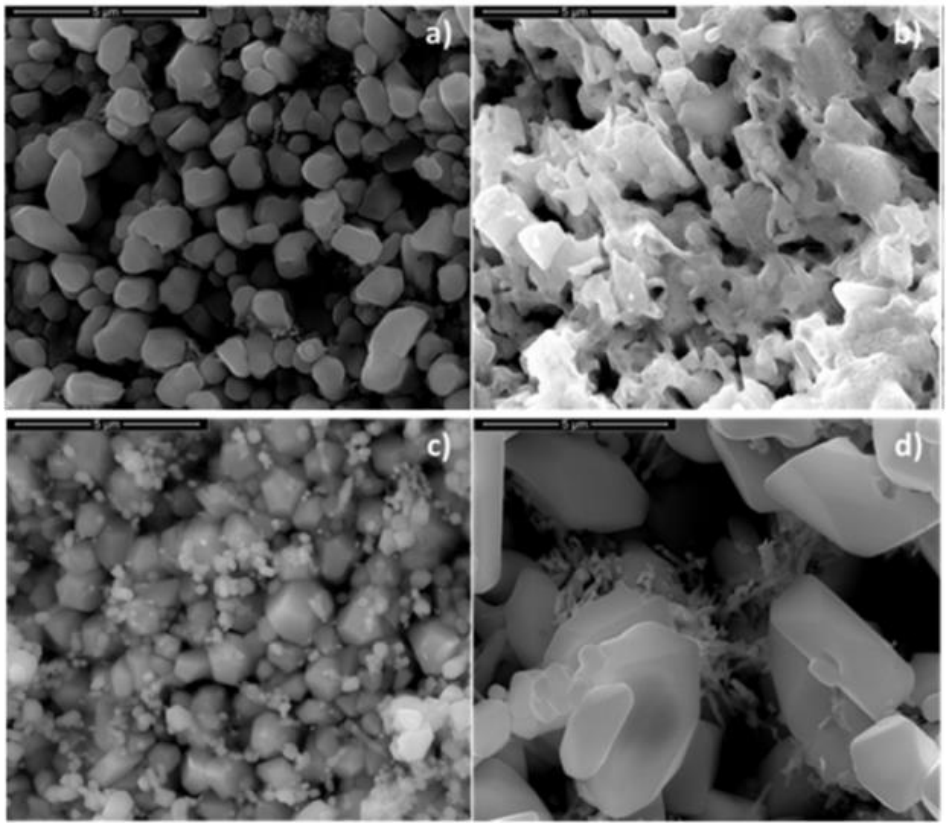

Figure 3.29 a) and b): SEM images of Pb and PbO_2 electrodes, respectively, cycled in contact with physical hydrogel. c) and d) SEM images of Pb and PbO_2 electrodes, respectively, cycled in contact with physical hydrogel. Cyclization was conducted at 1C and room temperature.

The cell used for this analysis is reported in the figure 3.30.

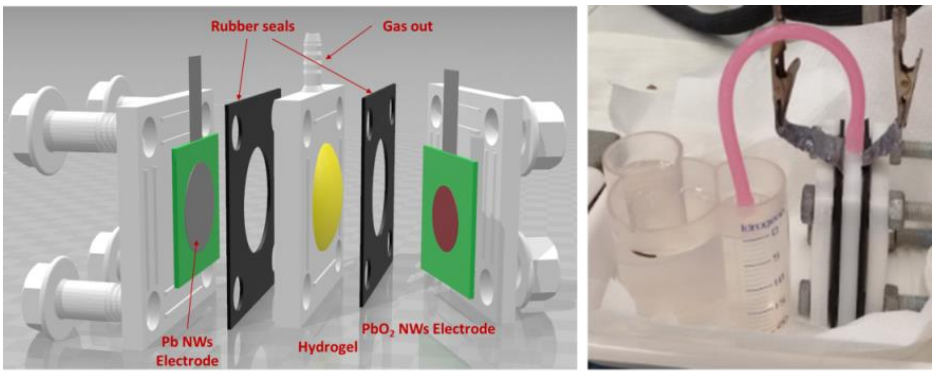

Figure 3.30 Cell used for checking gas evolution

- ***Characterization of hydrogels***

After drying of the gelled PVA, SEM analysis revealed an average grain size of 1.82 mm and 1.064 mm for the borax and physical hydrogel, respectively. The figure 3.31 shows the SEM images of the two types of hydrogel, and evidence that the borax hydrogel is more compact than the physical one, so that it is less suitable to absorb 5 M sulfuric acid. Therefore, the different swelling behaviour of the two types of hydrogel can be attributed to their more or less compact structure. The PVA powder used to produce the hydrogels was initially characterized by XRD to determine its crystallinity. The XRD patterns were compared with those of the two types of hydrogel before and after their use of a cell simulating a lead-acid battery. The figure 3.32 shows that the XRD pattern of no gelled PVA has three characteristic peaks ($2\theta = 13.5°$, $2\theta = 19.8°$, $2\theta = 22.5°$) that correspond to the crystalline regions of the PVA. The peaks agree with the findings by Seong et al. (2017) [39]. The most relevant results showed in figure 3.32a are: i) the invariance of the crystallinity after the physical gelling process, and ii) the appearance of a wave in place of the peaks at $2\theta = 19.8°$, $2\theta = 22.5°$ indicating some modification of the physical hydrogel under cycling. On the contrary, the borax hydrogel appears more amorphous than the no gelled PVA. Such a structural change is evidenced in figure 3.32b by the enlargement of the band at $2\theta=13.5°$ and the sharp weakening of the peak at $2\theta=19.8°$. Besides, figure 3.32b shows that XRD pattern of the hydrogel has the same trend of the no gelled PVA, therefore, the hydrogel has not incorporated borax. This conclusion is also supported by the absence of the most intense peak of the borax at $2\theta = 34.882°$. Also the borax hydrogel became more amorphous under cycling like the

physical hydrogel. This behaviour can be attributed to the absorption of the free sulfuric acid, which was added to the cell as a reservoir of electrolyte.

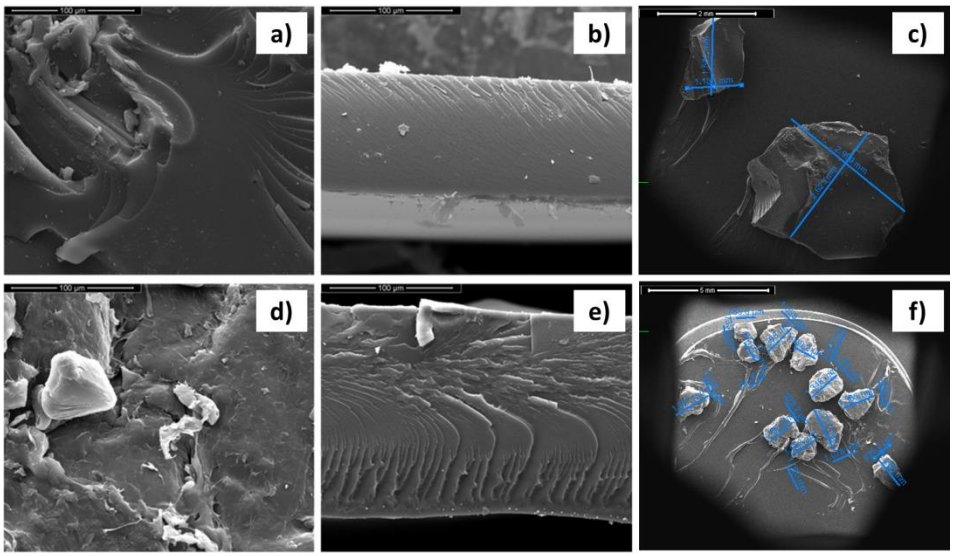

Figure 3.31 SEM images of dried hydrogels: a) powder of borax gelled PVA; b) section view of borax gelled PVA; c) grains measures of borax gelled PVA powder; d) powder of physically gelled PVA; d) section view of physically gelled PVA; e) grains measures of physically gelled PVA powder.

This is a crucial aspect for guaranteeing the long life of the gelled electrolyte and correct working of the battery. Water is consumed during overcharging, even if it is restored like in commercial battery equipped with gelled electrolyte. Since the total water loss under cycling cannot be exactly evaluated in advance, it is a precautionary approach to add free 5 M sulfuric acid in order to replenish the lost water. The major risk associated with water loss is the progressive drying of the hydrogels with their permanent damage, and consequently out of service of the battery. Another significant feature of the hydrogels is their chemical inertness evidenced in the present work by the absence of any incorporation of Pb and PbO_2 in the hydrogels at the end of cycling.

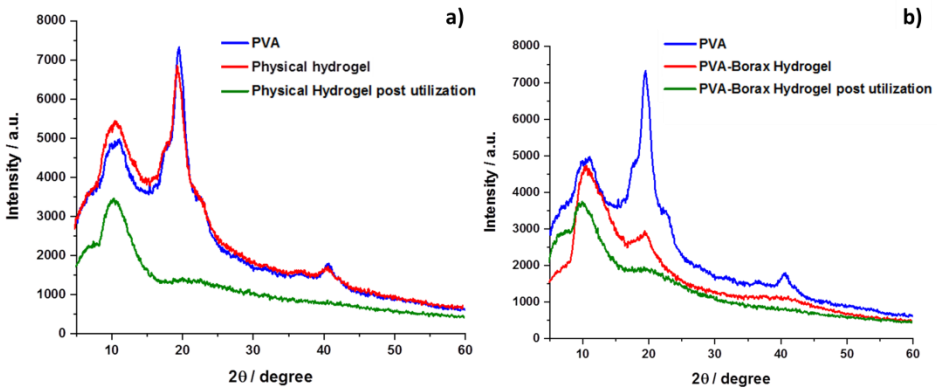

Figure 3.32 Results of XRD analysis on hydrogels: a) XRD pattern of PVA powder compared with physical hydrogel powder before and after its use as an electrolyte; b) XRD pattern of PVA powder compared with borax gelled powder before and after its use as an electrolyte.

3.3 Financial investigation

During the PhD period, a comparison was made between the performance of nanostructured batteries and commercial batteries in order to explore the possibility of a technology transfer, starting from the good laboratory results. A technology transfer activity was therefore launched with the aim of identifying the operational advantages of nanostructured batteries and being able to build a Canvas business model based on the potential of the system studied at the laboratory level. It is a "Business Model", as the activity is aimed at highlighting how value can be created up to profit by moving from the results of a research activity. The idea of starting a process of technology transfer of nanostructured lead batteries stems from the need to overcome the main problems of current lead-acid battery technology, which consist in the low use of active material and in the limited cycle speed; these parameters limit the field of application of this type of battery. For this reason, the use of a highly porous material, obtained through an electrodeposition process in a nanostructured template, could represent a suitable product in applications where a high speed of cyclization is required, for example, in the storage of energy from alternative sources, in UPS systems and for fast frequency regulation on the network. From the tests conducted on a 1mAh and 2V prototype, the results showed excellent

performance in terms of cycling speed. In particular, the batteries have been tested at a minimum C-rate of 1C (full charge in 1 hour), a particularly high value if compared with the usual value to which the batteries currently in charge are normally charged (C/5 corresponding to a full charge in 5 hours). In addition, tests were conducted at higher cyclization rates, reaching a C-rate of 30C (full charge in 2 minutes). It is also possible to set a DoD (Depth of Discharge) of 90% and a cut-off of 1.2V, which result in an almost complete discharge of the battery. Although the cycling conditions are very stressful for the battery itself, it is possible to obtain high efficiencies and better performance in terms of number of cycles (> 1000) and average discharge and charge voltages. The table 3.3 shows the main differences between the two technologies, which highlight the different cyclization conditions and the results obtained.

	Nanostructured Battery	**Commercial lead-acid battery**
C-rate	>10C	C/5 – C/10
Cut-off	1.2V	1.75V
DoD	90%	20%
Discharge efficiency	~90%	50% ÷ 70% (C/10)
Discharge curves	Constant during the dscharge	The voltage changes rapidly in the discharge time
Performances	Excellent performance at high cycling speeds, up to 30C	Good performance at C-rate < C/5
Utilization of active material	90%	30% ÷ 40%
Cycle-life	>1000 cycles	>1000 cycles
Temperature	It works well even at	Wide operating range:

dependence	low temperatures	-40 °C ÷ + 60 °C

Table 3.3 Comparison between the performances of nanostructured and commercial lead-acid batteries.

3.3.1 Lead-acid battery market

The lead-acid batteries represent approximately the 70% of the electrochemical accumulator market, mainly thanks to their diffusion in the automotive sector (SLI). Currently, their big advantage is linked to the low cost that undoubtedly derives from the economies of scale and experience (in the development of the production process) that characterizes them. In 2015, the lead battery market stood at around $ 47 billion. The automotive segment is the largest, accounting for approximately 59% of the global market. As for UPS systems, they represent a percentage of 10% and growth of around 7% is expected due to their growing use in industrial, commercial and residential sectors. A recent report [59] expects to reach a global market of $ 85 billion. The growth is linked to the expansion of the automotive sector in China, India, Brazil, Mexico, South-Africa, Indonesia and Germany. Furthermore, thanks to the increase in the use of this technology in storage systems and UPSs in many industries, the demand could grow further. In addition, by 2025, the use of electric bikes is expected to increase by 6% following the need to be able to move at zero cost, following the ever-increasing price of diesel, and to be able to significantly reduce CO_2 emissions.

3.3.2 Competitive scenario

The energy storage boasts a huge market and a wide range of devices capable of working in various conditions of use. The lead-acid battery market is fairly consolidated, although, over the years, it has faced competition from the ever-growing lithium battery market, used in portable devices and in some hybrid or electric machines. The cost of lithium batteries is, to date, much higher than lead batteries: lithium batteries cost around 700 €/kWh compared to 250 €/kWh of lead batteries, even if the cost differential between the two technologies it could drop to

75 €/kWh in 2025. Another competitor of nanostructured lead-acid batteries is represented by supercapacitors, which manage to provide high power density valuesmanaging to stabilize floating charges, also acting as power buffers. However, supercapacitors, when compared with batteries, are limited by the high cost and low energy density. The cost per unit of energy of the supercapacitors amounts to about 15000 €/kWh, so if you could produce a device that boasts the performance of a supercapacitor ensuring high energy densities, you could access a slice of the market of great interest.

3.3.3 Value proposition

The value proposition of this project consists in the production of nanostructured lead-acid batteries which, thanks to the high surface area, deriving from the nanostructured morphology of the electrodes, are able to obtain efficiencies close to 90% even at high C-rates (from 1C to 30C), speeds not reachable with commercial lead batteries. In addition to being placed on the market as a support for current batteries, as previously mentioned, they could be included in the field of application of supercapacitors. Other strengths of nanostructured batteries concern the electrode manufacturing process and the initial conditioning of the battery. In particular, the active material can be obtained directly through an electrodeposition process, which allows to eliminate many high energy consuming processes such as mixing, the curing process and the formation which are strictly necessary for obtaining the lead battery. Currently on the market. The steps required to obtain a nanostructured electrode are, however, only three: membrane sputtering, the electroplating process and the dissolution of the membrane, that can be recovered by distillation. The simplification of the production process represents a "value proposition" for lead-acid battery manufacturers, with whom partnerships could be created, such as alliances between competitors, in order to already have a market ready for the new product and reduce risks competition thanks to close collaboration. Sputtering is a process widely used in the electronics industry and is one of the most commonly used methods for making thin films. It is used for coating anti-reflective glass, with high optical properties, and in the semiconductor industry. It is a PVD (Physical Vapor Deposition) process and is used to deposit a material on a substrate through the condensation of the atoms emitted by the target.

As for the electroplating process, the process is very simple and widely used in the galvanizing industry. Among the best known processes we have nickel plating, chromium plating or galvanizing. The electroplating process, in addition to being easily scalable, can be easily integrated with renewable energy sources, does not provide for purification and separation costs (the material of our interest being produced directly) and allows to work at low temperatures and pressures.
Finally, for the dissolution of the organic membrane, the cost is related only to the price of the solvent. One of the advantages consists in the fact that it is possible to recover the solvent by distillation and also recover the polycarbonate of the membrane. Considering the fact that the price of the electrode is strongly influenced by the cost of the membranes, its recovery could represent a significant economic advantage. Furthermore, to lower production costs, one could think of creating a partnership with the membrane manufacturer.
One of the problems encountered in the realization of the first prototype concerns the price of the polycarbonate membrane used as a template. In particular, it currently has a high cost due to the fact that it is supplied in limited quantities for purely laboratory applications, in fact, these are membranes are used for microfiltrations. However, from a preliminary market investigation on the availability of larger formats, a significant decrease in price was observed in relation to the quantity requested as shown in the figure 3.33.

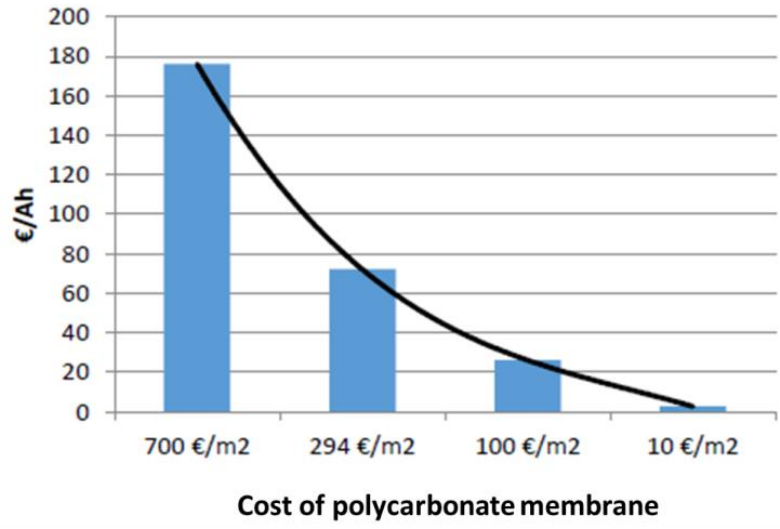

Figure 3.33 Trend in the cost of Ah as a function of the cost of the polycarbonate membrane.

We have estimated that the possibility of obtaining a membrane cost of less than 10 €/m^2 would make it possible to obtain an energy cost comparable to that of the current lead-acid battery.

3.3.4 Business model

Once the performance of the 1Ah and 6V products has been tested and validated, it would be necessary to create partnerships both with a company that deals with the production of the product at an industrial level and with the supplier of membranes in order to further reduce costs production and enter the market with a high added value product that can be added to current lead batteries. Our goal is to develop high-speed charging and discharging battery systems to be integrated with those currently on sale in collaboration with companies already active in the relevant markets and therefore to cooperate to own a range of products that can satisfy fields of application currently not covered by current lead-acid battery technology. A "business-to-business" strategy that will allow us to use the commercial channels already activated by our possible partners. The creation of a partnership could be aimed at acquiring new knowledge or licenses, customers or specific resources. From a more strictly economic point of view, typically, collaborations are established to optimize economies of scale and reduce costs. As reported on the Canvas business model, partnerships can be of a different type:

- Strategic alliances between non-competing companies: suppliers or companies that place within the production chain.
- Alliances between competitors: this is the case of companies that put themselves on the net to provide the customer with a similar value.
- Joint Venture to develop new businesses.

In the case of collaboration between competitors, the aim is to reduce the risk of a competitive environment characterized by uncertainties. It is not uncommon for companies to form an alliance in one sector while continuing to compete in other sectors.

The partnership could therefore become a key resource to support the business model. In addition to the key intellectual resources, such as the creation of a partnership or the know-now of a company, physical, human and financial resources are required. Our customers will be companies active in the Automotive and Energy Storage sectors.

3.3.5 Possible applications of nanostructured lead-acid batteries

Below there is a brief overview of the possible applications of nanostructured batteries in electrical systems and end uses.

- ***Braking with recovery of metropolitan trains***

The kinetic energy of the convoys when braking can be fed directly into the contact line to power the accelerating convoys and any excess part can, instead of being dissipated, be accumulated in groups of batteries arranged in the electrical power stations of the system to feed the station users and/or to be used in successive phases in which more trains are accelerating. The achievable advantages are represented by the recovery of energy, with consequent energy saving, and by the reduction of the power peaks required by the power supply equipment of the contact line. The battery groups could, alternatively, be housed on the same metropolitan trains, accumulating braking energy and supplying it to the train during acceleration and for powering the on-board services.

- ***Load leveling in hybrid vehicles***

Hybrid traction systems constitute an intermediate stage in the design of vehicle propulsion systems between conventional vehicles, using petroleum-based fuels, and pure electric traction not yet mature as regards the storage devices. The presence of storage systems allows the thermal engine to work in optimal conditions in terms of efficiency, while allowing the recovery of energy during braking and the reduction of the power developed by the diesel during the acceleration phases of the vehicle.

- ***Feeding of road transport vehicles***

In principle, the system consists of groups of batteries installed in correspondence with the canopies that charge in the time interval between the passage of two vehicles and groups of batteries installed on the means of transport, which through a "trunk" they charge by taking energy from the fixed batteries. The energy withdrawn is commensurate with that necessary to make the section between two successive stations complete. The short charging and discharging times make this type of battery particularly suitable for this type of application.

- ***Energy recovery in lifting systems, centrifuges etc.***

In these applications, the higher frequency of acceleration and braking makes the implementation of recovery during the descent of the cabins or the braking of the centrifuges of particular interest. The possibility of throwing the power directly into the network during braking, if on the one hand it would allow the energy recovery to be achieved more immediately, on the other hand it would not allow for "peak shaving", that is, it would not allow the containment of the peaks of power taken from the network and from the flicker associated with the continuous voltage variations related precisely to the sudden withdrawals of power. The containment of disturbances related to power fluctuations may require an oversizing of the electrical system upstream of the device. A final consideration of an economic nature is represented by the fact that the eventual sending of energy to the grid precisely for the ways in which it is available would be modestly remunerated.

- ***Hospital diagnostic equipment***

Many radiological equipment are characterized by large power absorption in the short intervals in which the examination is performed on the patient, interspersed with periods of modest absorption. The examination of the constitution of these machines highlights that they are often characterized by an AC/DC input stage which straightens the alternating current. One could then assume to insert on the DC side of these devices, groups of batteries suitable for containing the power peaks taken from the network and to avoid oversizing the power supply systems of the diagnostic equipment, made necessary to allow the regular operation of the

equipment powered by the same network. This oversizing would be uneconomical given the low number of hours of use of the installed power.

- ***Applications of nanostructured batteries in distributed generation***

A topic that is currently gaining some interest is the so-called Distributed Generation, that is, the introduction of small generation systems located near the user and connected to medium and low voltage networks. Among the motivations that push in this direction, the possibility of using clean energy sources such as the sun and the wind assumes importance. Also in this application the introduction of groups of nanostructured batteries could be of interest in relation to the discontinuity of primary energy sources. For example, the combination of such batteries in the production of electricity through wind turbines would seem to be attractive in that, reinforcing the intermediate DC bar of the generation system, during the transients, would allow in particular to level the rapid variations in power of the wind turbine.

- ***Improvement of the quality of the supply***

The combination of nanostructured batteries in uninterruptible power supplies could be of interest, for example, in the presence of loads with intermittent power withdrawals characterized by short-lasting power peaks. Once again, the combination of traditional batteries with groups of nanostructured batteries would make it possible to optimize the use of traditional batteries without being forced to oversize them to cope with the supply of the required powers even if for short periods of time. More generally, the use of nanostructured batteries, combined with suitable converters, could be promising in various equipment designed to improve the Power Quality of the system where power injections are required in short time intervals to allow continuity of power in the face of voltage dips or short-term interruptions. These are, in fact, disturbances present in the electrical networks that can cause the stoppage of entire production processes with often considerable damage and long restart times of the plant.

The foregoing provides a broad, albeit non-exhaustive, overview of the possibilities of using nanostructured batteries in electrical systems. The

reasons for interest are different, especially in terms of better use of energy resources and the sizing of the electrical system.

This chapter offers a broad overview of the performance of nanostructured lead-acid batteries and the possible applications of this innovative technology. As seen from the economic analysis carried out on nanostructured batteries, these currently have a higher price than that presented by current lead batteries, a price which however can be justified by the performance of the nanostructured technology, which does not intend to replace the current technology but to support it, taking the place of current supercapacitors coupled to electrochemical accumulators, bringing an economic and performance benefit to the coupling.

Chapter 4

Study on cyclic voltammetry on lead foil and lead nanowires and stability of carbonaceous additives

In this chapter results concerning the research activity at the Fraunhofer ISC of Wűrzburg with the supervisor of Jochen Settelein will be discussed. At the Fraunhofer, in particular a systematic Cyclic Voltammetry study on the Pb and PbO_2 NWs electrodes were performed and compared with the same tests carried out on lead sheets. Besides, the study of the stability of carbon additives (Carbon Black and Graphite) added to the positive pastes of the commercial lead-acid batteries were also performed.

4.1 Study on cyclic voltammetry on lead electrode in sulfuric acid

Cyclic Voltammetry is a very useful technique to study the redox reaction occurring at the electrode/ electrolyte interface. Visscher W.H.M. With this technique have studied the lead electrode in sulfuric acid solution [40]. He studied the oxidation of lead in 1.28 g/cm^3 H_2SO_4 in the potential range from --1.0 V to 2.6 V vs. R.H.E. In the potential range from +0.6 V to +2.6 V, the anodic voltammogram shows two peaks which indicate, the formation of α-PbO_2 and β-PbO_2 respectively. During the reverse sweep a main peak is present at 1.65 V and corresponds to the reduction of β-PbO_2 to $PbSO_4$. The reduction of α-PbO_2, leading to n-PbO* $PbSO_4$, does not have a defined voltage value. The basic lead sulphates are reduced at voltages below 0V. In figure 4.1 the typical cyclic voltammogram plot of lead electrode in aqueous solution of H_2SO_4, was shown.

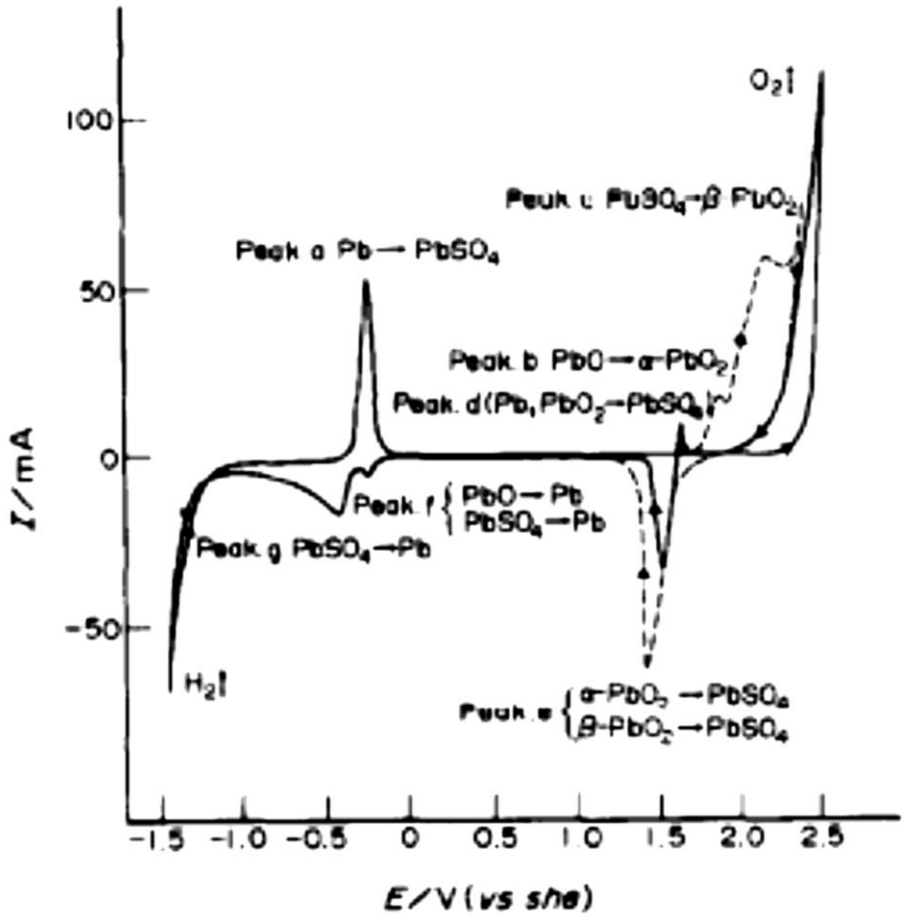

Figure 4.1 cyclic voltammograms for a lead electrode in aqueous H_2SO_4 solution [13].

4.1.1 Comparison between cyclic voltammetry in PAM range on PbO_2 NWs and oxidized lead foil

Firstly, the cyclic voltammogram study was carried out in PAM range. In particular the test was carried out on PbO_2 NWs electrode and oxidized lead foil. Both of the electrodes were tested in aqueous solution of sulfuric acid using as counter electrode a Pt wire and as reference electrode R.H.E. In both cases the geometric area of electrodes was equal to 0,38 cm^2. The figure 4.2 shows the typical cell used for cyclic voltammogram tests.

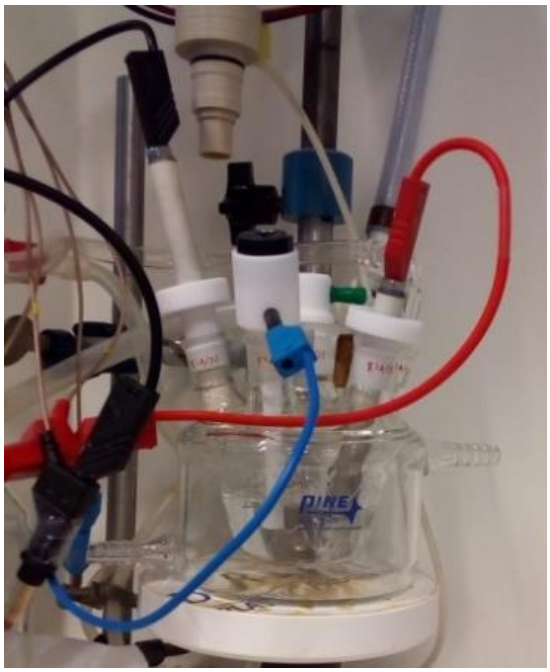

Figure 4.2 Typical cell used for cyclic voltammogram tests.

The electrochemical oxidation of lead foil leads to a mixture of α-PbO_2 and β-PbO_2. PbO_2 NWs electrode is constituted only of β-PbO_2, that is more electrochemically active of α-PbO_2. Cyclic Voltammetry was carried out with a scan speed equal to 10 mV/s in a range between 1V - 2.4V vs. RHE for PbO_2 NWs and 1.4V - 2.2V vs. RHE for the Pb foil. The figure 4.3 shows the cyclic voltammograms of the two different electrodes. From this plot it is possible to see how, despite the two electrodes have the same geometric area, the value of the current in case of PbO_2 NWs is higher than the value of oxidized Pb foil. In the range of reduction of PbO_2 to $PbSO_4$ the value of current for PbO_2 NWs electrode is equal to -0,0178 A and for oxidized Pb foil is equal to -0,054 A. In the range of oxidation of $PbSO_4$ to PbO_2 the value of current for PbO_2 NWs is equal to 0,0156 A and the value of Pb foil is equal to 0,0021 A.

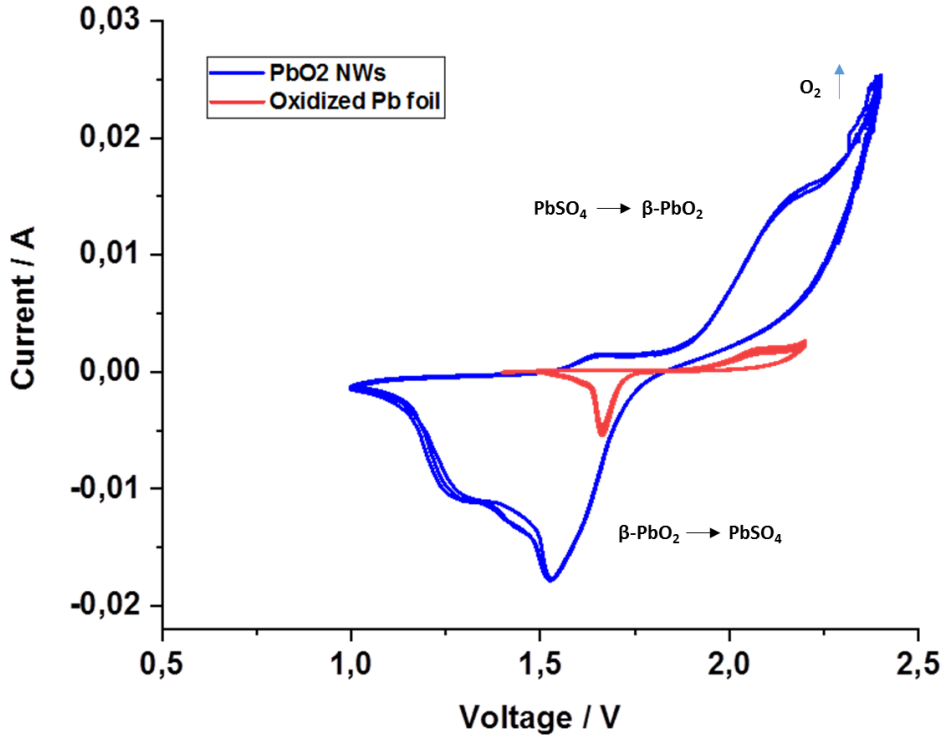

Figure 4.3 Comparison between cyclic voltammogram on oxidized Pb foil and PbO_2 NWs electrode.

Furthermore also the value of current for oxygen evolution is higher in case of PbO_2 NWs electrode than oxidized Pb foil. In fact, a value of current equal to 0,0254 A and 0,0026 A was measured respectively for nanowires and foil. The different values of current between the two electrodes are due to the high surface area of PbO_2 NWs. In a PAM range test at different potential scan rate were also performed, from 1mV/s to 100 mV/s. The figures 4.4 a) and c) show the results of these tests. Also in this case, the current is higher for PbO_2. To better evaluate the behaviour of both electrodes in the oxygen evolution range, also the potential range from 1.8V to 2.4V vs. RHE was analysed (figure 4.4, the final tension for lead foil is 2.2V).

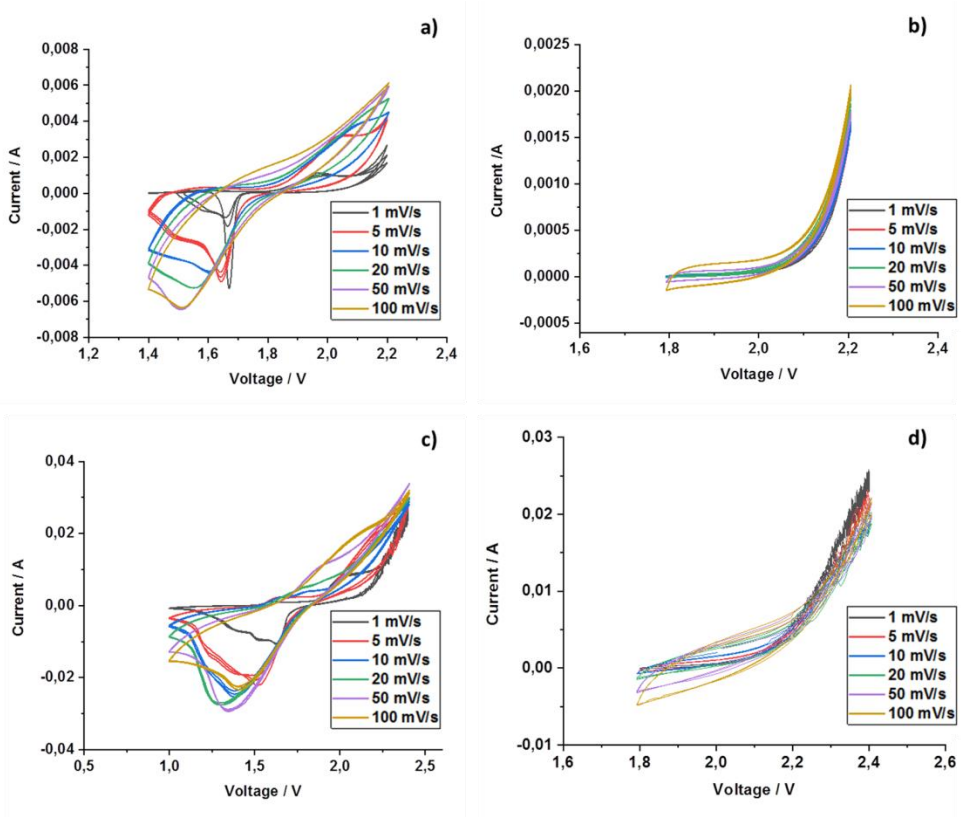

Figure 4.4 Cyclic voltammograms at different scan speed series: a) Cyclic voltammetry in PAM range on oxidized Pb foil; b) Cyclic voltammetry in PAM Overcharge range on oxidized Pb foil; c) Cyclic voltammetry in PAM range on PbO_2 NWs electrode; d) Cyclic voltammetry in PAM Overcharge range on PbO_2 NWs electrode.

Also in this range, the current is higher for nanowires. Thus, from these results it can be concluded that PbO_2 nanowires have a very good electrocatalytic behaviour thanks to their high surface area.

4.1.2 Comparison between cyclic voltammetry in NAM range on Pb NWs and lead foil

The same studies carried out on PbO_2 NWs electrodes were carried out on Pb NWs electrodes.. The figures 4.5 and 4.6 show the results of these tests.

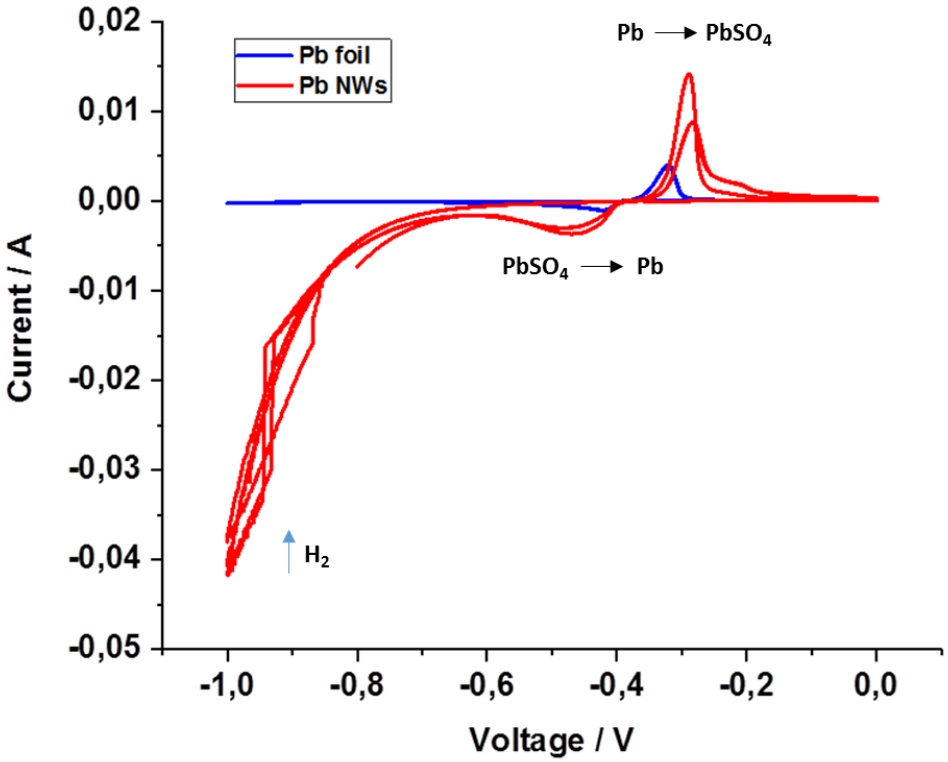

Figure 4.5 Comparison between cyclic voltammogram on Pb foil and Pb NWs electrode.

The Cyclic Voltammetry in NAM range was carried out on both electrodes in a scan range between -1V - 0V vs. RHE. Also in this case the value of current of the Pb NWs electrode is higher than the value of current of the Pb foil, despite the same geometric area and the same electrolyte. The value of current on the Pb NWs electrode, for lead oxidation, is equal to -0,0036 A against the -0,0012 A of Pb foil. Also the values of current for lead reduction and hydrogen evolution are higher for Pb NWs than Pb foil.

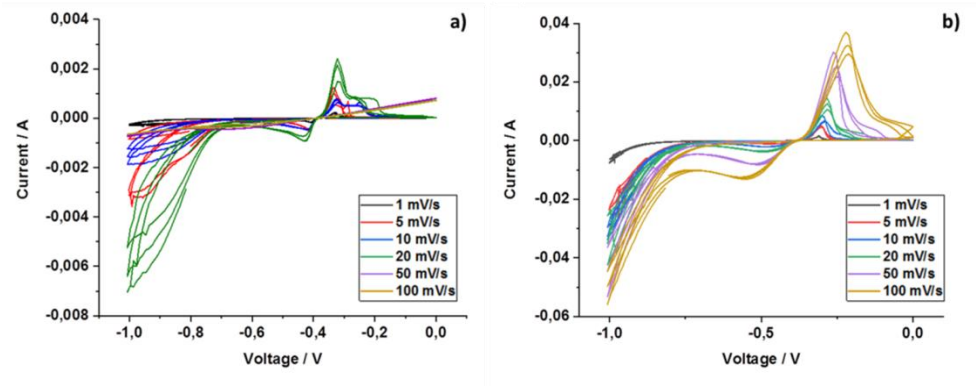

Figure 4.6 Cyclic voltammograms at different scan speed series: a) Cyclic voltammetry in NAM range on Pb foil; b) Cyclic voltammetry in NAM range on PbO_2 NWs electrode.

4.1.3 Comparison between cyclic voltammetry in NAM range on Pb NWs and lead foil with carbon additives

In the last years carbon additives are used into NAM pastes of commercial lead-acid batteries to improve their performance under HRPSoC (high-rate partial-state of charge) and increase their cycle life. Shiomi et al. affirm that the carbon added to the NAM leads to the formation of a conductive layer between $PbSO_4$ crystals, formed into the paste during discharge, and carbon. This conductive layer improves the rechargeability of the negative plate [41]. Spence et al. showed that the positive effect of carbon in negative plate is due to the formation of a porous structure of the NAM [42]. For Moseley, the carbon increases the electrical conductivity of the NAM. Another effect of carbon into the NAM is the creation of smaller PbSO4 crystals, that facilitate their dissolution during charge. Furthermore, carbon increases the capacity of negative plate, acting as a capacitive component [43,44]. Considering these advantages of carbon additives in the negative lead plate, the behaviour of Pb NWs electrodes and Pb foils added with Carbon Black and Graphite was studied. The electrodes with carbon additives were made by droop casting. In particular, a solution constituted by 0,1 g of Carbon Black (or Graphite), 8 g H_2O, 2g of Ethanol and 100 µl of Nafion was used. The characteristics of carbon additives are reported in table 4.1.

	BET surface area (m^2/g)	Average particle size	Oil absorption number (ml/100g)
Lamp Black 101	29	95 nm	140
Graphite BNB 90	28.4	85 µm	180

Table 4.1 Main characteristics of carbon additives used for cyclic voltammetry [45].

The electrodes coated with carbon solutions were dried in air. For these tests we used the same cell used above.

The tests were carried out in a NAM range from -1 V to 0 V vs. RHE and the plots of cyclic voltammetry are reported in figure 4.7.

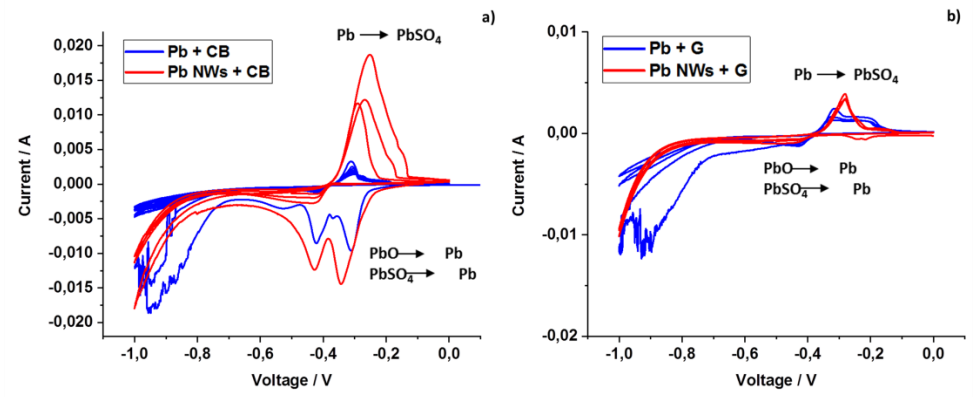

Figure 4.7 Comparison between cyclic voltammetry on Pb foil and Pb NWs electrodes with carbon additives: a) Cyclic voltammogram on Pb foil and Pb NWs with Carbon Black; b) Cyclic voltammogram on Pb foil and Pb NWs with Graphite.

The figure 4.7a shows the Cyclic Voltammetry of lead foil and Pb NWs electrodes added with carbon black. The current on Pb NWs electrode are higher than the Pb foil, thus in Pb NWs electrodes added with carbon black the reaction of lead is more favourite than in case of lead foil. The figure 4.7b shows the cyclic voltammograms of Pb NWs electrode and Pb foil added with graphite. In

this case, the performances of both electrodes are almost the same. Thus the addition of carbon black on the surface of electrode improve the performance of nanostructured electrode, in fact an increase in the value of electric current for reduction and oxidation of lead was measured. Instead, the adding of graphite causes a decrease of the performance of nanostructured electrode, in fact, there is a decrease of current of the electrode, as the figures 4.8 a) and b) show. This effect is probably due to the particle size of graphite. The relative large dimension of graphite particles caused a decrease of real porosity of nanostructured electrode and then of the active area available for charge/discharge reactions.

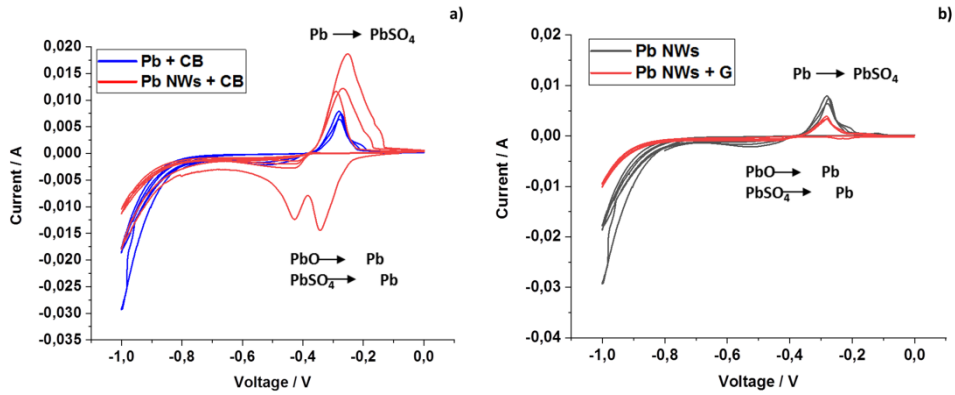

Figure 4.8: Comparison between cyclic voltammograms on pure Pb NWs and Pb NWs with carbon additives: a) Cyclic voltammogram on pure Pb NWs and Pb NWs added with Carbon Black; b) Cyclic voltammogram on pure Pb NWs and Pb NWs added with Graphite.

4.1.4 Study in cyclic voltammetry of carbon additives on FTO substrate

The FTO (Fluorine-doped tin oxide) coated glass is electrically conductive and ideal for use in a wide range of devices. The FTO has been recognized as a very promising material because it is relatively chemically inert, mechanically hard, stable under atmospheric conditions and high-temperature, has a high tolerance to physical abrasion and is less expensive than indium tin oxide. Thus, it was used as substrate in order to characterize the stability of carbonaceous material used as additive.

Figures 4.9 a) – d) show the electrochemical characteristics of FTO used for our tests.

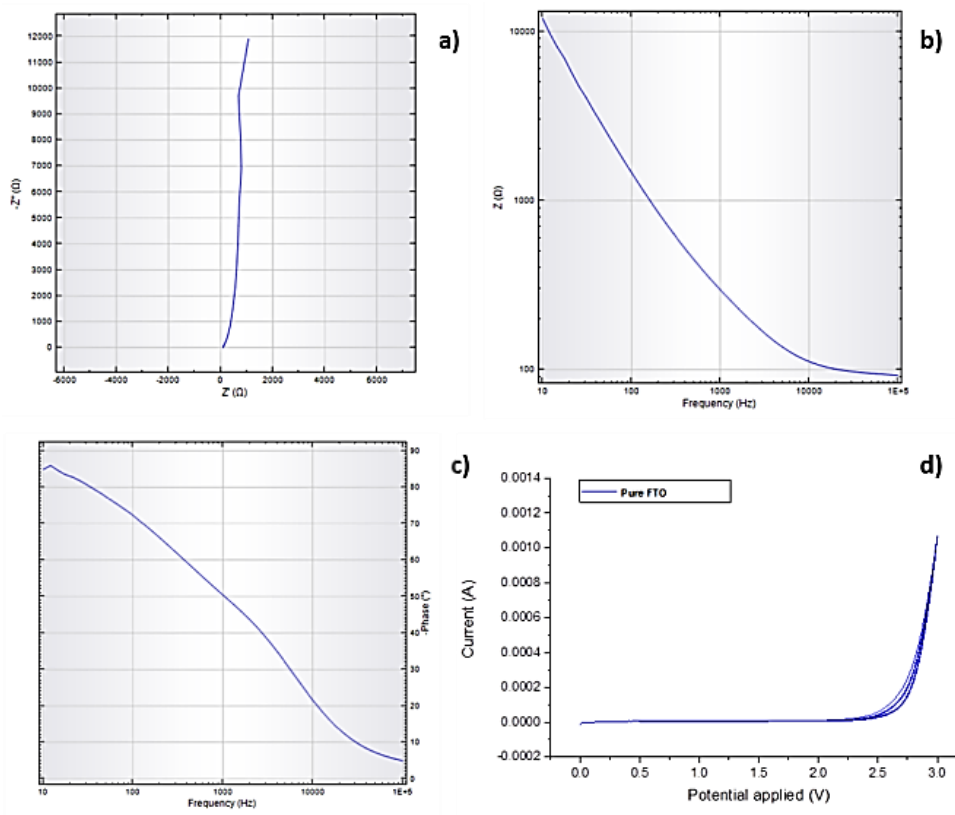

Figure 4.9 Electrochemical characteristics of FTO: a) Nyquist diagram of FTO; b) Bode modulus diagram of FTO; c) Bode phase diagram of FTO; d) Cyclic voltammogram of FTO.

The electrolyte used for these test was sulfuric acid 1.28 g/cm^3 and the Cyclic Voltammetry was carried out in a range equal to 0 V - 3 V vs. RHE. EIS measurements show that the FTO samples are very conductive with a negligible resistance and the cyclic voltammogram shows its high stability. The electrodes coated with carbon solutions were obtained by droop casting coating and dried in air.

For electrochemical tests, the counter electrode was a Pt wire, the reference electrode was RHE and the electrolyte was an aqueous solution of sulfuric acid with acid density equal to 1.146 g/cm^3 (formation acid for lead-acid batteries) and

1.28 g/cm^3 (utilization acid for lead-acid batteries). The figures 4.10 a) and b) show the cyclic voltammograms of FTO+CB.

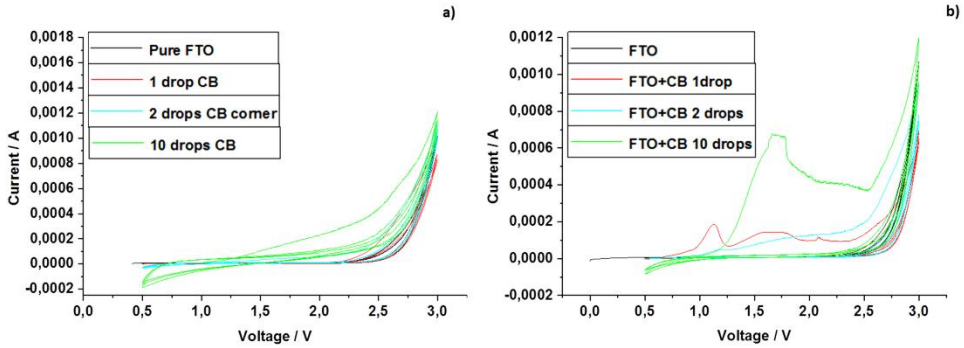

Figure 4.10 Cyclic voltammograms of FTO+CB in H_2SO_4: a) Cyclic voltammogram in sulfuric acid with acid density of 1.146 g/cm^3; b) Cyclic voltammogram in sulfuric acid with acid density of 1.28 g/cm^3.

The cyclic voltammograms, obtained in a range equal to 0 V - 3 V vs. RHE, of CB show the typical pattern of this carbon additive [46]. The Cyclic Voltammetry on FTO+CB was carried on electrodes with different quantitaties of carbon additive. The behaviour of carbon black is different in the two cases and the typical pattern of CB oxidation is more visible with sulfuric acid with a density of 1.28 g/cm^3. Furthermore the value of electric current of CB oxidation depends also from the quantity of carbon additive on the FTO surface, in fact the current increases with the increase of CB higher (figures 4.10) a) and b)).
The same tests were carried out on FTO coated with graphite and the figures 4.14 a) and b) show the cyclic voltammograms of FTO+G with different amount of graphite additive.

The typical pattern of graphite oxidation is more visible with sulfuric acid with a density of 1.28 g/cm^3 [47]. Also in this case with the increase of graphite the circulating current increases. In all plots of the figures 4.10 and 4.11 it is possible to see that after the first cycle the performance of carbon additives decrease and this is due either the degradation of carbon and its fall down because of the gas evolution.

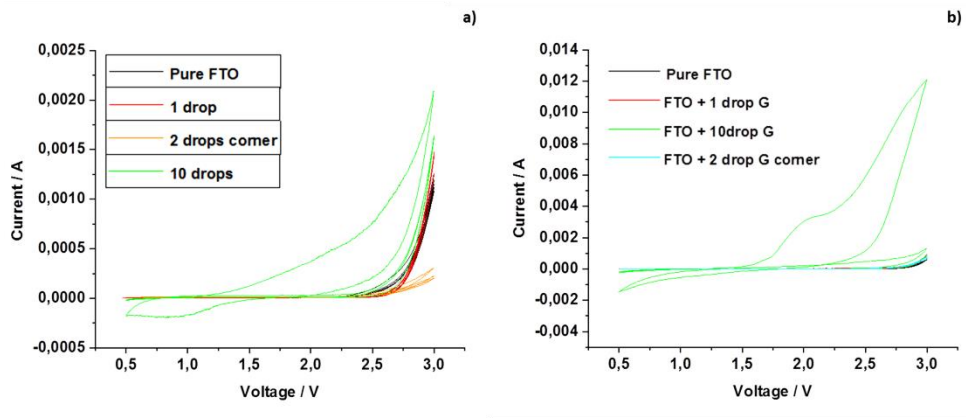

Figure 4.11 Cyclic voltammograms of FTO+G in H_2SO_4: a) Cyclic voltammogram in sulfuric acid with acid density of 1.146 g/cm^3; b) Cyclic voltammogram in sulfuric acid with acid density of 1.28 g/cm^3.

The figures 4.12 a) and b) show how change the conductivity of FTO coated with graphite and carbon black.

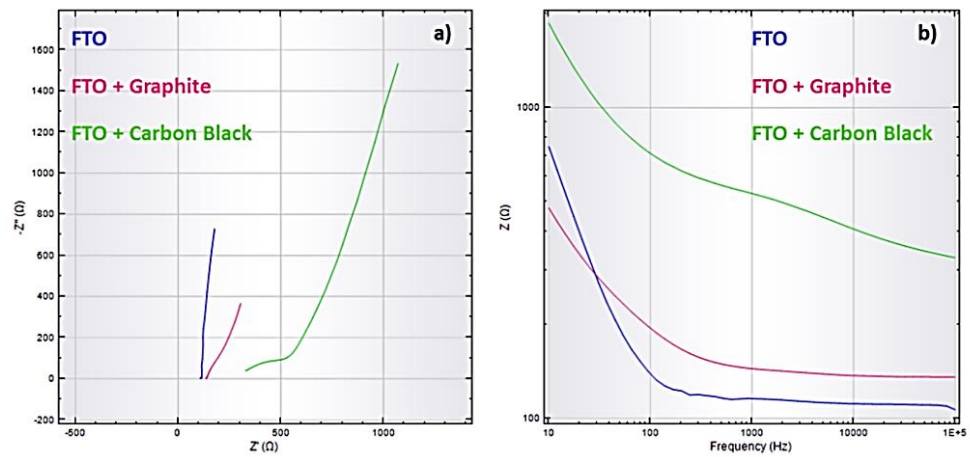

Figure 4.12 a) Nyquist diagram of FTO and FTO coated with carbon additives; b) Bode modulus diagram of FTO and FTO coated with carbon additives.

4.2 Effect of carbon additives in positive plates of lead-acid battery

In the last years, some scientists studied the possibility to use the carbon additives to improve the performance of lead-acid batteries. In particular Witantyo et al. in our studies affirm that the addition of acetylene black coated on the positive plates of a lead-acid battery improves the cycle life of this type of accumulator [48]. The battery experts of the Fraunhofer R&D Center Electromobility Bavaria located at the Fraunhofer Institute for Silicate Research ISC collaborate at the project AddESun aiming to safeguard the future of lead-acid batteries launched in September 2017. In particular to the Fraunhofer ISC was assigned the key task of researching new additives and their effect on battery properties. The goal of this project is to improve service life and energy density by up to 30 percent. The task of the Fraunhofer ISC within the AddESun project is to investigate the correlation between the physical and chemical structure of the additives and to understand what part they play in the battery. The scientists of the Fraunhofer ISC pay special attention to the effect of additives on the porosity of the active mass, on a battery‘s mechanical stability and conductivity. The AddESun project is coordinated by EXIDE Technologies Operations GmbH & Co. KG and the partners of this project are: EXIDE Technologies Operations GmbH & Co. KG, Büdingen, Evonik Resource Efficiency GmbH, Hanau, PENOX GmbH, Ohrdruf, SGL Carbon GmbH, Meitingen, RWTH, Aachen [49]. At the Fraunhofer ISC of Wűrzburg, I worked also to the project AddESun, and in particular I studied the cyclic voltammograms of positive plates coated with different amount of carbon black and graphite and the corrosion of these carbon additives in the positive plates of lead-acid batteries during formation phase at different potentials.

4.2.2 Study of carbon black corrosion in positive plate of lead-acid battery

The positive plate was fabricated using different amount of carbon black, additive much used to improve the performance of lead-acid battery. In particular, 2% and 4% by weight of CB was used. Three different types of paste for positive plate were prepared:

- 90.2 g (60.6% ww) of negative mixture powder, 38.7 g (26% ww) of positive mixture powder and 22.6 g (14.3% ww) of water. The total weight of this paste was equal to 151.5 g.

- 90.2 g (60.6% ww) of negative mixture powder, 38.7 g (26% ww) of positive mixture powder, 3 g (2% ww) of CB and 26 g (17.2% ww) of water. The total weight of this paste was equal to 157.9 g.
- 90.2 g (60.6% ww) of negative mixture powder, 38.7 g (26% ww) of positive mixture powder 6 g (4% ww) of CB and 32 g (21.1% ww) of water. The total weight of this paste was equal to 166.9 g.

To prepare these paste the positive powder, the negative powder and carbon black are firstly premixed to homogenize the initial composition in a mixer at 800 rpm for 60s. After this first step water was added to the powders and all was mixed at 2000 rpm for three times for 20s with a cycle of cooling after each mix step. The pastes so manufactured were spread on the positive commercial grids, and then put in an oven at 45 °C, with controlled humidity, for 10 hours. After this time the plates were dried at the same temperature for 2 hours. The average weights obtained from the three different types of plates are reported in table 4.2.

Type of positive plate	Average weight of grid [g]	Average weight plate before drying [g]	Average weight plate after drying [g]
Plate without CB	16.807	39.415	37.012
Plate with 2% of CB	16.372	37.08	35.427
Plate with 4% of CB	16.815	35.392	32.867

Table 4.2 Average weight obtained in the different steps of positive plates preparation.

After curing phase the positive plates were subject to the electrochemical tests. The first test carried out on the positive plates was the Cyclic Voltammetry. The cell for these tests was constituted by two commercial negative plate, a polyethylene separator with in a positive plate, put between the two negative electrodes, and a RHE reference electrode. To blocked the electrodes in their position the Teflon sheets (2 for side) are set in the back of the negative electrodes. For the tests an aqueous solution of sulfuric acid with gravity density

equal to 1.146 g/cm^3 (formation acid) and 1.28 g/cm^3 (utilization acid) were used. The tests were carried out at room temperature. Before Cyclic Voltammetry tests, the impedance of the positive plate, the voltage of positive plate and the voltage of negative plates were measured. The values of these measurements are reported in table 4.3.

Type of positive plate	Impedance [Ω]	Voltage of positive plate vs. RHE [V]	Voltage of negative plate vs. RHE [V]	Acid density [g/cm^3]
Plate without CB	2.360	-0.105	-0.300	1.146
	2.950	-0.109	-0.300	1.280
Plate with 2% of CB	0.854	-0.120	-0.320	1.146
	0.595	-0.120	-0.320	1.280
Plate with 4% of CB	7.270	0.160	-0.320	1.146
	4.53	0.220	-0.310	1.280

Table 4.3 Characteristics of electrodes used for cyclic voltammetry tests.

In figures 4.13 a) and b) the cyclic voltammograms of positive plates with different amount of CB and in the two different types of electrolyte were reported. The Cyclic Voltammetry tests were carried out in a range between 0 V and 2.2 V vs. RHE. The presence of a greater concentration of carbon black has the effect of making uniform the conductivity of the electrode, moreover a greater concentration of the acid, according to Nernst's law, facilitates the conversion. After the Cyclic Voltammetry tests the cells were subject to the formation process in potentiostatic conditions. They were done five different tests with a different potential with values from 1.6 V to 2 V vs. RHE. The formation was performed for 40 h in charge (in the potentiostatic condition) at the set voltage followed by a measure of OCV for 20 h.

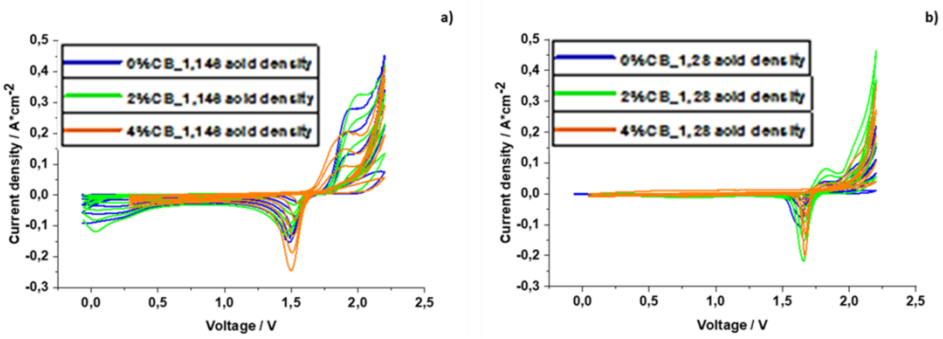

Figure 4.13 Cyclic voltammograms on positive plates: a) Cyclic voltammograms in sulfuric acid with acid density of 1.146 g/cm^3; b) Cyclic voltammograms in sulfuric acid with acid density of 1.28 g/cm^3.

The characteristics of the electrodes used for formation with sulfuric acid with density of 1.146 g/cm^3 are reported in table 4.4.

Type of positive plate	Impedance [Ω]	Voltage of positive plate vs. RHE [V]	Voltage of negative plate vs. RHE [V]	Formation types
Plate without CB	2.360	-0.026	-0.300	Formation at 1.6 V
	1.662	-0.099	-0.302	Formation at 1.7 V
	2.360	-0.105	-0.300	Formation at 1.8 V
	1.223	-0.026	-0.300	Formation at 2 V
Plate with 2% of CB	0.522	0.0056	-0.300	Formation at 1.6 V
	0.366	-0.036	-0.299	Formation at 1.7 V
	0.840	-0.990	-0.320	Formation at 1.8 V
	0.854	-0.120	-0.320	Formation at 2 V
Plate with 4% of CB	0.100	0.230	-0.300	Formation at 1.6 V
	8.400	0.192	-0.304	Formation at 1.7 V

	0.101 7.270	0.0004 0.160	-0.320 -0,320	Formation at 1.8 V Formation at 2 V

Table 4.4 Characteristics of electrodes used for cyclic voltammetry tests in sulfuric acid with 1.146 g/cm^3.

The figure 4.14 a) - d) show the diagrams of the current in function of the time during the formation phase in sulfuric acid with a gravity density equal to 1.146 g/cm^3. In the figures 4.14 a) c), that represent the formation at the voltages of 1.6 V, 1.7V and 1.8 V respectively, it can be seen that, despite an initial increase, the current decreases after a few hours, reaching the same (or lower) value of current of the positive plate without carbon black. For formation carried out at 2V, the behaviour is different only for plates with 4% of CB.

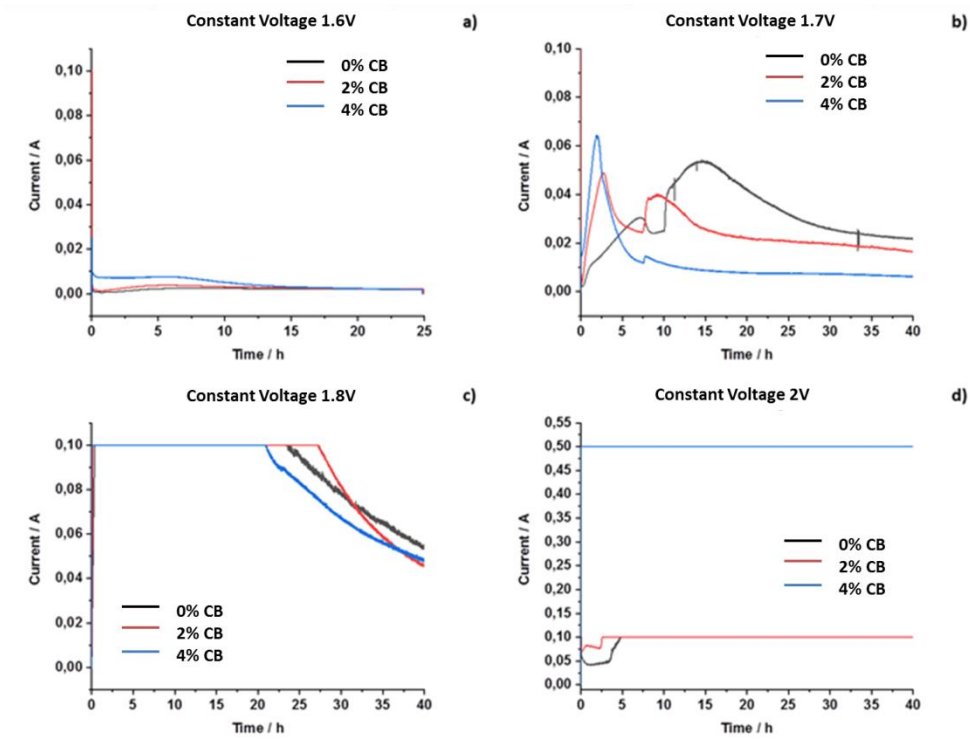

Figure 4.14 Diagrams of current formation phase in sulfuric acid with a gravity density equal to 1.146 g/cm^3: a) Formation at 1.6 V; b) Formation at 1.7 V; c) Formation at 1.8 V; d) Formation at 2 V.

After formation phase positive plates were subject to the chemical analysis to detect the residual quantity of carbon into the paste. The results of these analyses are reported in table 4.5. The chemical analysis was carried out with LECO CS744. This machine can determine the quantity of carbon and sulfur presents in metals, minerals and other inorganic materials. The positive plates after formation phase were smashed and pulverized with a mortar to homogenize the powder obtained from all parts of the plate. After pulverization around 0.5g of powder were put into the LECO to determine its quantity of carbon. The LECO has a combustion furnace with variable power and an IR optical lector, to define the quantities of carbon and sulfur into the sample.

From the table 4.5 it is possible to see that the quantity of carbon black decreases during formation phase and it decreases depending to the applied voltage. Also a morphological analysis was carried out on the samples to verify how the electrode morphology changes during formation phase and if the quantity of carbon has any influence.

	0% (ww) CB	**2% (ww) CB**	**4% (ww) CB**
Cured	0	2.34 ± 0.00265	4.74 ± 0.0132
1.6V	0	2.40 ± 0.0934	3.30 ± 0.179
1.7V	0	1.69 ± 0.101	3.66 ± 0.0334
1.8V	0	1.11 ± 0.0881	2.83 ± 0.0435
1.9 V	0	0.509 ± 0.0174	1.35 ± 0.112
2 V	0	0.000698 ± 0.00577	0.543 ± 0.00279

Table 4.5 Quantitative of carbon black into the positive plates after formation phase in sulfuric acid with density of 1.146 g/cm^3.

The figures 4.15 shows the SEM images obtained from this analysis.

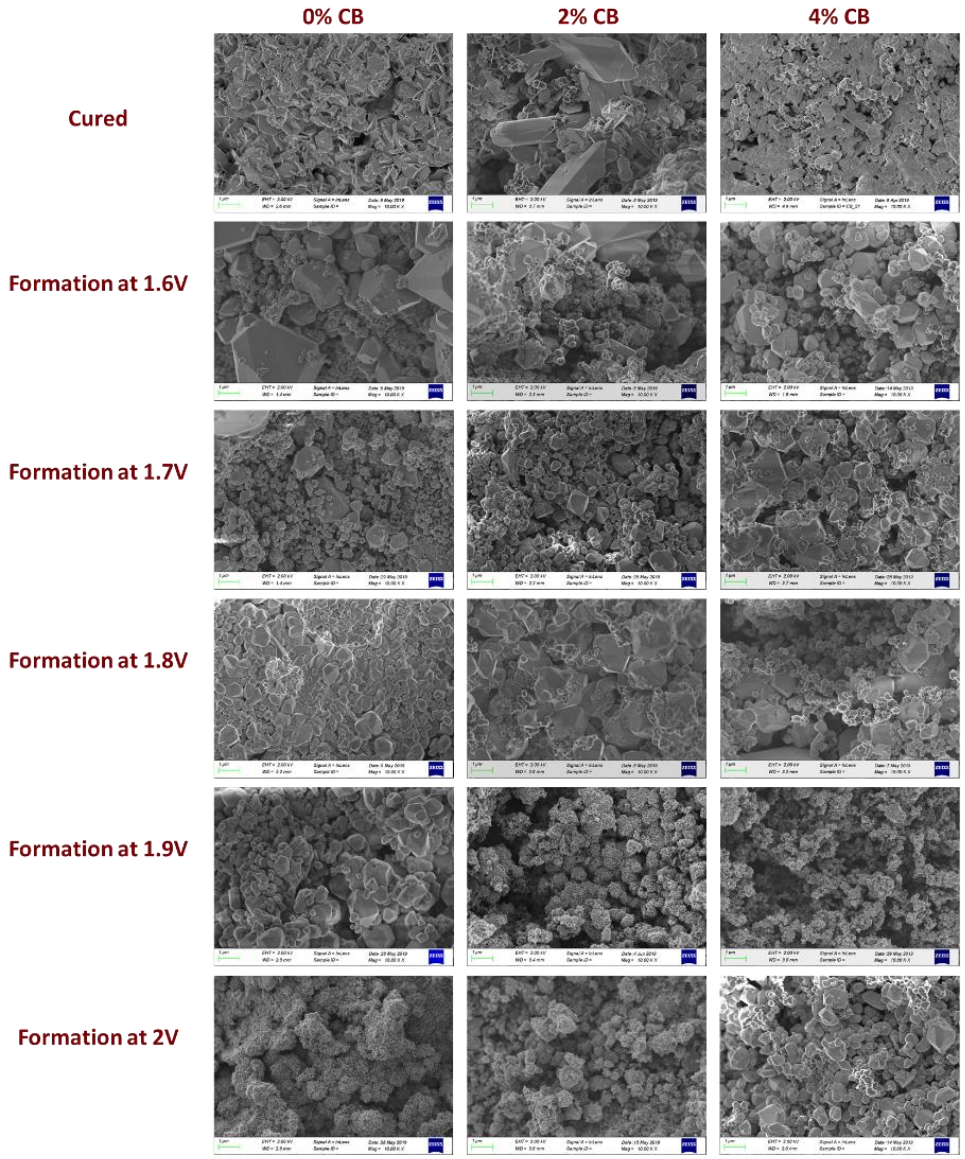

Figure 4.16 SEM images of positive plates after formation phase at different set potentials.

From SEM analysis, it is possible to see that the morphology changes with the potential applied and with the quantity of carbon black into the plate. In fact, the

sizes of crystals decreasing with the increase of potential. The corrosion of carbon, during the formation phase, creates some vacuums into the paste of the positive plates, making the plate more porous.

4.2.3 Study of graphite corrosion in positive plate of lead-acid battery

The corrosion of graphite into the pastes of positive plates was also studied, because this is another carbon additive much used in the lead-acid battery. The positive plates were fabricated using different amount of graphite, in particular, they were used the 1%, the 2% and 4% in weight of graphite. They were prepared three different types of pastes for positive plate:

- 90.2 g (60.6% ww) of negative mixture powder, 38.7 g (26% ww) of positive mixture powder, 1.5 g (1% ww) of graphite and 28 g (17.7% ww) of water. The total weight of this paste was equal to 158.4 g.
- 90.2 g (60.6% ww) of negative mixture powder, 38.7 g (26% ww) of positive mixture powder, 3 g (2% ww) of graphite and 33 g (20.8% ww) of water. The total weight of this paste was equal to 164.9 g.
- 90.2 g (60.6% ww) of negative mixture powder, 38.7 g (26% ww) of positive mixture powder 6 g (4% ww) of graphite and 38 g (24% ww) of water. The total weight of this paste was equal to 172.9 g.

To prepare these paste the positive powder, the negative powder and the graphite are firstly premixed to homogenize the initial composition in a mixer at 800 rpm for 60s. After this first step the water was added to the powders and all was mixed at 2000 rpm for four times for 20s with a cycle of cooling after each mix step with a duration equal to 1 minute. The pastes so manufactured were spread on the positive commercial grids, from which a third of the grid was eliminated, and then put in an oven at 45 °C, with controlled humidity, for 10 hours. After this time the plates were dried at the same temperature for 2 hours. The average weights obtained from the three different types of plates are reported in table 4.6.

Type of positive plate	Average weight of grid [g]	Average weight plate before drying [g]	Average weight plate after drying [g]
Plate without CB	16.758	37.703	34.836
Plate with 2% of CB	16.787	36.835	33.878
Plate with 4% of CB	17.420	34.888	31.764

Table 4.6 Average weight obtained in the different steps of positive plates preparation.

The plates so prepared were used for electrochemical tests and in particular the first electrochemical test was the Cyclic Voltammetry test. The Cyclic Voltammetry tests were carried out at room temperature, using the same configuration of positive plates with carbon black additive. The figures 4.16 a) and b) show the Cyclic Voltammograms of positive plate coated with different quantity of graphite in sulfuric acid with two different values of gravity density. The Cyclic Voltammetry range of the positive plates in sulfuric acid with density of 1.146 g/cm^3 was set between 0 V and 2 V vs. RHE, because at higher voltage values we reached the limit value of the machine. The Cyclic Voltammetry of positive plates in sulfuric acid with density equal to 1.28 g/cm^3 was set between 0 V and 2.2 V vs. RHE. From the figure 4.23a, that shows the Cyclic Voltammograms in sulfuric acid with density of 1.146 g/cm^3, it is possible to see that with the addition of graphite to the positive plate in the current decreases. It is possible to see that the presence of a greater concentration of carbon black has the effect of making uniform the conductivity of the electrode, moreover a greater concentration of the acid, according to Nernst's law, facilitates the conversion. The positive plates containing graphite, after curing, were subjected to formation phase at different applied potential to study the corrosion of graphite and its effects on the positive plates. The formation phase was carried out in a potential range between 1.6 V and 2 V vs. RHE, using as an electrolyte sulfuric acid with gravimetric density equal to 1.146 g/cm^3. The figures 4.17 a) - e) show the trend of the current as a function of time during the training phase to the different

potentials applied. The initial electrochemical characteristics of positive plates subject of formation phase are reported in table 4.7.

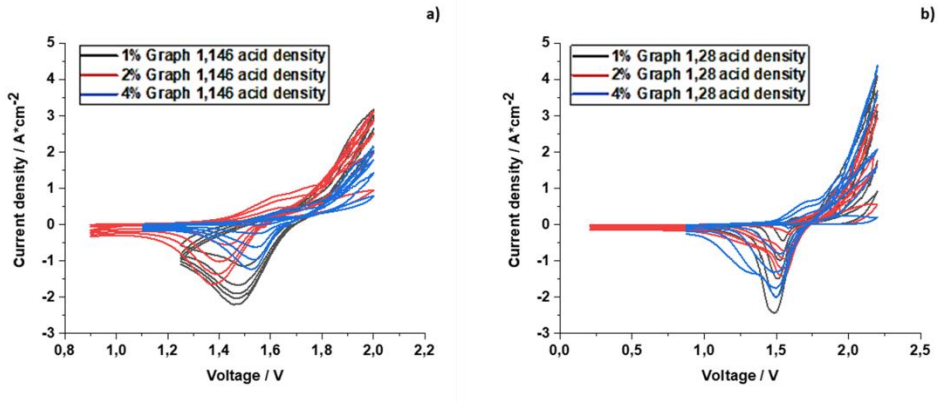

Figure 4.16 Cyclic voltammograms on positive plates: a) Cyclic voltammograms in sulfuric acid with acid density of 1.146 g/cm^3; b) Cyclic voltammograms in sulfuric acid with acid density of 1.28 g/cm^3.

Type of positive plate	Impedance [Ω]	Voltage of positive plate vs. RHE [V]	Voltage of negative plate vs. RHE [V]	Formation types
Plate with 1% of G	0.280	-0.092	-0.324	Formation at 1.6 V
	0.860	-0.069	-0.325	Formation at 1.7 V
	0.418	-0.990	-0.325	Formation at 1.8 V
	0.542	-0.086	-0.324	Formation at 1.9 V
	0.564	-0.082	-0.329	Formation at 2 V
Plate with 2% of G	4.130	0.048	-0.321	Formation at 1.6 V
	3.970	0.010	-0.370	Formation at 1.7 V
	4.550	0.011	-0.379	Formation at 1.8 V

	5.770 4.950	0.087 -0.004	-0.325 -0.332	Formation at 1.9 V Formation at 2 V
Plate with 4% of G	5.370 4.570 6.430 0.052 0.095	0.696 0.731 0.619 -0.529 -0.222	-0.321 -0.323 -0.324 -0.662 -0.323	Formation at 1.6 V Formation at 1.7 V Formation at 1.8 V Formation at 1.9 V Formation at 2 V

Table 4.7 Characteristics of electrodes used for cyclic voltammetry tests in sulfuric acid with 1.146 g/cm^3.

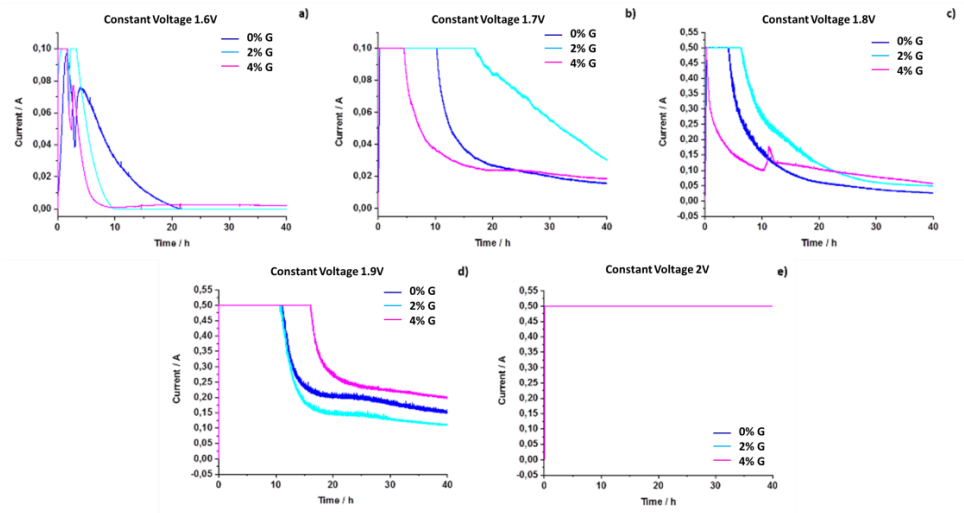

Figure 4.17 Diagrams of current formation phase in sulfuric acid with a gravity density equal to 1.146 g/cm^3: a) Formation at 1.6 V; b) Formation at 1.7 V; c) Formation at 1.8 V; d) Formation at 1.9 V; e) Formation at 2 V.

The formation phase, carried out in a range of potential between 1.6V vs. RHE and 2 V vs. RHE. After an initial increase, the current decreases after few hours of formation. The value of current reached from the positive plates with 4% of graphite is higher than the value of current reached from the positive plates without carbon additives (figures 4.17, pink curves) for the potential values from

1.8 V to 2 V. After formation phase the positive pastes were reduced in powder and analysed to the LECO to verify the amount of graphite lost during the formation phase. The table 4.8 reports the results of chemical analysis. The quantity of graphite decreases during formation phase and the corrosion of carbon additive is higher at higher applied potentials.

	1% (ww) G	**2% (ww) G**	**4% (ww) G**
Cured	1.89 ± 0.0102	3.12 ± 0.0218	5.46 ± 0.0491
1.6V	0.974 ± 0.0787	1.94 ± 0.0239	3.79 ± 0.0199
1.7V	0.828 ± 0.0207	1.59 ± 0.0444	3.15 ± 0.0452
1.8V	0.409 ± 0.0216	0.784 ± 0.0570	2.02 ± 0.0117
1.9 V	0.299 ± 0.00218	0.764 ± 0.0272	1.53 ± 0.0545
2 V	0.306 ± 0.0102	0.740 ± 0.0568	1.43 ± 0.0143

Table 4.8 Quantitative of graphite into the positive plates after formation phase in sulfuric acid with density of 1.146 g/cm^3.

Also, SEM analysis was carried out on the samples post-formation. The figure 4.18 shows the results of this analysis. The presence of graphite into the positive plate causes a higher porosity of positive plates than the plates without carbon. Furthermore, the porosity increases, increasing the applied potential, because there is a higher lost in the amount of graphite generating vacuum spaces into the paste of the positive plates. It is possible to see also the presence of graphite into the pastes in all analysed plates.

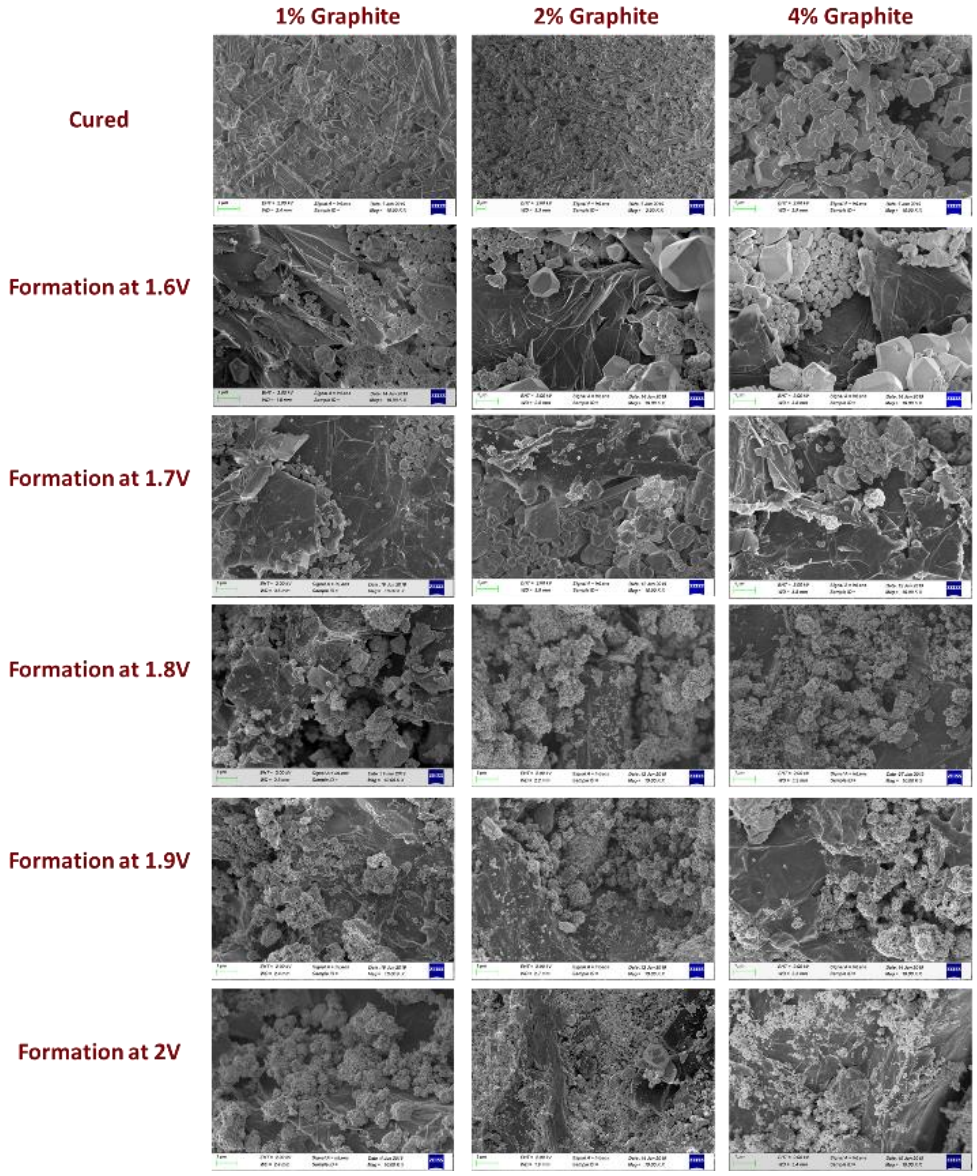

Figure 4.18 SEM images of positive plates after formation phase at different set potentials.

Chapter 5

Disposal of exhausted batteries and accumulators

In this chapter the re-conversion process of plates of spent lead-acid batteries will be discussed. In particular, to re-convert the plates a new method will be presented. This method has been patented by the Laboratory of Applied Physical Chemistry of the University of Palermo. For comparison a brief summary of the conventional recycling methods of lead acid batteries will also be reported.

5.1 Lead-acid battery recycling process

Lead-acid batteries, once exhausted, can be a potential danger to the environment, as they contain highly toxic components. In fact, they contain lead, that is heavy and toxic metal, and the electrolyte, sulfuric acid, that is a very corrosive acid. From exhausted lead acid battery, it is possible to extract the lead and other components such as the electrolyte, the plastic of the case and separators.

Lead metal from exhausted batteries represents over 40% of Italian lead production as well as 37% of the national metal requirement [50]. This secondary production of lead requires less energy than that required for the processing of the mineral.

The first phase of recycling of lead-acid batteries provides for their *crushing*. From the storage area the batteries are loaded into a hopper and, via conveyor belts, are sent to the crushing section consisting of hammer mills. The crushed product with a calibrated size is transferred to a wet screening system where the accurate separation of the fine metal part oxidized by the mix of metal grids and plastic materials takes place. The fine metal part, called *pastel*, is transferred to a filter press. The mix of metal grids and plastic materials is started, by means of tapes, to the hydrodynamic separator in counter-current which, taking advantage of the difference in density of the various crushed components, separates the plastic components from the metallic ones. The plastic, polypropylene and PVC,

are carefully washed and reduced to flakes and is ready to be reused, for example, to produce new battery boxes.

In this phase the liquid part of the battery is also released, an aqueous solution of sulfuric acid, which is sent to the neutralization plant. In the neutralization plant the acid attack with hydrated lime takes place according to the reaction:

$$Ca(OH)_2 + H_2SO_4 \rightarrow CaSO_4 + 2H_2O$$

and with flocculating agents that allow the settling of dissolved solids and the achievement of neutralization of the liquid at the values set by the legislation on effluents. The *melting phase* of the pastel follows the crushing phase. The melting of the pastel occurs at a temperature of about 800 ÷ 1000 °C in direct flame rotary kilns fed with methane and oxygen. Downstream dust collection and abatement systems with bag filters allow continuous control of emissions into the atmosphere, in compliance with the criteria imposed by law. In the ovens the material is reduced from sulfate ($PbSO_4$) and lead oxide (PbO) to metal lead (Pb^0) through the addition of special reagents including iron. Such *opera lead*. it is then sent for *refining - alloying* to obtain refined lead or alloys for various uses. The last phase of the process is the *refining phase* of the work lead. The lead in blocks or in liquid form, coming from the foundry, is placed in boilers, where it undergoes different treatments depending on the final product to be obtained. The figure 5.1 shows the scheme of the lead-acid battery recovery process.

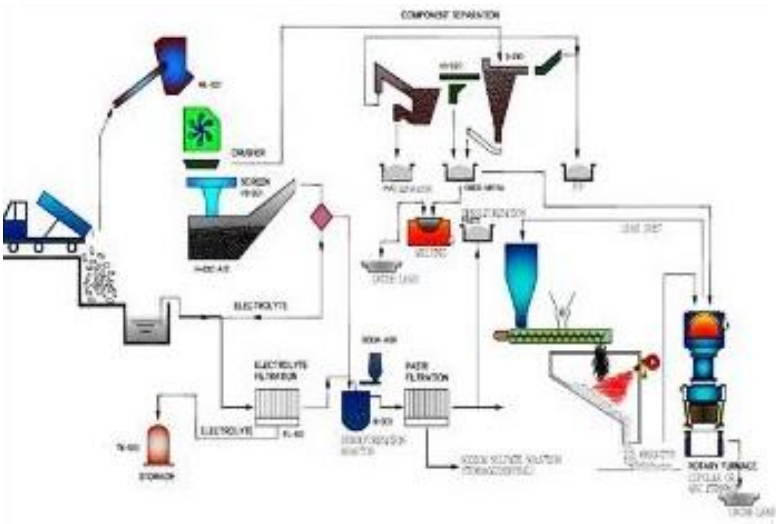

Figure 5.1 Lead-acid battery recycling plant [14].

5.2 Patent on the recycling of lead-acid batteries

The new method proposed in the Applied Physical Chemistry Lab, permits to re-convert the plates of spent lead-acid batteries, without their dismantling and is based on cementation reaction. In particular, a galvanic connection of the plates with aluminium sacrificial anode provides the driving force of the desulfurization reaction of exhausted plates of the lead-acid batteries.

In a galvanic couple, the less noble metal (lower electrochemical standard potential) works as an anode (negative pole) while the other is the cathode (positive pole). Thus, in this case the plates are the cathode, while aluminium is the anode.

The process for converting exhaust active material to metallic lead can be conducted through two different procedures. The first one involves the conversion of negative and positive plate, separately. In this case, two distinct galvanic connections must be established between each terminal of the battery with one sacrificial anode which must be distinct for a negative or positive plate with electrolytic connection for every plate. In the alternative, the two battery terminals can be short circuited and connected to a single sacrificial anode which drives the simultaneous desulfurization of both negative and positive plates.

For conducting a successful desulfurization of exhausted lead acid plates, some parameters must be controlled. The fundamental are temperature and cathodic to anodic surface ratio. The temperature enhances the reaction rate, but, conversely, increases also the evaporation of the electrolyte. In this context, temperatures between 25 and 65 °C were found to be the best compromise between the opposite effects. The surface area ratio of anode to cathode also greatly influences the desulfurization rate. All possible ratios can be employed for better controlling the process rate [51].

- ***Desulfurization of the Negative Plate***

The negative plate of lead acid battery at the end of life was connected to a less noble, in this case Al, metal through an electronic conductor and both were immersed in H_2SO_4 aqueous solution at concentration of 5 M. Through the connection sacrificial anode/electrolyte/exhausted plate, it is possible to convert

the $PbSO_4$ present on the negative plate to metallic lead. The reaction that occurs at the negative plates is:

$$PbSO_4 + 2e^- = Pb + SO_4^{2-} \qquad (E_{cat} = E°_{PbSO4/Pb} = -0.36 \text{ V/NHE}) \qquad (1)$$

The anodic reaction involves aluminium dissolution according to the reaction:

$$Al = Al^{3+} + 3e^- \qquad (E_{an} = E°_{Al^{3+}/Al}) \qquad (2)$$

The overall cell reaction is:

$$nPbSO_4 + 2Al = nPb + nSO_4^{2-} + 2\,Al^{3+} \qquad (E = E_{cat} - E_{an}) \qquad (3)$$

leading to metallic lead and an aqueous solution containing ions of the sacrificial anode.
Parasitic reduction reactions are:

$$4H^+ + O_2 + 4e^- = 2H_2O \qquad (E = 1.23 - 0.059\ pH \ \text{V/NHE}) \qquad (4)$$

$$2H^+ + 2e^- = H_2 \qquad (E = 0 - 0.059\ pH \ \text{V/NHE}) \qquad (5)$$

The role of both these reactions is negligible, because both occur at low extent owing to the very low oxygen concentration (reaction (4)), and large overpotential for hydrogen evolution on lead (reaction (5)). In the presence of sulphate ions, the following reaction occurs in the bulk of the solution:

$$2Al^{3+} + 3SO_4^{2-} = Al_2(SO_4)_3 \qquad (6)$$

Therefore, aluminium sulphate is the main species present in solution, as confirmed by analysis carried out on the electrolyte. After the complete oxidation of the sacrificial anode, for optimizing the process, it is necessary to conduct a purification step of the exhaust solution in order to recycle it. The purification step can be conducted using sodium hydroxide as a neutralizing agent causing the precipitation of aluminium as hydroxide in accordance with the following reaction:

$$Al_2(SO_4)_3 + 6NaOH = 2Al(OH)_3 + 3Na_2SO_4 \qquad (7)$$

The aluminium hydroxide, having a very low solubility in water, precipitates on the bottom tank and it can be separated from a solution by filtration. The product obtained has a value and it may be used for the production of alumina. Instead, the remaining solution can be sent to crystallization for recovering sodium sulfate, which has a market value. The purified solution, after pH correction by H_2SO_4, can be recycled into the process.

- ***Desulfurization of the Positive Plate***

The same process described for negative plate can be conducted for desulfurization of the positive plate with formation of metallic lead. The most significant difference with the negative plate is the presence of PbO_2 that can be reduced to PbSO4, and then to Pb. This last step is identical to that one for negative plate, while the first step is

$PbO_2(s) + SO_4^{2-}(aq) + 4H^+(aq) + 2e^- = PbSO_4\ (s) + 2H_2O\ (l)$
$(E_{cat} = E^0 = +1.69\ V/NHE)$ (8)

Also, this step can be driven through a galvanic connection with a sacrificial anode. The reduction process can occur at higher rate owing to the very noble electrochemical potential of the reaction (7).

5.2.3 Laboratory tests

The desulfurization of exhausted plates (positive or negative) was carried out using an aqueous solution of H_2SO_4 5M. The plate was connected through a lead wire to the sacrificial anode (aluminium) and the connection was isolated to avoid its corrosion during desulfurization phase. The solution was magnetically stirred, and the desulfurization was carried out at room temperature. The scheme of the cementation cells is reported in the figure 5.2. The figure 5.2a shows the arrangement of the electrodes when they are immersed in the same vessel. The figure 5.2b shows the arrangement of cementation cell when exhausted plate and sacrificial anode are immersed in the separate vessels. In this case it is necessary to use a salt bridge to connect the electrolytes into the vessels. The desulfurization of lead plate was carried out with five steps of cementation and after each one the XRD analysis was carried out to verify the evolution of peaks of lead sulfate and lead on the plate.

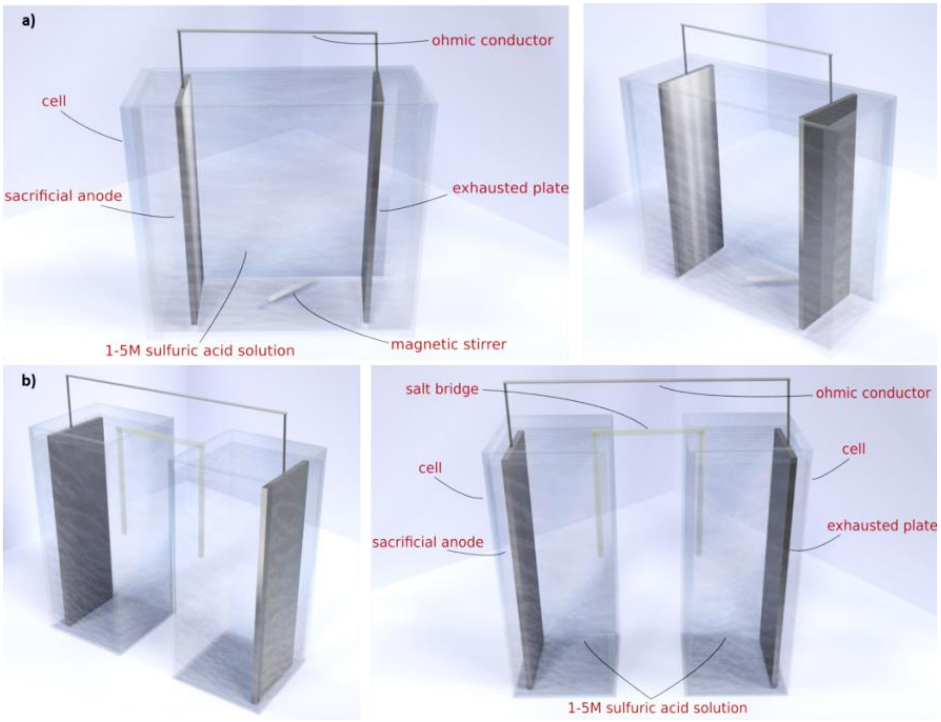

Figure 5.2 Scheme of the cementation cells: a) Arrangement when exhausted plate and sacrificial anode are immersed in the same vessel; b) Arrangement when exhausted plate and sacrificial anode are immersed in the separate vessels [15].

The figure 5.3 shows the XRD patterns of the lead plate before and after desulfurization.

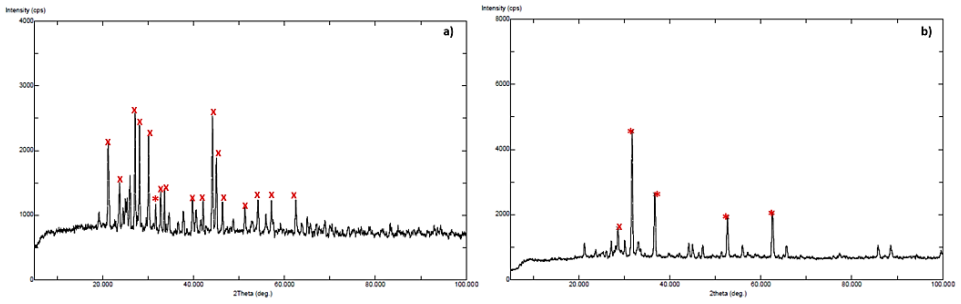

Figure 5.3 XRD patterns of Pb plate: a) XRD pattern of exhausted Pb plate; b) XRD pattern of Pb plate after cementation.

After the cementation processes, XRD patterns show a decrease in the lead sulphate and an increase of lead. Prior cementation, Figure 5.3a shows a largely presence of $PbSO_4$, [52] in fact, its characteristic peaks at the angles 2-theta 29.68°, 26.71° and 20.81° were found. In figure 5.3b, pattern after cementation, the presence of Pb characteristic peaks at the angles 2-theta 31.27°, 36.26° and 52.22° [52], were also found. In table 5.1 the evolution of the main peaks of the XRD pattern before and after desulfurization is reported.

Species	**2Theta (Before cementation)**	**Instensity (Before cementation)**	**I/I_0 (Before cementation)**	**2Theta (After cementation)**	**Instensity (After cementation)**	**I/I_0 (After cementation)**
$PbSO_4$	27.132	2585	100	28.592	1590	35
	28.088	2114	82	-	-	-
	21.220	2537	99	-	-	-
Pb	31.660	1159	45	31.692	4563	100
	-	-	-	36.688	2624	58
	-	-	-	62.560	2063	46
	-	-	-	52.640	1924	43

Table 5.1 Peaks' evolution of lead sulphate and lead of XRD patterns on Pb plate before and after cementation.

Also the exhausted positive plate was subject to the desulfurization process through the cementation in the same condition of the negative plate, but without stirred. We carried out three steps of cementation and after each step the positive plate was subject to XRD analysis and the figures 5.4 a) and b) show the patterns before and after cementation.

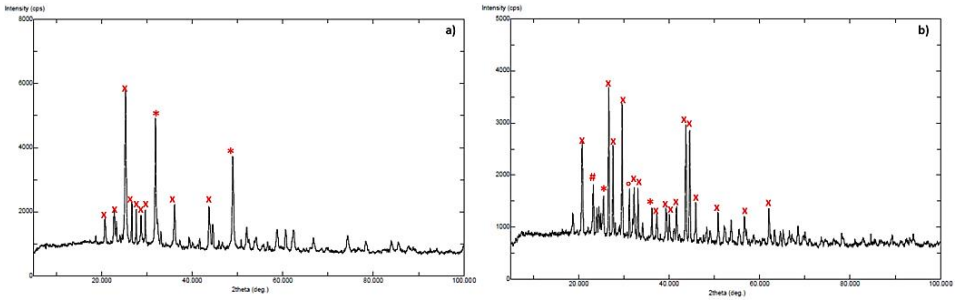

Figure 5.4 XRD patterns of PbO_2 plate: a) XRD pattern of exhausted PbO_2 plate; b) XRD pattern of PbO_2 plate after cementation.

In the exhausted positive plate is present lead sulphate and β-PbO_2, [52].

Species	2Theta (Before cementation)	Instensity (Before cementation)	I/I_0 (Before cementation)	2Theta (After cementation)	Instensity (After cementation)	I/I_0 (After cementation)
$PbSO_4$	26.660	2307	40	26.640	3680	100
	43.700	2149	38	29.604	3384	92
	29.628	2059	36	43.672	2976	81
	20.756	1834	32	20.752	2627	72
α-PbO_2	-	-	-	23.232	1816	50
β-PbO_2	25.276	5793	100	25.504	1592	44
	31.892	4923	85	36.184	1370	38
	48.972	3721	65	-	-	-
Pb	-	-	-	31.204	1734	48

Table 5.2 Peaks' evolution of lead sulfate and lead of XRD patterns on PbO_2 plate before and after cementation.

After the cementation the peaks of Pb and α-PbO_2 appear. Table 5.2 shows the evolution of the peaks of the species [52].

Thus, the desulfurization of the active paste of spent lead acid battery can be obtained through galvanic method. This technique is easy, more environmentally friendly if compared with the actual recycling processes, and scalable to industrial level.

Conclusions

The goal of this research activity work was to prepare nanostructured lead and lead oxide electrodes to test in lead acid batteries. Initially, the attention was focused on the study of the performance of the nanostructured lead electrode, because, as known in the literature, the negative plates have worse performance in comparison to positive plate. In fact, negative plate must overcome some limits to guarantee a longer duration, to increase the charge acceptance and to prevent the sulfurization phenomena that prematurely damage the electrode. The most common approach is to add additives to the active material in order to improve its characteristics, closely related to the specific surface of the electrode. In fact, one of the main problems of lead-acid batteries is related to the high molecular weight of lead, which limits the specific energy of the electrodes. In order to overcome this limitation, in this PhD thesis the electrodeposition process of the Pb in the template has been optimized, with the aim to increase the surface available for the sulfation/desulfation reactions occurring respectively during the discharge/charge cycles. The electrodeposition was carried out in nano-porous template, obtaining electrodes consisting of nanowire arrays supported by a current collector, also obtained by electrodeposition. Before the electrochemical tests, the membrane is dissolved and the nanostructured electrode was analysed to study morphology, composition and crystallinity. Thus, nanostructured electrodes are tested by simulating the operating conditions of commercial batteries. In particular, the electrodes were assembled in a zero-gap configuration, consisting of nanostructured electrodes, an AGM type separator and a high capacity positive plate. The cell is then tested in a 5M sulfuric acid solution. All tests were conducted in much more drastic conditions than those typical of commercial battery. In particular the tests were conducted at C-rate greater than or equal to 1C (for commercial batteries the operating C-rate is lower or equal to 0.2C), and a greater discharge depth. In fact, a very low cut-off voltage (1.2 V, while the usual commercial battery voltage is 1.75 V) was imposed with a deep of discharge of 90% (in commercial battery never exceeding 80%). Although these conditions are very "stressful", the results were quite satisfactory in terms of drainage capacity. For the first charge, a step-by-step charging method (which concerns only the first charge of the first battery start-up) was imposed to gradually charge the electrode and prevent the excessive generation of hydrogen.

The battery tests carried out at 1C showed the achievement of an efficiency of about 84%. The discharge curves have a plateau that increases with the number of cycles, which translates into greater usable energy. The tests made at C-rate of 2C, 5C and 10C have shown more stable performance, reaching an efficiency value of 90% which remains constant until the end of battery life. This result is attributable to the different Pb sulfate morphology that is generated at a higher cyclization rate.

Battery with both nanostructured electrodes was also tested. Also, in this case the results obtained were satisfactory and interesting conclusions were deduced from these tests. In fact, the performance of nanostructured battery is stable in terms of efficiency and shape of discharge curves. The very good performance are attributed to the high surface area of nanostructured electrodes that greatly affects the charge-discharge characteristics, confirming the importance of the development and use of nanostructured electrodes. During discharge/charge phases, the nanostructures undergo a considerable variation from a morphological point of view. The morphology variation leads to the formation of very spongy and non-compact structures, characterized by a presence of macro-voids that ensure electrolyte penetration even in the most internal areas. Thus, a large part of the active mass of the electrode becomes easily accessible to the electrolyte, and this implies a high degree of utilization of the material from which good performance is achieved. Therefore, using nanostructures, it is possible to increase the specific energy (Wh/kg) and the power density (W/L) of the batteries thanks to the drastic reduction in both the weight of the active material and the volume, and it is also possible to increase the cycling speed.

At the Fraunhofer ISC of Wűrzburg, Germany, where there are the specialists in the field of lead-acid batteries, we studied, by Cyclic Voltammetric tests, the performance of nanostructured electrodes in comparison with the lead sheets. From these tests it was found that both nanostructured electrodes show a much higher current density than that detected on the lead sheets and this gives us confirmation of the high surface area presented by the nanostructured electrodes.

The results obtained so far show that it is possible to propose an innovative device that can compete with already well-established technologies.

Bibliography

[1] D. Linden, T. B. Reddy Edt.s, Handbook of Batteries, 4th Edition, McGraw-Hill, New-York, 2010.
[2] Alfredo Testa, Appunti di sistemi elettrici di bordo, 2005.
[3] Velarossa.it, Batterie al Piombo, www.velarossa.it.
[4] B. University, «BU-806a: How Heat and Loading affect Battery Life,» 26 05 2016.https://batteryuniversity.com/index.php/learn/article/how_heat_and_harsh_loading_reduces_battery_life.
[5] D. Diemand, «Automotive Batteries at Low Temperatues,» in Cold Regions Technical Digest, Hanover, New Hampshire, USA Cold Regions Reasearch and Engineering Laboratory, 1991.
[6] R. Inguanta, S. Randazzo, A. Moncada, M. C. Mistretta, S. Piazza, C. Sunseri, Growth and Electrochemical Performance of Lead and Lead Oxide Nanowire Arrays as Electrodes for Lead-Acid Batteries, Chemical Engineering Transactions, Vol. 32, (2013) 2227 - 2232.
[7] COBAC, Batterie, www.cobac.it.
[8] P. Křivík, K. Micka, Petr Bača, Karel Tonar, Pavel Tošer, Effect of additives on the performance of negative lead-acid battery electrodes during formation and partial state of charge operation, J Power Sources 209 (2012) 15– 19.
[9] Storage Battery Systems– Battery Specialists Since 1915, Stationary Lead-Acid Batteries With Selenium Alloys.
[10] P. Bača, P. Křivík, P.Tošer, S. Vaculík, Negative Lead-Acid Battery Electrodes Doped with Glass Fibres, Int. J. Electrochem. Sci., 10 (2015) 2206 – 2219.
[11] N. Boudieb, M. Bounoughaz, M. Nazef-Allaoua, Influence of surfactant as an electrolyte additive on the electrochemical and corrosion behaviors of lead-acid battery, University M'Hamed Bougara-UMBB-Boumerdes, Faculty of Engineering Science, Laboratory of Polymers Treatment and Forming; Avenue of Independence –Boumedes- 35000- Algeria. Department of Corrosion, Development & Technologies Division, Upstream Activity, Sonatrach2 1th November Avenue, Boumedes- 35000 ALGERIA.
[12] J. Zhu, G. Hu, X. Yue1, D. Wang, 2016, Study of Graphene as a Negative Additive for Valve-Regulated Lead-Acid Batteries Working under High-Rate Partial-State-Of-Charge Conditions, Int. J. Electrochem. Sci., 11, 700 – 709.
[13] N. Sugumaran, P. Everill, S.W. Swogger, D.P. Dubey, Lead acid battery

performance and cycle life increased through addition of discrete carbon nanotubes to both electrodes, Journal of Power Sources 279 (2015) 281e293.
[14] M. Saravanan, P. Sennu, M. Ganesan and S. Ambalavanan, Multi-Walled Carbon Nanotubes Percolation Network Enhanced the Performance of Negative Electrode for Lead-Acid Battery, Journal of The Electrochemical Society J. Electrochem. Soc. 2013, Volume 160, Issue 1, Pages A70-A76.
[15] P.T. Moseley, Positive plate additives, Journal of Power Sources 64 (1997) 47-50.
[16] S. Salih, A. Gad-Allah, A. Abd El-Wahab, H. Abd El-Rahman, Effect of boric acid on corrosion and electrochemical performance of Pb-0.08% Ca-1.1% Sn alloys containing Cu, As, and Sb impurities for manufacture of grids of lead-acid batteries, Turk J Chem (2014) 38: 260 – 274 ©TÜBİTAK doi:10.3906/kim-1212-76.
[17] K. McGregor, Active-material additives for high-rate lead/acid batteries: have there been any positive advances?, Journal of Power Sources 59 (1996) 31-43.
[18] M. Sorge, T. Bean, T. Woodland, J. Canning, I. F. Cheng, D.B. Edwards, Investigating the use of porous, hollow glass microspheres in positive lead acid battery plates, Journal of Power Sources 266 (2014) 496-511.
[19] A. Moncada, S. Piazza, C. Sunseri, R. Inguanta, Recent improvements in PbO_2 nanowire electrodes for lead-acid battery, Journal of Power Sources 275 (2015) 181-188.
[20] A. Moncada, M.C. Mistretta, S. Randazzo, S. Piazza, C. Sunseri, R. Inguanta, High-performance of PbO_2 nanowire electrodes for lead-acid battery, Journal of Power Sources 256 (2014) 72-79.
[21] A. N. Fleming, J.A. Harrison, The Aqueous System Pb^{2+}/Pb - Chapter 1. The Electrochemistry of Lead. A. T. Kuhn, London, 1979.
[22] D. Pavlov, Pastes and Grid Pasting - Chapter 6. Lead Acid Batteries: Science and Technology, Elsevier, Amsterdam, 2011.
[23] M. G. Insinga, R. L. Oliveri, C. Sunseri, R. Inguanta, Template electrodeposition and characterization of nanostructured Pb as a negative electrode for lead-acid battery, Journal of Power Sources, 413 (2019) 107–116.
[24] D. Pavlov, Pastes and Grid Pasting – Appendix 2. Lead Acid Batteries: Science and Technology, Elsevier, Amsterdam, 2011.
[25] D. Pavlov, Lead-acid Batteries: Science and Technology a Handbook of Lead-acid Battery Technology and its Influence on the Product, Elsevier, Amsterdam, 2017.

[26] E. Budevski, G. Staikov, W.J. Lorenz, Electrocrystallization Nucleation and growth phenomena, Electrochim. Acta 45 (2000) 2559–2574, https://doi.org/10.1016/ S0013-4686(00)00353-4.
[27] L. Rodrıguez-Sanchez, M.C. Blanco, M.A. Lopez-Quintela, Electrochemical synthesis of silver nanoparticles, J. Phys. Chem. B 104 (2000) 9683–9688, https://doi.org/ 10.1021/jp001761r Table 3.
[28] Secondary cells and batteries for renewable energy storage – General requirements and methods of test - Part 1: Photovoltaic off-grid application, BSI Standards Publication, BS EN 61427-1:2013.
[29] R. H., Sandia National Laboratories, Temperature effects on sealed lead acid batteries and charging techniques to prolong cycle life, 2004.
[30] J. L. J. T. A. D.-V. L. T. J. V. F. H. A. D. G. S. Grugeon-Dewaele, «Soaking and formation of tetrabasic lead sulfate,» Journal of Power Sources, vol. 64, pp. 71 - 80, 1997.
[31] M.G. Insinga, S. Pisana, R.L. Oliveri, C. Sunseri, R. Inguanta, Performance of lead-acid batteries with nanostructured electrodes at different temperature, IEEE, 2018, DOI: 10.1109/RTSI.2018.8548446.
[32] G. Feuillade, P. Perche, 1975, Ion-conductive macromolecular gels and membranes for solid lithium cells, J. Appl. Electrochem., 5, 63-69.
[33] N.A. Peppas, 1975, Turbidimetric studies of aqueous poly(vinyl alcohol) solutions, Macromol. Chem. And Pysics, 176, 3433-3440.
[34] M. Nambu, 1984, Freeze-dried poly(vinyl alchool) gel, US Patent 4,472,542.
[35] F. Yokoyama, I. Masada, K. Shimamura, T. Ikawa, K. Monobe.,1986, Morphology and structure of highly elastic poly(vinyl alcohol) hydrogel prepared by repeated freezing-and-melting, Colloid Polym Sci, 264, 595-601.
[36] C.W. Bunn, 1948, Crystal Structure of Polyvinyl Alcohol. Nature, 161, 929-930.
[37] H.E. Harris, J.F. Kenney, G.W. Willcockson, R. Chiang, H.N. Friedlander, 1966, Structure–property relationships of poly(vinyl alcohol). II. The influence of molecular regularity on the crystallization–dissolution temperature relationships of poly(vinyl alcohol), Polym Sci., 4, 665-677.
[38] M.G. Insinga, A. Derelitto, S. Pisana, R.L. Oliveri, C. Sunseri, R. Inguanta, Gelled Electrolyte for Nanostructured Lead-acid Battery, Chemical Engineering Transactions, 2019, Vol. 73, 25–30.
[39] Seong B. Y. , Sung H. Y. , Joon S. L. , Jong W. K., Jeong H. Y., 2017, Surface Properties of a Novel Poly(vinylalcohol) Film Prepared by

Heterogeneous Saponification of Poly(vinyl acetate) Film, Polymers MDPI, 9, 493.
[40] Visscher, W.H.M., Cyclic voltammetry on lead electrodes in sulphuric acid solution, Journal of Power Sources, 1977, DOI: 10.1016/0378-7753(76)81003-8.
[41] M. Shiomi, T. Funato, K. Nakamura, K. Takahashi, M. Tsubota ―Effects of Carbon in Negative Plates on Cycle-life Performance of Calve-regulated Lead/Acid Batteries.‖ Journal of Power Sources, 64 (1997). pp. 147-152.
[42] M. A. Spence, D. P. Boden, T. D. Wojcinski, ―Identification of the Optimum Specification for Carbon to be Included in the Negative Active Material of a Valve-Regulated Battery in Order to Avoid Accumulation of Lead Sulfate During High-Rate Partial-State-of-Charge Operation.‖ ALABC Research Project Designation C1.1/2.1A, Progress Report 4, October 2009.
[43] P.T. Moseley, R.F. Nelson, A.F. Hollenkamp ―The Role of Carbon in Valve-regulated Lead-acid Battery Technology.‖ Journal of Power Sources, 157 (2006). pp.3-10.
[44] P.T. Moseley ―Consequences of Including Carbon in the Negative Plates of Valve-regulated Lead-acid Batteries Exposed to High-rate Partial-state-of-charge Operation.‖ Journal of Power Sources, 191 (2009). pp. 134-138.
[45] https://www.sigmaaldrich.com/materials-science/material-science-products.html?TablePage=106837645.
[46] L. Dong, Q. Liu, K. Chen, Graphene-Supported Platinum and Platinum-Ruthenium
Nanoparticles for Fuel Cell Applications, 2011, InTech, DOI: 10.5772/14422.
[47] A.J. S. Ahammada, P. R. Pala, S. S. Shahb, T. Islama, Md. M. Hasana, M. A. A. Qasemb, N. Odhikaria, S. Sarkerc, D. M. Kimc, Md. A. Aziz, Activated jute carbon paste screen-printed FTO electrodes for nonenzymatic amperometric determination of nitrite, Journal of Electroanalytical Chemistry 832 (2019) 368–379.
[48] Witantyo, Suwarno, N. K. Sholihah, A. Shahab, Influences Of Carbon Additives In The Positive Active Material Of Lead-acid Batteries To Improve Capacity And Life Cycles, Conference Paper in AIP Conference Proceedings, 2018, DOI: 10.1063/1.5046289.
[49] https://www.isc.fraunhofer.de/en/press-and-media/press-releases/faster-lighter-better-addesun-a-new-generation-of-lead-acid-batteries.html.
[50] http://automazione-plus.it/cobat-il-processo-di-riciclaggio-delle-batterie-al-piombo-esauste_3481/

[51] R. Inguanta, C. Cocchiara, M. G. Insinga, C. Sunseri, Metodo E Kit Per Il Recupero Di Piombo Metallico Da Componenti Di Un Accumulatore Esausto Al Piombo-Acido, Italian Patent 102017000141056 del 6/12/2017.
[52]D. Pavlov, Pastes and Grid Pasting – Appendix 2. Lead Acid Batteries: Science and Technology, Elsevier, Amsterdam, 2011.
[53] Lead Acid Battery Market Size to Reach $84.46 Billions by 2025 –January 2017.

Images bibliography

[1] M. A. Hannan, Md. Murshadul Hoque, A. Mohamed, A. Ayob, Review of energy storage systems for electric vehicle applications: Issues and challenges, Renewable and Sustainable Energy Reviews 69(2017):771-789 DOI: 10.1016/j.rser.2016.11.171.
[2] Global surces, Shenzhen Glink Hardware&Plastic Co. Ltd, https://www.globalsources.com.
[3] UPS Battery Center Canada, https://www.upsbatterycenter.ca/12v-45ah-sealed-lead-acid-battery-with-f11-terminals.
[4] A. Moncada, Accumulo e conversione di energia per via elettrochimica attraverso batterie piombo-acido con elettrodi nano-strutturati, Doctoral thesis 2017.
[5] Velarossa.it, Batterie al Piombo, www.velarossa.it.
[6] Technologies | Storage, distribution, electrical, convertors, http://www.joules-project.eu/Joules/technologies/storage_distribution_electrical_convertors.
[7] Lithium Ion Battery Assembly Challenges, https://www.ecnmag.com/article/2011/01/lithium-ion-battery-assembly-challenges.
[8] D. Diemand, «Automotive Batteries at Low Temperatues,» in Cold Regions Technical Digest, Hanover, New Hampshire, USA Cold Regions Reasearch and Engineering Laboratory, 1991.
[9] D. Pavlov, Pastes and Grid Pasting - Chapter 6. Lead Acid Batteries: Science and Technology, Elsevier, Amsterdam, 2011.
[10] M. G. Insinga, R. L. Oliveri, C. Sunseri, R. Inguanta, Template electrodeposition and characterization of nanostructured Pb as a negative electrode for lead-acid battery, Journal of Power Sources, 413 (2019) 107–116.
[11] M.G. Insinga, S. Pisana, R.L. Oliveri, C. Sunseri, R. Inguanta, Performance of lead-acid batteries with nanostructured electrodes at different temperature, IEEE, 2018, DOI: 10.1109/RTSI.2018.8548446.
[12] A. Derelitto, Elettroliti gelificati per batterie piombo acido nanostrutturate, Tesi di Laurea Magistrale in Ingegneria Chimica, A.A. 2017 – 2018.
[13] Y.Yamamoto, K. Fumino, T. Ueda, M. Namew, A potentiodynamic study of the lead electrode in sulphuric acid solution, Elecmchimica Acta, Vol.3 7, N° 2, pp.199 – 203, 1992.
[14] https://unikor.en.ec21.com/Waste-Battery-Recycling-Plant--6_8413309.html

[15] R. Inguanta, C. Cocchiara, M. G. Insinga, C. Sunseri, Metodo E Kit Per Il Recupero Di Piombo Metallico Da Componenti Di Un Accumulatore Esausto Al Piombo-Acido, Italian Patent 102017000141056 del 6/12/2017.